EUROPEAN COMMISSION

Community Research

SEVENTH FRAMEWORK PROGRAMME

ARCHER

Collaborative Project (CP)

Co-funded by the European Commission under the Euratom Research and Training Programme on Nuclear Energy within the Seventh Framework Programme

Grant Agreement Number : 269892

Start date : 01/02/2011 Duration : 48 Months

www.archer-project.eu

Archer

Advanced Reactor for Cogeneration of Heat & Electricity-R&D

Report on test results and comparison with pre and post-calculations

Authors : Claudia Druska, Kathrin Trollmann, Stefan Kasselmann (FZJ), B^{a}rbel Schl^{o}gl, Dinesh Singh (RWTH)

ARCHER - Contract Number: 269892
Advanced High-Temperature Reactors for Cogeneration of Heat and Electricity R&D
EC Scientific Officer: Dr. Panagiotis Manolatos

Document title	Report on test results and comparison with pre and post-calculations
Author(s)	Claudia Druska, Kathrin Trollmann, Stefan Kasselmann (FZJ), Bärbel Schlögl, Dinesh Singh (RWTH)
Number of pages	66
Document type	Deliverable
Work Package	WP 21
Document number	D21.12
Issued by	FZJ
Date of completion	04/03/2015
Dissemination level	Confidential, only for members of the consortium (including the Commission Services).

Summary

This document contains the description of the Boudouard tests in the NACOK II facility. First the theoretical background of the graphite oxidation, especially the Boudouard reaction in case of an air ingress accident is given. After the description of the test facility NACOK, the experimental set-up of the Boudouard experiments is described. The first experiment is dealing with graphite blocks, in the second experiment a pebble-bed of graphite spheres is used. The experiments were accompanied by pre- and post-calculations with the 3-dimensional reactor dynamics code MGT. The simulation results are compared with the experimental data and a final evaluation of the project is given.

Approval

Date	By
11/03/2015	Stefan KASSELMAN
11/03/2015	Norbert KOHTZ
11/03/2015	Steven KNOL

Distribution list

Name	Organisation	Comments
P. Manolatos	EC DG RTD	Through the EC participant portal
All beneficiaries	ARCHER	Through the private online workspace

Table of contents

Table of figures

Table of tables

1 Introduction

In the event of an HTR air ingress accident, carbon dioxide is produced during the initial oxidation of the reactor's graphite by atmospheric oxygen in the graphite reflector, from which it might flow into the reactor core and cause damage as a result of corrosion. The overall aim of this work package is therefore to study effects of the so called Boudouard reaction (a secondary reaction of air induced graphite corrosion by CO_2) using state-of-the-art instrumentation systems of the new NACOK II facility for a better understanding of coupled fluid dynamics and reaction kinetics.

The graphite oxidation by CO_2 (Boudouard reaction) will be investigated without influence of the primary (air induced) reaction at a temperature level at which the Boudouard reaction can take place at significant reaction rates. In the first experiment a block geometry and in the second experiment a pebble bed geometry is used.

These experiments are accompanied by pre- and post-calculations with the reactor dynamics code MGT-3D. The MGT-3D code system in general deals with the nuclear and the thermal transient behaviour of the primary circuit of a high temperature gas cooled reactor and is based on the well-known code TINTE. MGT-3D takes into account the mutual feedback effects in three-dimensional R-Z-Phi geometry. As the R-coordinate is not restricted to start at $R \approx 0$, by starting at a considerable large radial value a pseudo X-Y-Z geometry may be simulated as well. MGT contains also models for simulating air ingress into the primary circuit of an HTR. For this reason 2D and 3D models are developed and compared.

2 Graphite oxidation

Chemical reactions in which all of the reactants are in the same phase are called homogeneous reactions, and chemical reactions between reactants that are in two or more different phases are called heterogeneous reactions. Heterogeneous reactions are much more dependent on mass transport than homogeneous reactions. Graphite-gas reactions are therefore considered heterogeneous reactions, and reactions between gaseous reactants are considered homogenous.

No.	Reaction	ΔH_R (kJ/mol)
(1a)	$2C + O_2 \rightarrow 2CO$	-221.04
(1b)	$C + O_2 \rightarrow CO_2$	-393.51
(2)	$C + CO_2 \leftrightarrow 2CO$	+172.47
(3)	$C + H_2O \leftrightarrow CO + H_2$	+130.29
(4)	$C + 2\,H_2 \leftrightarrow CH_4$	-74.77
(5)	$2CO + O_2 \rightarrow 2CO_2$	-565.98
(6)	$CO + H_2O \leftrightarrow CO_2 + H_2$	-40.38

Table 1: Reactions taking place during the oxidation of carbon in air or water vapour

Chemical reactions generally tend to depend more strongly on temperature than on mass transport by gas diffusion. The reaction rate is determined by the chemical reaction at low temperatures and by mass transport at higher temperatures. Therefore, with respect to thermal reactions between gases and porous solid materials, there are three different chemical reaction regimes, controlled respectively by the slowest of the steps involved in the reaction, that have to be taken into consideration.

At low temperatures, the slowest reaction step is the actual chemical reaction, therefore it is called chemical regime (CR) or Regime I. In a Regime I reaction, the chemical reaction progresses so slowly that mass transport simply has no influence at all. Since the reactant gases penetrating the graphite do not form a concentration profile, the corrosion affects all of the solid material largely homogeneously.

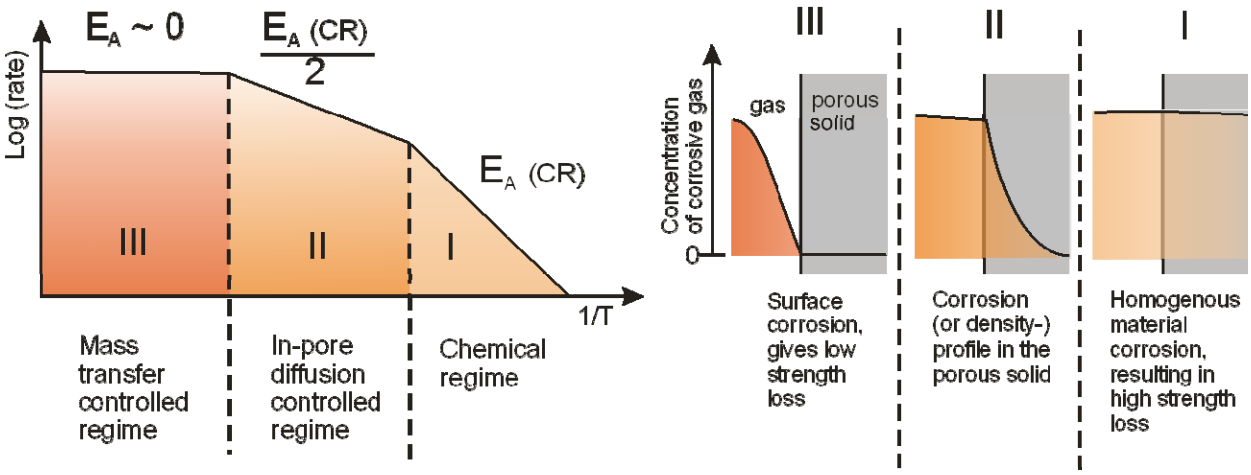

Figure 1: Graphite oxidation (heterogeneous reaction) reaction regimes

At medium temperatures, pore diffusion or Regime II determines the oxidation rate. Since at these temperatures, gas transport through the pores and the chemical reaction overlap, the reaction rate is determined by both the chemical reaction rate and pore diffusion. The high concentration profile of the reactant gases inside the solid material also leads to the formation of a corrosion profile in the graphite.

At high temperatures, the corrosion rate is determined solely by boundary layer diffusion and is therefore called boundary layer diffusion or Regime III. At these temperatures, corrosion occurs only on the graphite's surface. This temperature-controlled chemical reaction happens so quickly that the reactant gases are fully consumed at the graphite's surface long before they are able to penetrate the porous solid matter.

The temperature ranges of these different regimes strongly depend on the oxidants, their flow rates, and the graphite's porosity. The higher the purely chemical reaction rate, the lower the regimes' temperature ranges. The Regime II thresholds for CO_2 are ~1000°C to ~1300°C, while the Regime II thresholds for reactant air, which has a higher reactivity, are ~600°C to ~900°C, depending on porosity.

3 MGT-3D

The TINTE (**TI**me dependent **N**eutronics and **TE**mperatures) reactor dynamics code /1/ has been developed some decades ago to simulate the transient behaviour of gas-cooled high temperature reactors in operational as well as in accidental situations. The code has gained world-wide attention in the past ten years and has been licensed several times in the international community.

During the last years with the development of MGT (**M**ulti-**G**roup-**T**INTE) /2/ major extensions have been applied to TINTE. So the restriction of TINTE to two energy groups has been removed as now the group structure may be deliberately chosen. Furthermore the nuclear data base is now more flexible. While in TINTE the only option was a parametric polynomial expansion of the cross-sections, in MGT polynoms, tables and as major innovation a direct calculation of cross sections during the run of a transient are available. Substantial operating experience with MGT has been collected during the last years.

For certain analyses a three-dimensional description is highly favourable however. Thus the explicit representation of control rods and gas risers requests a 3-D picture. The questions that arose with the latest discussions around the AVR reactor can only be answered with a 3-D model. Finally 3-D models of reactors become more and more a standard. Thus it was intended to extend the MGT code to three spatial dimensions. Considering the fact, that a cylindrical geometry is the natural geometry for high-temperature reactors, a R-Z-Φ representation was chosen. As will be seen later, by some clever use of the 3-D cylindrical geometry a pseudo X-Y-Z geometry may approximately be described as well.

The three-dimensional reactor dynamics program MGT-3D today is able to treat reactor models in R-Z-Φ geometry. Caused by the requirements of the 3-D geometry compared to TINTE, new features have been implemented into MGT-3D. The fluid-dynamics equations for multi-gas mixtures, as they occur e.g. in graphite corrosion calculations have completely been revised and rewritten. A much better approximation of the momentum transfer equations has been implemented, so that now extremely fast propagating waves may be treated in MGT-3D. The treatment of the 1-D component network has been corrected and modified. In total, MGT-3D presents itself as a complete 3-dimensional (R-Z-Φ) tool to describe equilibrium and transient situations of high temperature reactors in operating and accident conditions.

MGT-3D can also be applied to pure neutronics or fluid dyamics problems. In the latter case a graphite corrosion model is available which takes into account the most important homogeneous (reactions in the gas phase) and heterogeneous (gas/wall interactions) reactions. The following chemical reactions are implemented so far:

- CO oxidation: $2\,CO + O_2 \Rightarrow 2\,CO_2$
- H2 oxidation: $2\,H_2 + O_2 \Rightarrow 2\,H_2O$
- Water shift reaction: $H_2O + CO \Leftrightarrow H_2 + CO_2$
- Water gas reaction: $H_2O + C \Leftrightarrow H_2 + CO$
- Boudouard reaction: $CO_2 + C \Leftrightarrow 2\,CO$
- Heterog. oxidation: $O_2 + C \Leftrightarrow CO_2$

Additional reactions are neglected to be able to get an analytical solution of the balance equation system. As a result a nuclide vector for each mesh is derived depending on the concentrations of the neighbouring meshes. In addition the chemical sources and sinks are being calculated which are used in the gas mixing and transport part of MGT.

The model was already successfully applied to experiments like VELUNA or NACOK-I, but is still in the validation phase. The model up to now was only used to simulate pebble bed arrangements. So it can be expected that there are still significant deviations between experimental results and MGT simulations for block type setups. A more detailed study about this issue is currently underway.

4 Experimental Set-Up and Instrumentation in NACOK II

4.1 NACOK II

The old NACOK (NAturzug im COre mit Korrosion) facility of the Institute for Nuclear Waste Management and Reactor Safety (IEK-6) of Forschungszentrum Jülich has been optimized, modernized and reactivated according to a new assignment of objectives (see Fig. 2). It is a 5 m high integral experiment for fluid mechanics and graphite corrosion processes under natural convection conditions or forced gas flow. The modular structure of the electrically heated ceramic flow channel allows flexible handling of samples such as spherical fuel elements and prismatic blocks. Optical access for PIV flow field measurements is provided by window segments. The new NACOK II reaches 1200°C after 1,2m entry length with normal air or defined gases and gas mixtures of N_2, O_2, He, CO_2 up to a flow rate of 50m³/h. The facility was brought into operation at the end of 2012.

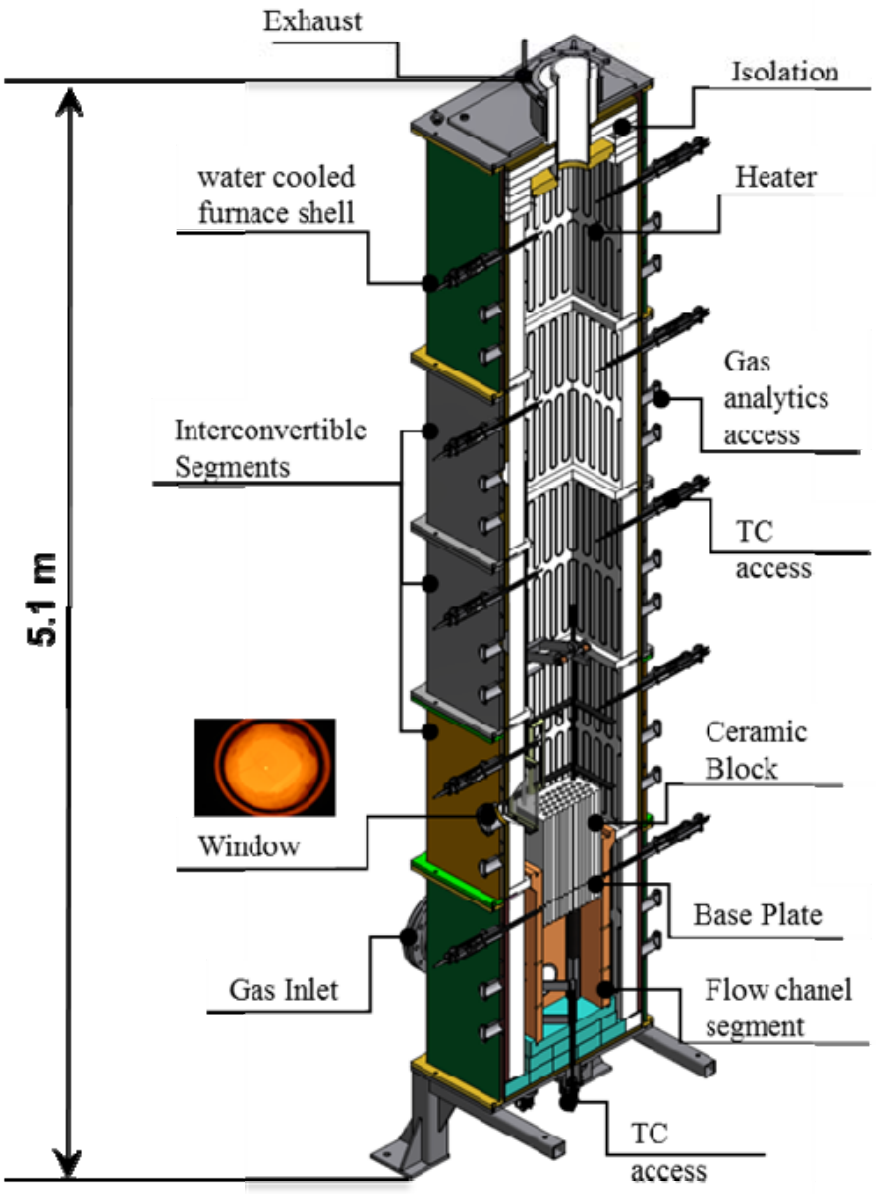

Figure 2: Schematic of NACOK II main parts

The new NACOK II has a ceramic flow channel stacked with five segments, each with a height of 0.8m and able to withstand temperatures up to 1600°C (maximal temperature of the entire facility is 1200°C). The cross section of the channel is rectangular and allows sample sizes of 300mm x 300mm. The height of those samples, like prismatic blocks, should not exceed 400mm for handling and instrumentation. The furnace shell is water-cooled and provides defined boundary conditions. The heating power of the lower three furnace segments is 40kW each, while the upper segments have a heating capacity of 25kW each. That results in a 170kW total maximum heating capacity of the furnace.

The second segment, which is interchangeable with segment three and four, is equipped with windows for optical access. This allows the implementation of Particle Image Velocimetry (PIV) to investigate the flow field above samples inside the flow channel. For the oxidation experiments this measurement technique can´t be used reasonable. The use of particles in the test facility would give a far higher oxidation surface in relation to the investigated graphite geometries and therefore affect the intended results.

Number of segments	5 (upgradeable)
Height of each segment	0.8m
Height of furnace	5.1m
Maximum temperature	1200°C
Maximum flow length to reach T_{max}	1.2m
Maximum total heating power	170kW
Maximum heating rate	30°C/h
Maximum gas flow	50Nm³/h

Table 2: NACOK II main data

The NACOK II facility has been optimized for graphite oxidation experiments. Therefore it must be assured, that no oxidation gases can enter the graphite geometry unintentionally. The water-cooled shell of the furnace allows the use of silicon seals in the cold area to get a gastight facility. There is the possibility to use pneumatic valves in the gas inlet (especially for natural convection experiments) and in the gas outlet lines. The pneumatic valve in the exhaust line has to be protected from temperatures higher than 200°C by installation of a water-cooled bend and a gas cooler before the valve.

For the balancing of the heating power, the current and voltage of each heating zone is recorded as well as the amount and temperature of the cooling water. Every heating zone, the cooled bend and the gas cooler has a separate, adjustable cooling water supply with measurement of the inlet and outlet temperature.

To control and monitor the gas concentration inside the flow channel and in the heating zone between ceramic flow channel and furnace heating rods, a system of gas tubes and magnetic valves was installed (see Fig. 3). This area can be ventilated with nitrogen to remove oxygen remaining from experiment preparations or in case of a leak during the experiment.

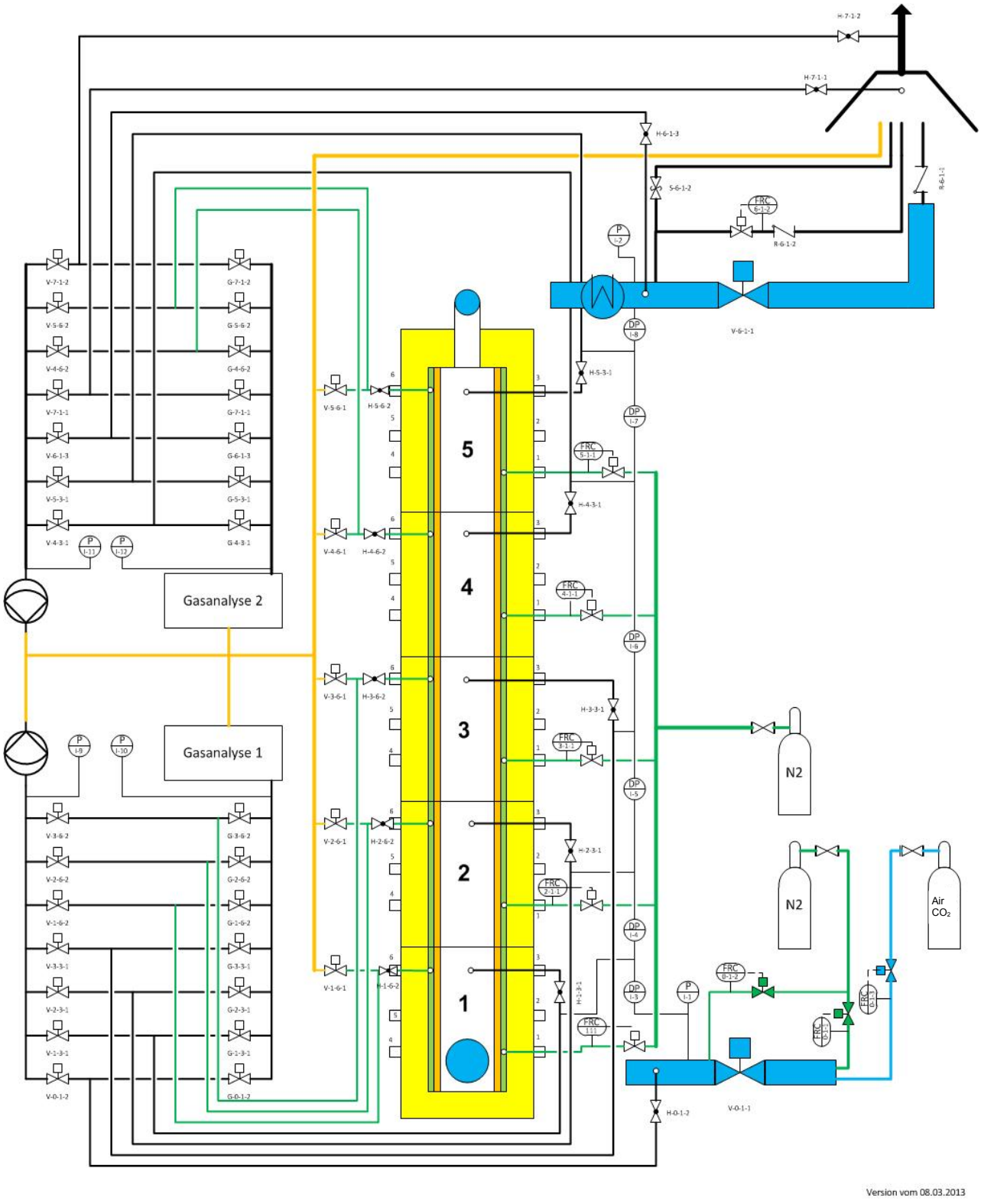

Figure 3: Schematics of gas analysis and gas flow in NACOK-II

Within the ARCHER programme in the NACOK II test facility the Boudouard reaction is investigated. Two experiments - complementary to each other – are defined as following:

In the first experiment a block type geometry with bore holes is studied, in the second experiment a pebble bed geometry. For comparability the surface of the graphite geometry in both experiments is similar.

The furnace heats the graphite up to 1100 - 1200°C with a constant nitrogen gas flow of 7 m^3_N/h to vent out remaining oxygen in the system. After having reached the desired temperature, the heating power of the furnace is kept at a constant level Are stable conditions reached at the desired temperature, the oxidation starts when a mixture of 21 Vol.-% CO_2 in Nitrogen enters the system with a flow rate of 7 m^3_N/h. Temperatures and gas concentration are measured during the oxidation.

Due to the high temperatures in an HTR, the exothermic primary reaction ($C + O_2 \rightarrow CO_2$) would occur immediately in case of an air ingress, producing the carbon dioxide for the secondary so called Boudouard reaction ($C + CO_2 \rightarrow 2CO$, endothermic). To study the effects of the Boudouard reaction separately, the oxidation gas is a mixture of CO_2 in nitrogen.

Table 3 shows the main data of the two experiments

Feature	First experiment	Second experiment
Number of graphite blocks	5 (10 half blocks: x.1 and x.2)	
Overall height of stacked graphite	2.0m	
Flow channel diameter	15.9mm	
Number of flow channels	82	
Graphite surface	8,192m²	8,200m²
Pebble diameter		60mm
Number of pebbles		725 (fits 29 layers)
Height of pebble-bed		1.5m
Type of graphite	NBG-18 (from SGL)	MLRF-1 (from SGL)
Ceramic geometry below graphite geometry	2 blocks, 100mm and 400mm height	1 block, 400mm height and 3 layers of pebbles
Graphite temperature at start	1185°C (Ox1), 1125°C (Ox2)	1175°C (Ox1) 1135°C (Ox2) 1095°C (Ox3)
Gas flow	7 Nm³/h	7 Nm³/h
Oxidation gas	21Vol.-% CO_2 in N_2	21Vol.-% CO_2 in N_2
Inert gas (heating and cooling phase)	Nitrogen	Nitrogen
Maximum heating rate	30°C/h	30°C/h
Heating power	170 kW	170 kW
Heating time to stable state before oxidation	49h	57h
Cooling down phase	>72h	>72h

Table 3: Comparison of the main parameters of both experiments

4.2 First experiment: Block Geometry

For the first experiment in NACOK, the following set up is given: Five graphite blocks (NBG-18) with boreholes are stacked inside the flow channel with an overall height of 2m. The furnace heats the graphite up to 1100 - 1200°C with a constant nitrogen gas flow of 7 m^3_N/h to vent out remaining oxygen in the system. After having reached stable conditions at the desired temperature, the oxidation starts when a mixture of 21 Vol.-% CO_2 in Nitrogen enters the system with a flow rate of 7 m^3_N/h. Temperatures and gas concentration are measured during the oxidation.

Due to the high temperatures in an HTR, the exothermic primary reaction ($C + O_2 \rightarrow CO_2$) would occur immediately in case of an air ingress, producing the carbon dioxide for the secondary so called Boudouard reaction ($C + CO_2 \rightarrow 2CO$, endothermic). To study the effects of the Boudouard reaction separately, the oxidation gas is a mixture of CO_2 in nitrogen. For stability reasons the experiment is stopped at a maximum weight loss of 25% at the lowest block.

The samples in the first experiment are block-shaped allowing for instrumentation with thermocouples and gas analytics. In this geometry it is possible to measure the gas concentration at different heights of the stacked blocks. An additional advantage of the block-shaped geometry over a pebble bed is the stability of the measurement points. Depending on the oxidation regime, there can be significant material loss due to oxidation. In a pebble bed, the set up may change and start to move downwards unpredictably with increasing material loss. For the block-type geometry the measurement points stay in place, even when significantly corroded.

Figure 4 shows a block before the instrumentation with thermocouples. 82 boreholes with a diameter of 15.9 mm and four slots for guiding the thermocouples in the corners are presented. The borehole geometry is defined by the base plate, so the gas can flow through the channels without further disturbances. For mechanical treatment, handling, and instrumentation, the 5 graphite blocks are cut in two parts (so-called block 1.1 and 1.2 from block 1, block 2.1 and 2.2 from block 2 etc.) and stacked above each other (figure 5).

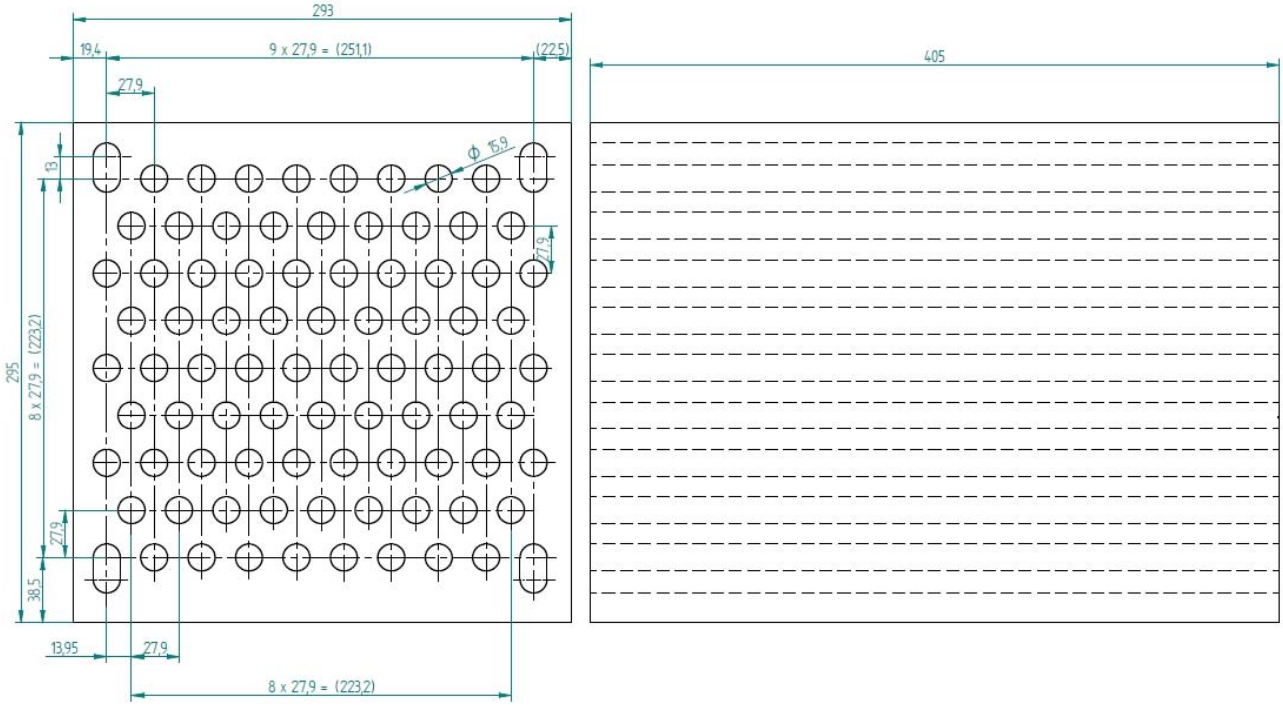

Figure 4: Geometry of sample shape (before cutting into two parts)

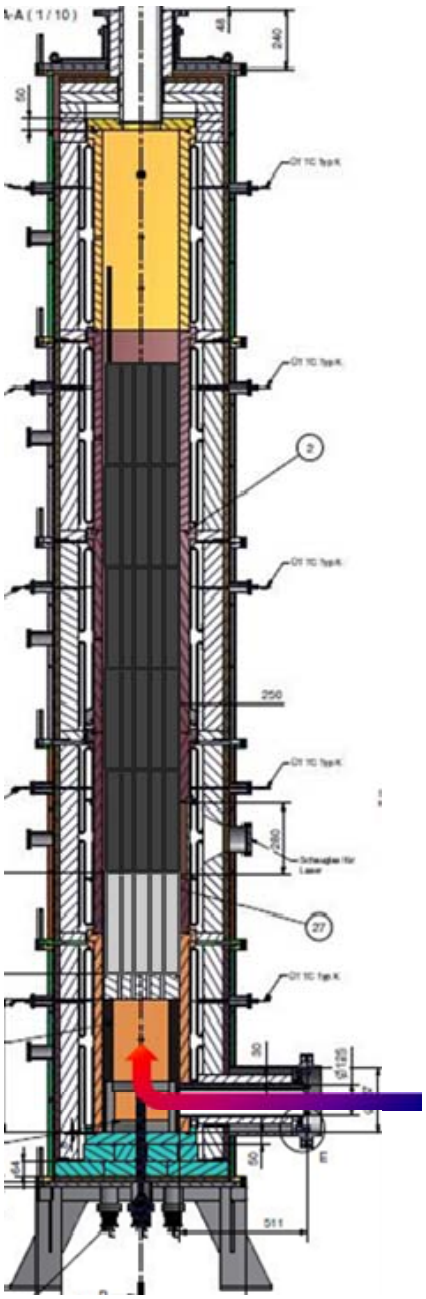

Figure 5: Schematic of sample set up and gas flow of NCAOK-II

The oxidation gas enters the flow channel and is heated up in the lower part. For a good investigation of the Boudouard reaction the temperature of all graphite blocks should be in the same range. To ensure this several pre-calculations with MGT were done (see chapter 5) and the results modified the build-up of the experiment as following: two additional ceramic blocks (total height of 500mm) are implemented in the geometry below the graphite blocks for heating of the oxidation gas before entering the graphite-zone. At 1100 - 1300°C, the Boudouard reaction is in the in-pore diffusion controlled regime. Due to the endothermic character of the investigated reaction, the oxidation should start at preferably high temperatures (1100 – 1200°C). The Boudouard reaction reduces the temperature in the graphite geometry. The relatively low flow rate of 7m³N/h is recommended to allow the Boudouard reaction to take place in the whole test section for a better investigation of this effect.

The oxidation progress in the experiment is monitored with a dense grid of thermocouples (at least 7 per block, up to 17 in the lower part) and with gas analytics to measure the gas concentration of oxygen, carbon dioxide, and carbon monoxide at the upper part of every block (1.2 – 5.2). Also in the ceramic channel above the graphite geometry as well as behind the gas cooler the gas concentration is analysed (oben, Austritt). By integrating the measured carbon dioxide and carbon monoxide, the mass loss of every block can be monitored during the experiment. The oxidation gas is stopped, when 25% mass loss

in the lowest block is reached, which would compromise the structural integrity. The oxidation must also be stopped, if the cooling rate in the ceramic part is higher than 30°C/h
For safety reasons, also the gas concentrations in the heating zone between ceramic flow channel and furnace-heating rods is measured (W1 – W5)

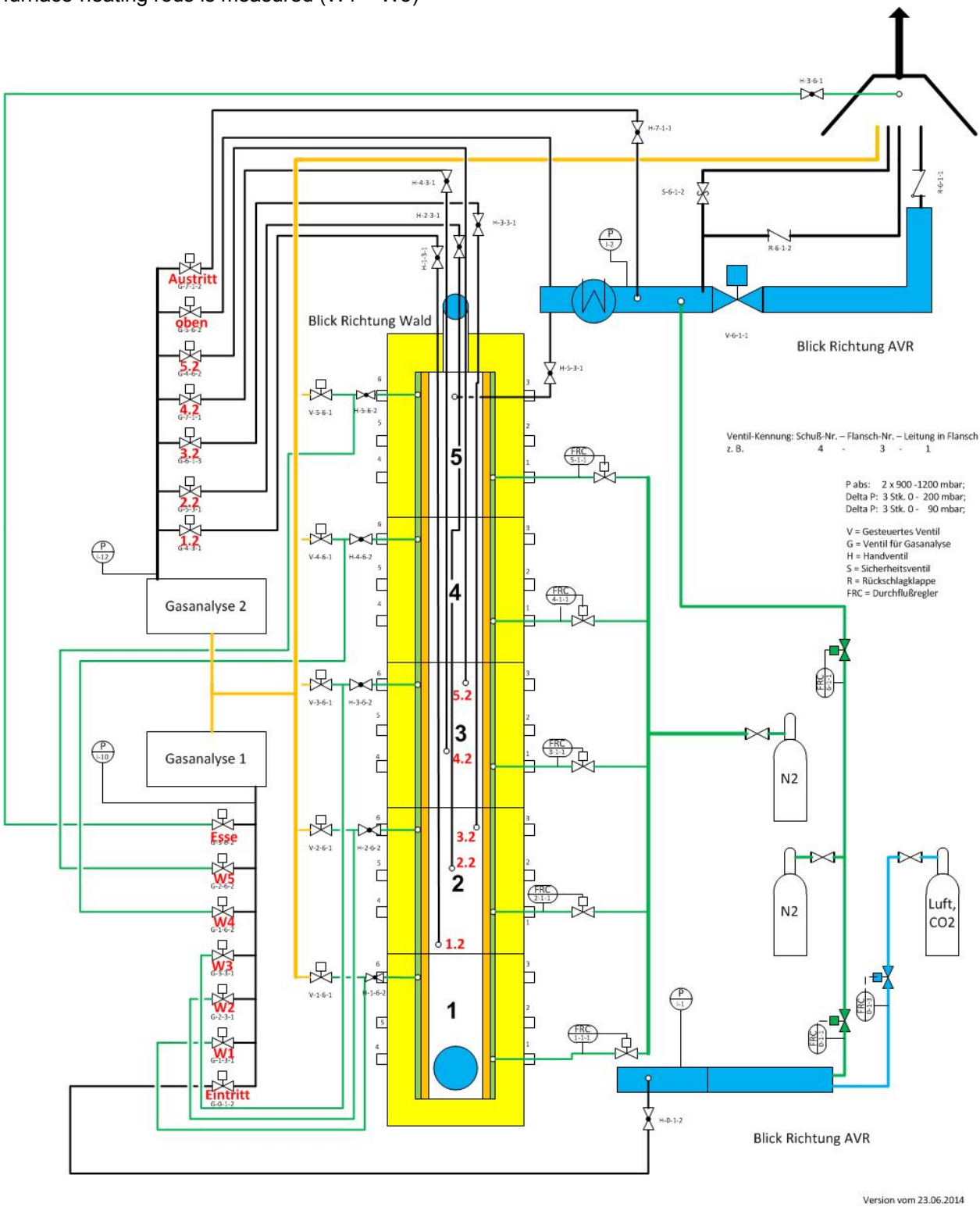

Figure 6: Schematic of the position of the gas analytics

Figures 7-12 provide an overview of the positions of the thermocouples in the different graphite blocks. The instrumentation of the lower graphite blocks (1.1 and 1.2) is denser than in the upper blocks to ensure a good knowledge of the temperature distribution. This is of special interest in the lower part, because there heated oxidation gas enters first and we assume the reaction to have the highest rate in this part.

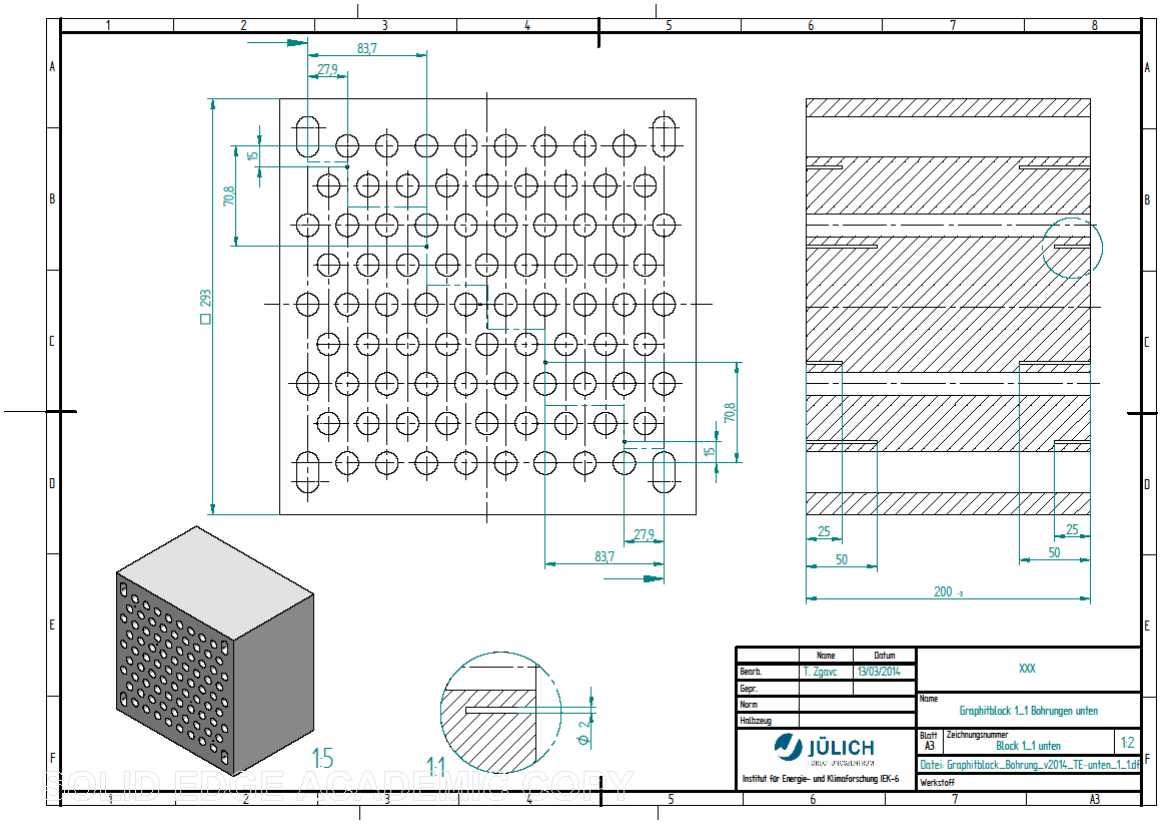

Figure 7: Position of thermocouples at the bottom of block1.1

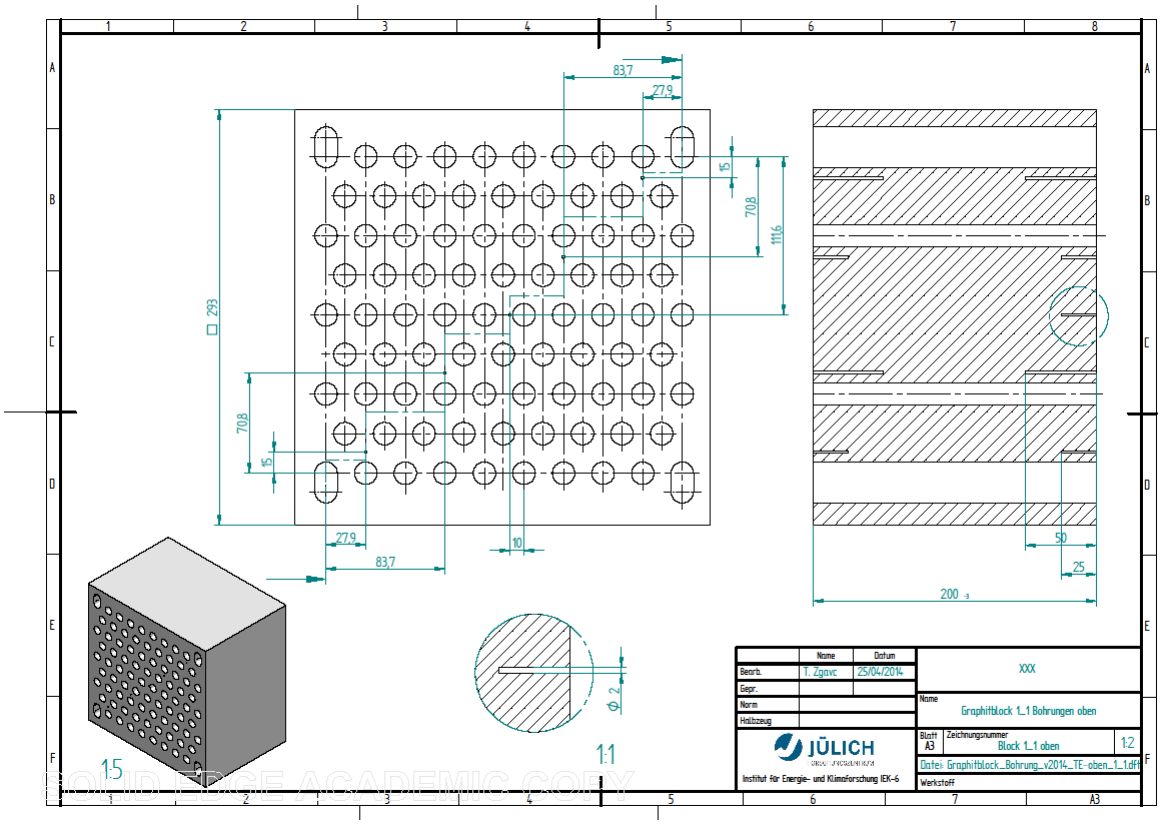

Figure 8: Position of thermocouples at the upper part of block 1.1

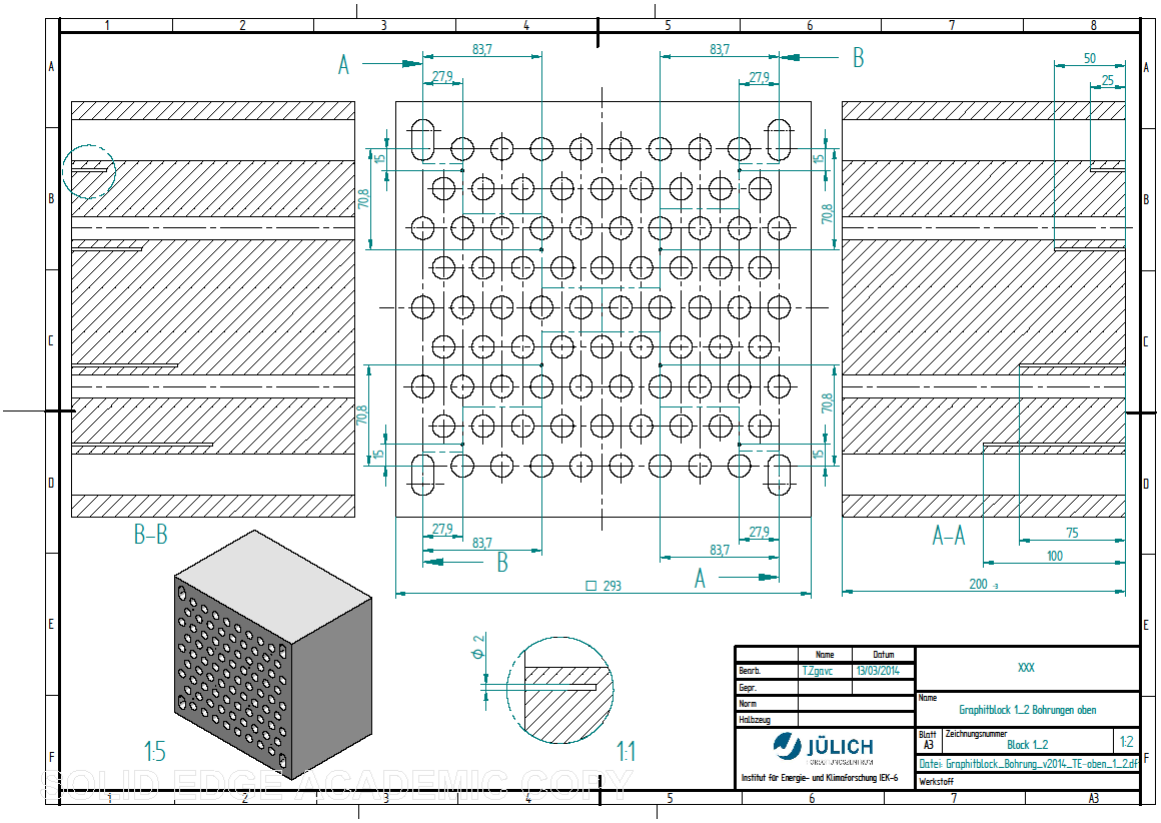

Figure 9: Position of thermocouples at top of block 1.2

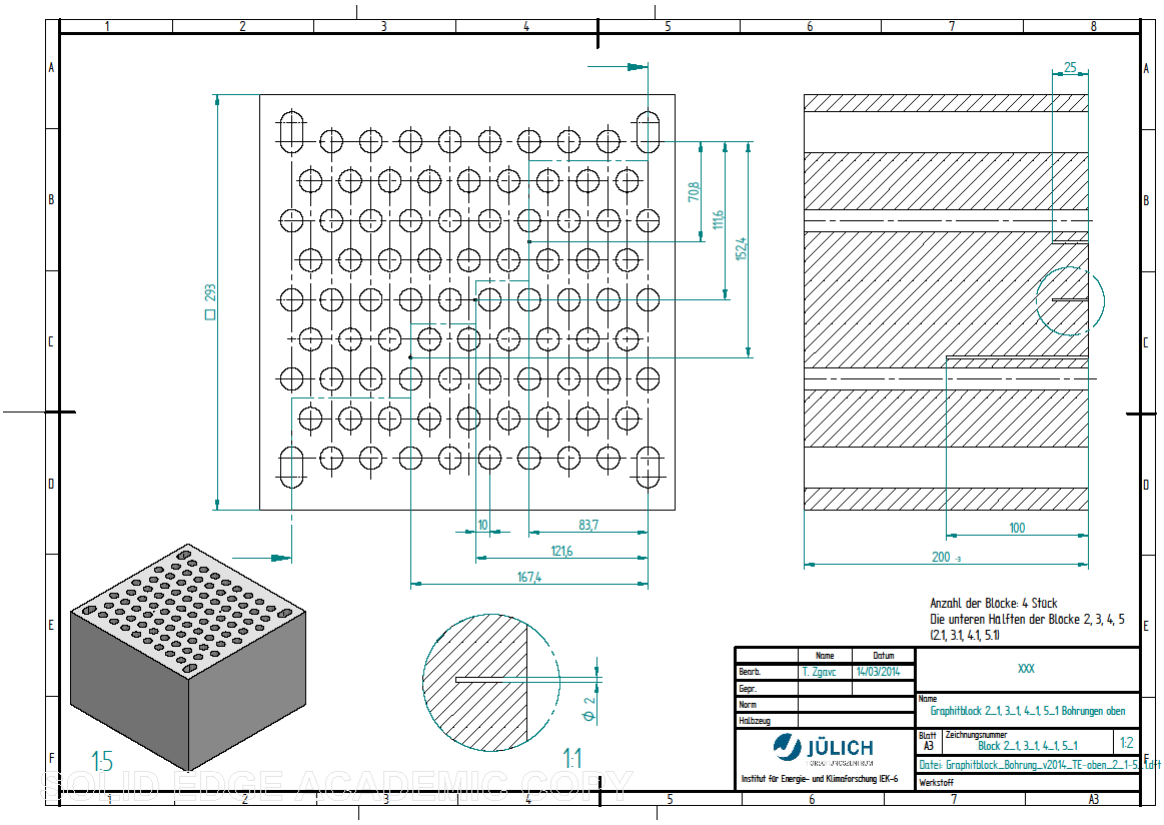

Figure 10: Position of thermocouples at top of block 2.1 – 5.1

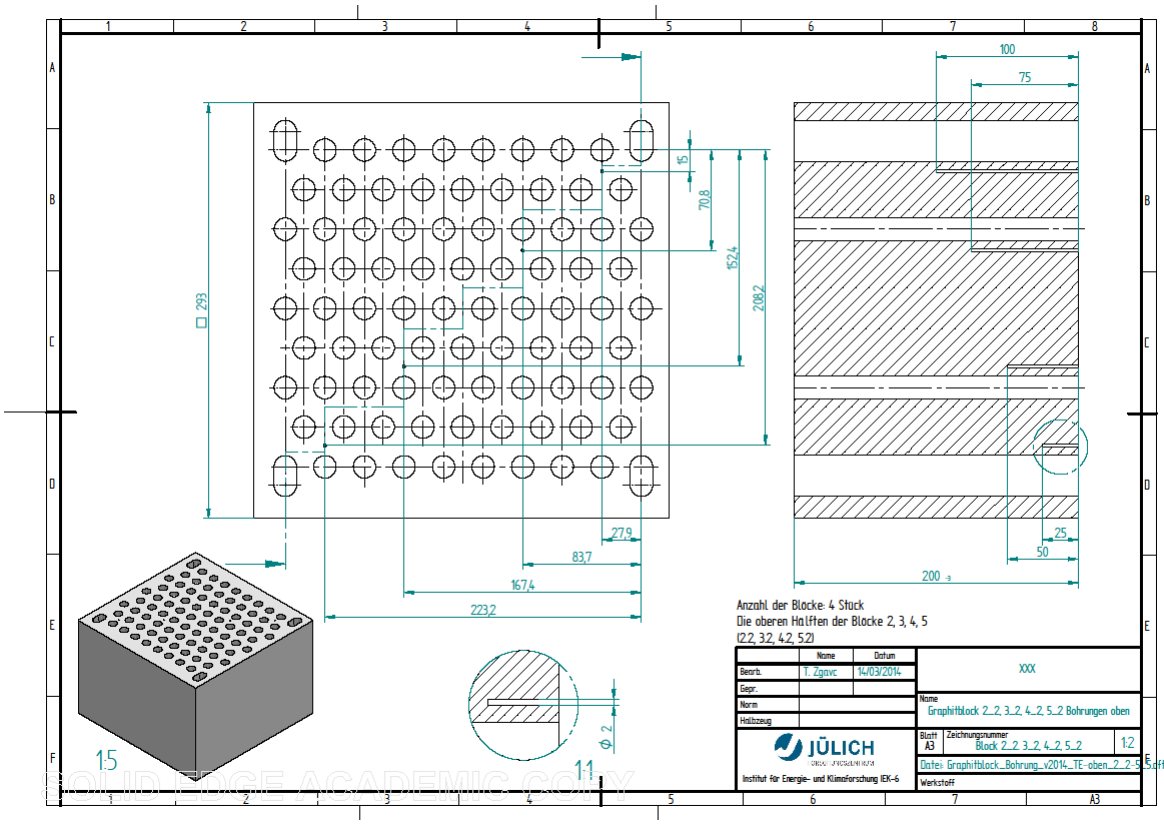

Figure 11: Position of thermocouples at top of block 2.2 – 5.2

One of the instrumented blocks is shown in figure 12. The thermocouples lay in different flutes, so that the graphite blocks can be stacked over each other without disturbances.

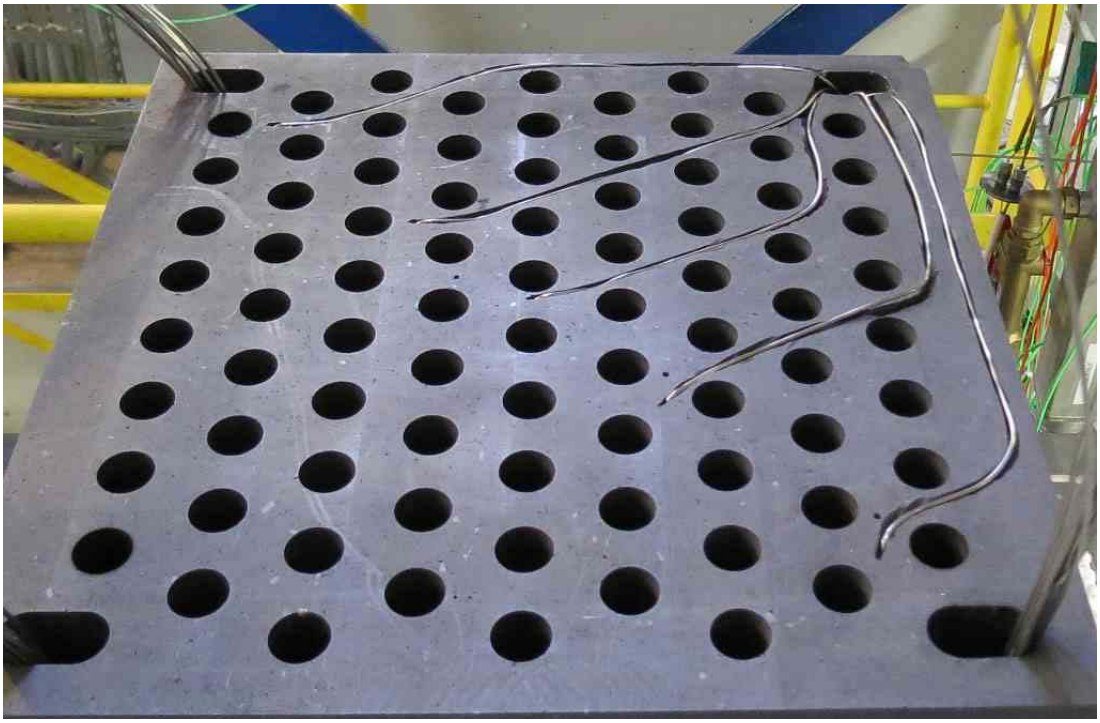

Figure 12: Assembly of thermocouples in one of the graphite blocks

Figure 13 shows the entire instrumentation of the graphite blocks over height and the denomination of each thermocouple.

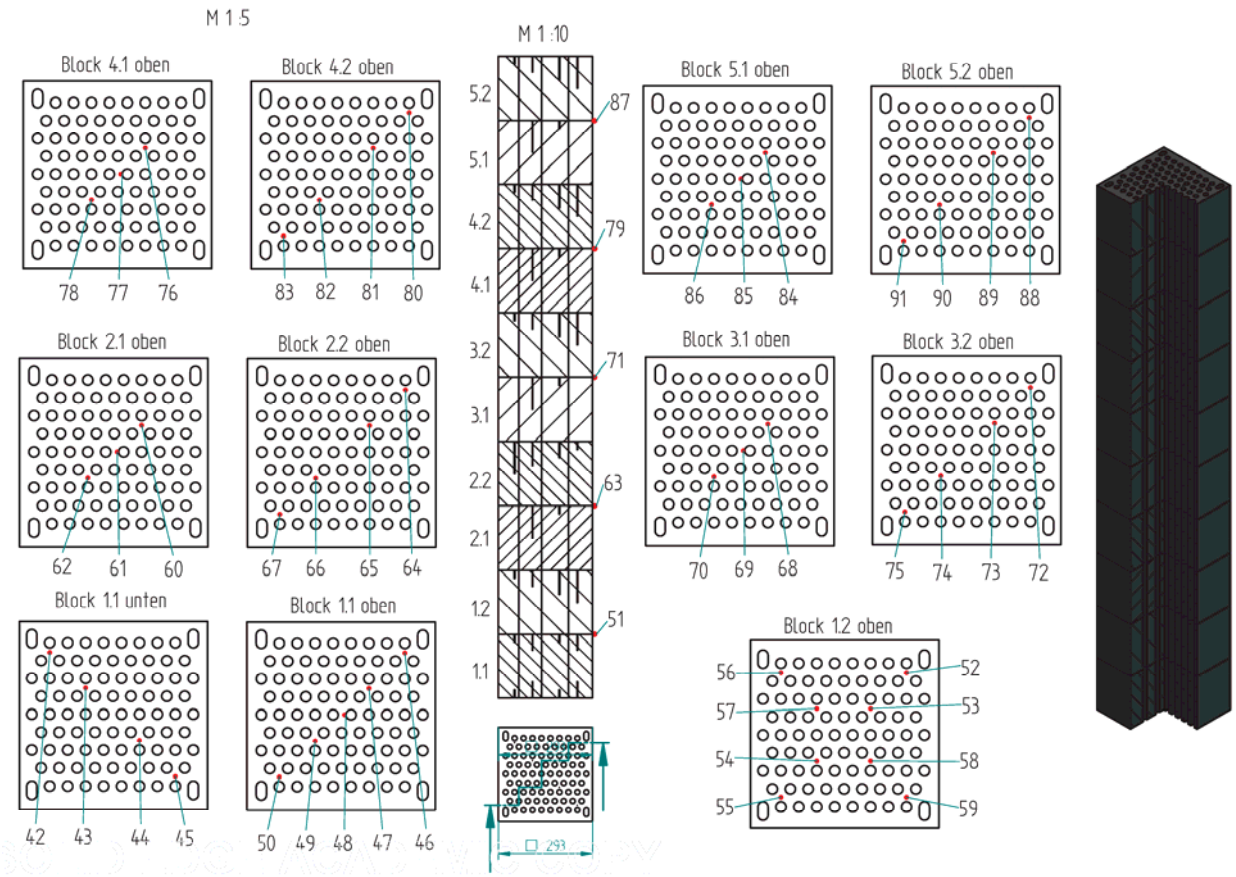

Figure 13: Instrumentation of the graphite blocks

In Table 4 are the planned as well as the experimentally reached features listed.

Feature	planned	first experiment
Number of graphite blocks	5 (10 half blocks: x.1 and x.2)	5 (10 half blocks: x.1 and x.2)
Type of graphite	NBG-18 (from SGL)	NBG-18 (from SGL)
Height of graphite block	0.4m (0,2m for half block)	0.4m (0,2m for half block)
Overall height of stacked graphite	2.0m	2.0m
Flow channel diameter	15.9mm	15.9mm
Number of flow channels	82	82
Graphite temperature at start	1100-1200°C	1185°C
Gas flow	7 Nm³/h	7 Nm³/h
Oxidation gas	21Vol.-% CO_2 in N_2	21Vol.-% CO_2 in N_2
Inert gas (heating and cooling phase)	Nitrogen	Nitrogen
Maximum heating rate	30°C/h	30°C/h
Heating power	170 kW	170 kW
Heating time to stable state before oxidation	48h	49h
Cooling down phase	72h	>72h

Table 4: Oxidation experiment main data

4.3 Second experiment: Pebble-Bed Geometry

The second experiment in NACOK II is complementary to the first one, but uses a pebble-bed geometry instead of the stacked blocks. For a good comparison between the two experiments the second experiment is done under the same boundary conditions as the first experiment (21Vol.-% CO_2 in nitrogen, 7m³N/h, 1100 - 1200°C). In addition to the direct comparison between both geometries, the set of these two NACOK experiments provides data for the Boudouard reaction, which is less well known compared to the primary corrosion reaction.
Based on the results of the first experiment, the stability of the graphite after the Boudouard reaction is quite good. The stability of the pebble-bed geometry should also be assured if the reaction takes place in the in-pore diffusion regime and if the duration of the oxidation part of the experiment is similar to the first experiment.

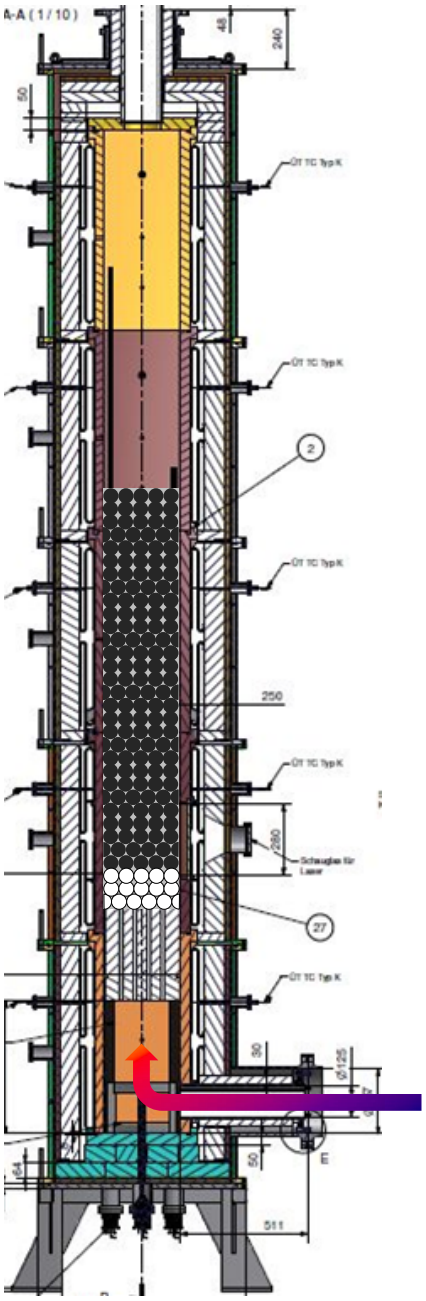

Figure 14: Schematic of the sample set up with pebble-bed geometry

Analoge to the first experiment the oxidation gas enters the flow channel and is heated up in the lower part. To ensure a comparable temperature distribution within the graphite pebble bed, one ceramic block (400mm height) and 3 layers of ceramic pebbles (d=60mm) are implemented below the graphite geometry. The additional ceramic pebbles should minimise effects on the oxidation behaviour of the first graphite pebble layer due to flow effects (different flow in the transition between block and pebble-bed and within a pebble-bed).

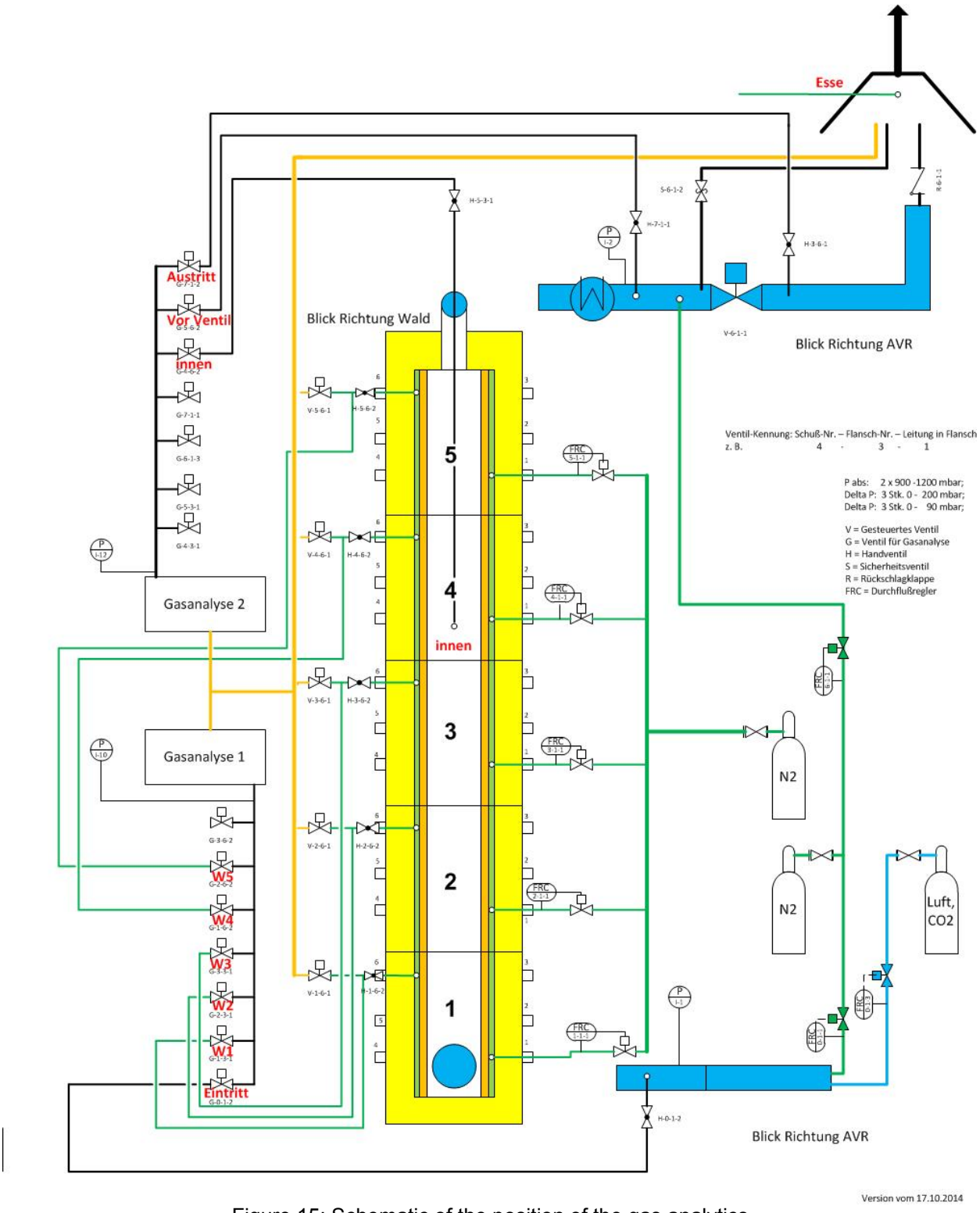

Figure 15: Schematic of the position of the gas analytics

The oxidation progress in the experiment is monitored with a dense grid of thermocouples and with gas analytics. As shown in figure 14 the gas concentration of oxygen, carbon dioxide and carbon monoxide is measured for three measurement points: above the pebble bed (innen), behind the gas cooler (Vor Ventil) and after dilution with additional Nitrogen (Austritt). The dilution keeps the CO-concentration under the inflammable limit and is installed for safety reasons. Concentration measurement within the pebble-bed geometry is not possible. By integrating the measured carbon dioxide and carbon monoxide, the mass loss in the geometry can be monitored during the experiment. The oxidation gas is stopped after a comparable oxidation rate or time of oxidation. It must also be stopped if the cooling-rate in the ceramic part is higher than 30°C/h.
For safety reasons, also the gas concentrations in the heating zone between ceramic flow channel and furnace heating rods is measured (W1 – W5).

Figure 16 shows 8 layers of the pebble-bed geometry. The first layer is 5x5 spheres, like the third, fifth, and every other odd layer of the pebble-bed. In the second layer are 4x5 intact spheres, and 5 spheres cut into half, laying on two sides. Also the fourth layer are 4x5 intact spheres and 5 spheres cut into half, but now with a 180° rotation with respect to the second layer. The sixth layer is the same like the second, the eighth layer is like the fourth and so on. The total height of the pebble-bed is 29 layers (1.5m). With this well-defined geometry it is also possible to calculate the filling factor.

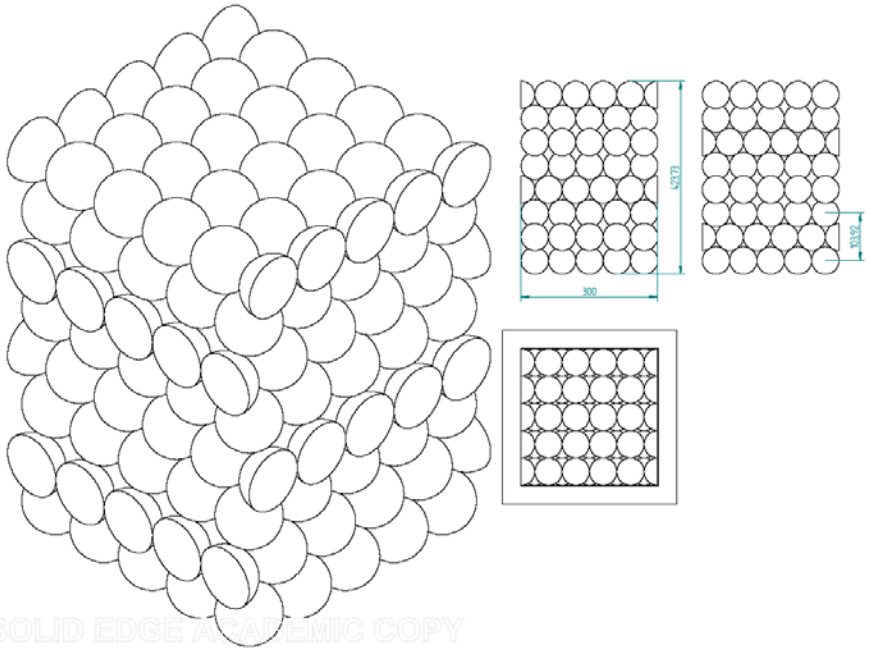

Figure 16: Geometry of the pebble bed

There are more thermocouples in the lower part of the pebble-bed to get a good knowledge of the temperature distribution in the geometry (Figure 17). The lower part is of special interest, because here enters the heated gas the graphite structure and the oxidation takes place with higher reaction rates. As there is no possibility to measure the gas concentration within the pebble-bed, the temperature drop in the geometry gives an impression of the progress in oxidation for the different layers.

Additional thermocouples are positioned in three different heights in the ceramic block and below the ceramic block. The temperature between ceramic block and the ceramic channel (wall temperature) is also measured.

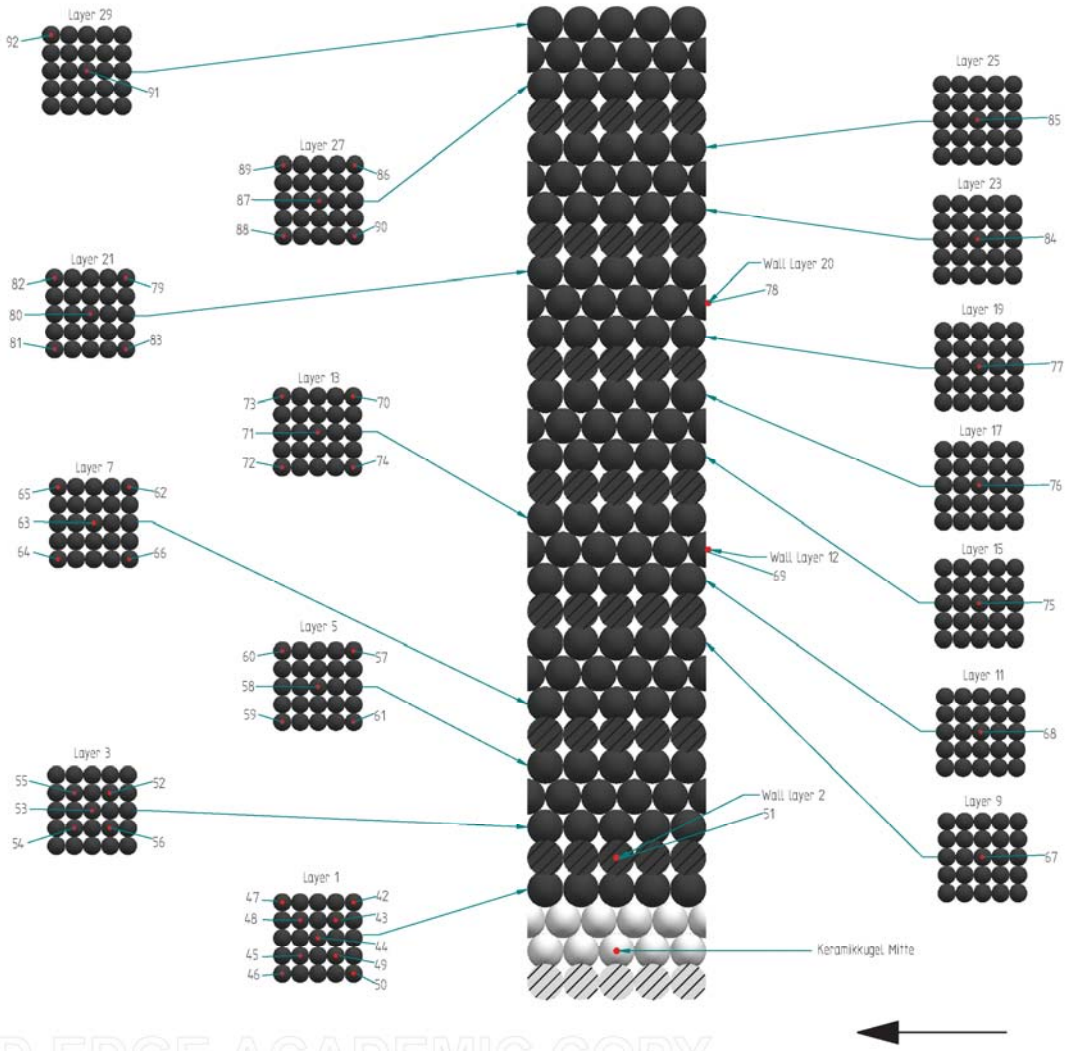

Figure 17: Instrumentation of the pebble bed

In Table 5 are the planned as well as the experimentally reached features listed.

Feature	planned	first experiment
Number of graphite pebbles	725	725
Pebble diameter	60mm	60mm
Type of graphite	MLRF-1 (from SGL)	MLRF-1 (from SGL)
Height of pebble-bed	1,5m	1,5m
Graphite temperature at start	1100-1200°C	1175°C
Gas flow	7 Nm³/h	7 Nm³/h
Oxidation gas	21Vol.-% CO_2 in N_2	21Vol.-% CO_2 in N_2
Inert gas (heating and cooling phase)	Nitrogen	Nitrogen
Maximum heating rate	30°C/h	30°C/h
Heating power	170 kW	170 kW
Heating time to stable state before oxidation	48h	57h
Cooling down phase	72h	>72h

Table 5: Oxidation experiment main data

5 Pre-Calculations with MGT-3D

Some experiments in the NACOK II test facility were previously performed for a better understanding of the system and their control to be carried out in preparation for the oxidation experiments. The first preliminary experiments were carried out in the empty NACOK II test facility, which means there was neither the inner ceramic channel nor any graphite geometry inside. These preliminary experiments were also used in order to create various two- and three-dimensional models in MGT. The comparison with the experimental data should then take the decision in which model the oxidation calculations should later be performed.

5.1 Calculations for heating-up experiments

As mentioned in the introduction to this section, the first preliminary experiments are designed to understand the control of the test facility better because there were some changes in the persons responsible for the facility before. The focus of this heating up experiments lay in the change from a temperature towards a power-controlled heating and the question how long does it take until the system is in steady state condition.

There are a total of three preliminary experiments for heating up. For all experiments, the performance was identical in design. First there is a power controlled heating up until a predefined temperature (1000 °C) is reached. From this time point a constant heating power has to be hold and the system reverts into a steady state behavior. The temperatures within the heating channel are measured by one thermocouple per heating element and one thermocouple in the outlet during the experiment.

The heating phase at a level of 1000 °C during the first experiment takes 4 hours at a mass flow rate of 5 m^3 /h of air. Five water cooling zones along the furnace were perfused with 4 l/min, and the bend heat exchanger with 18l/min. Following the heating process, the heating capacities of the five furnace segments are repeatedly adjusted to reach a steady state at a given target temperature over three hours. After this there is a constant heating power in zones 1 to 5. However, after further 2.5 hours experimental time the temperature are still rising, no steady state conditions are reached and the experiment is terminated at this point in time. For the second experiment additional thermocouples are installed in the water cooling system and the screw connections of thermocouples in the heating zones are now soldered and not glued as before. After heating up to 1000°C and adjusting the heating power 6.5 hours are awaited at constant power. But there is again no steady state behavior (rising temperatures with 3-4 K/h) and the experiment stops. One more experiment is done with one more thermocouple in the insulation at the top of the NACOK II to check the heating power in the 5th heating zone. All other boundary conditions are the same as before.

Fig. 18 shows the “bathtub curve” of the temperature behavior. This means that the temperatures drop by reducing the heating power and then turn into an apparent steady state. However, looking at a larger time interval, it is found that the temperatures gradually rise again. After 2.5 hours they are still not constant.

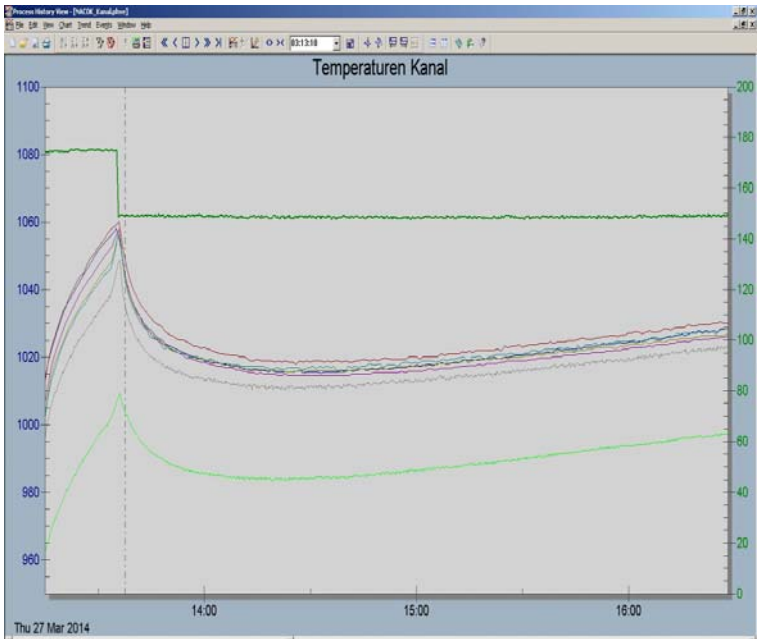

Figure 18: “bath tube curve” of temperatures during heating experiment

Based on these pre-experiments a detailed 2D model of MGT-3D was developed with 16 meshes in r direction and 64 meshes in z direction (see Fig. 19). Due to the r-z-geometry the gas inlet and outlet is in a central position and the circular area matches to the quadratic cross sectional area. The model has seven meshes in the core region. The two windows for optical measurements are not considered. If possible heat loss of the windows be taken into account in the model, this can be dealt with by negative external heat sources in the mesh at appropriate points. The different colors in the model represent different material regions of the test facility. The most important material regions are

- empty channel (yellow)
- heating zone (red)
- insulation (green)
- water cooling (blue)
- meshes with defined boundary temperatures (brown)

In the lower core region there are finer axial meshes as in the rest of the model due to the focus on the area during the oxidation experiments later on. Values for heat conductivities and heat capacities of the different materials are given by the manufacturers of these materials. Also, when simulating the heating process the prescribed boundary temperatures and mass flow set in the experiment were used.

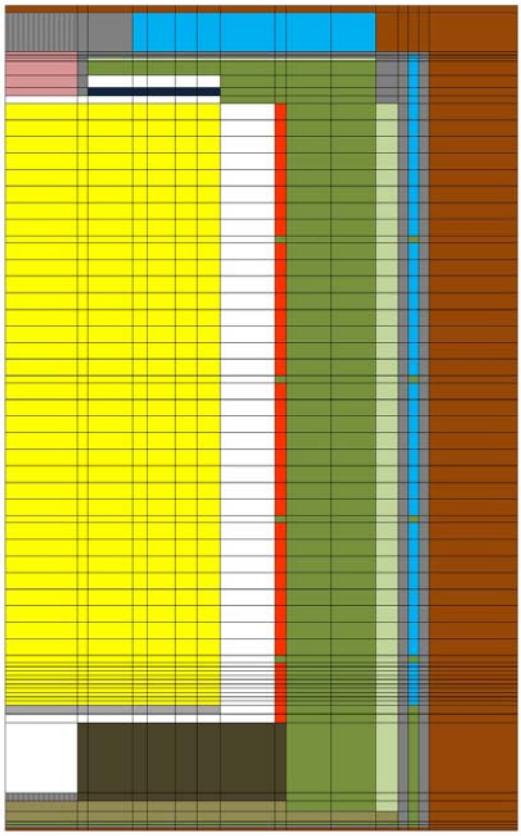

Figure 19: Detailed 2D-model for MGT calculation

With the model described above the quasi steady state phase of the second pre-experiment was simulated (calculation time: 945 CPUs) and the result is shown in Fig. 20. For a better understanding of the mesh grid a picture of the test facility is integrated into the graph to explain the position of the r- and z-axes.

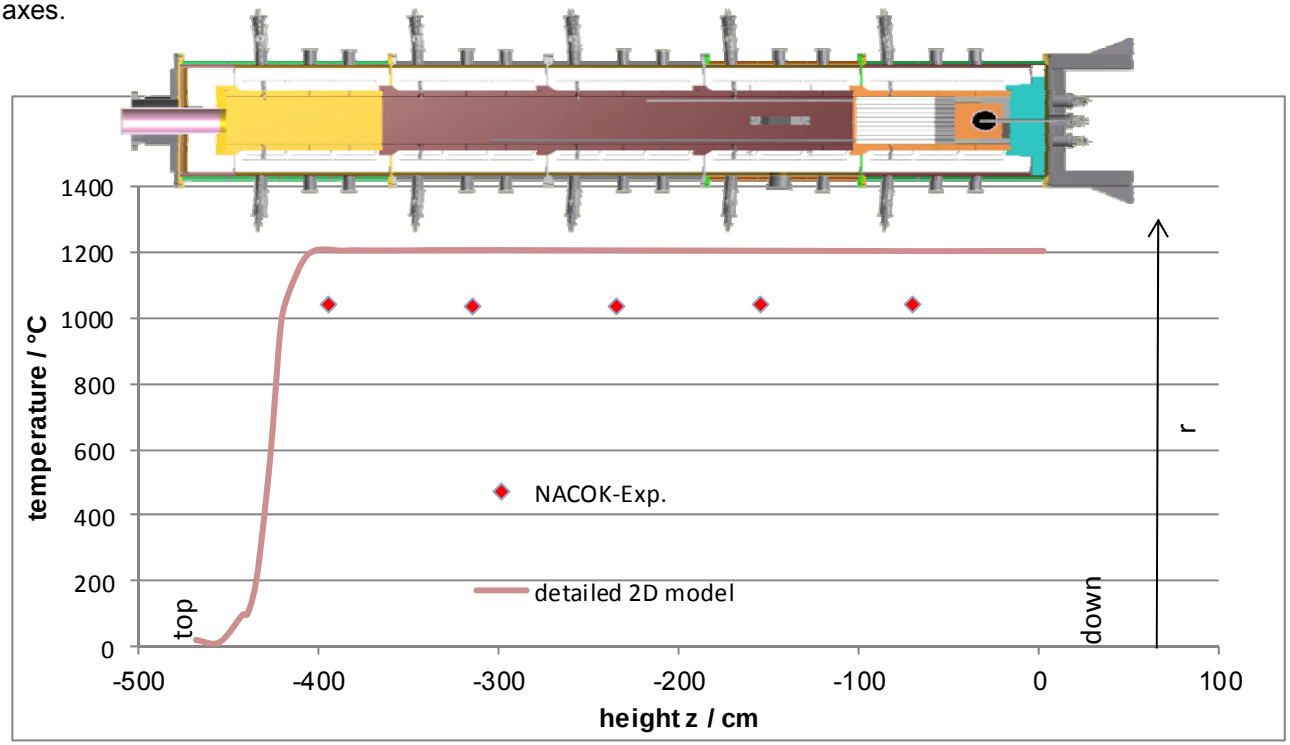

Figure 20: Comparison between calculated and experimental temperatures

As it is shown there is a deviation in the values of the temperatures between experiment and simulation of about 150°C – 180°C. A first idea to improve the simulation model is to select not the cross-sectional area of the test object, but the scale as the basis for calculating the radii in the model. The result of this adaption is shown in Fig. 21 and presents a better agreement with the experimental data.

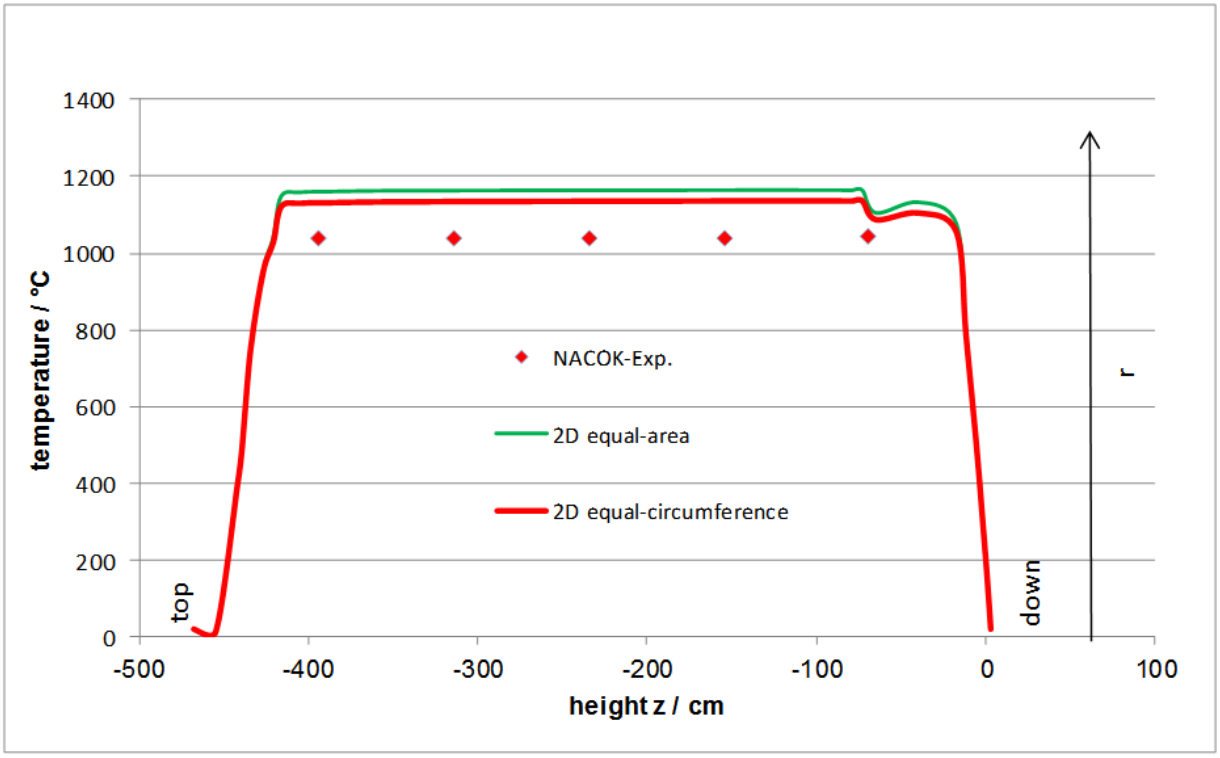

Figure 21: Temperature comparison between experimental data and different 2D models

The next step is to develop a 3D model based on this detailed 2D model. To listen to the square plan of the test facility as realistic as possible, it makes sense to choose a pseudo-XYZ geometry. The 3D model was designed in that way that the windows are taken into account and the lateral gas inlet is considered. The numbers of meshes in x-, y- and z-direction result from the different materials used in NACOK II. Therefore, the following dimensions for the grid resulted

- 14 meshes in radial direction
- 40 meshes in axial direction
- 14 meshes in azimuthal direction.

The innermost radial mesh has a radius of 50.000 cm in order to realize the pseudo-xyz geometry. The idea of a pseudo-xyz-geometry is given in Fig. 22. The very large radius of the innermost radial mesh causes the neighbor mesh form outward to be approximately rectangular.

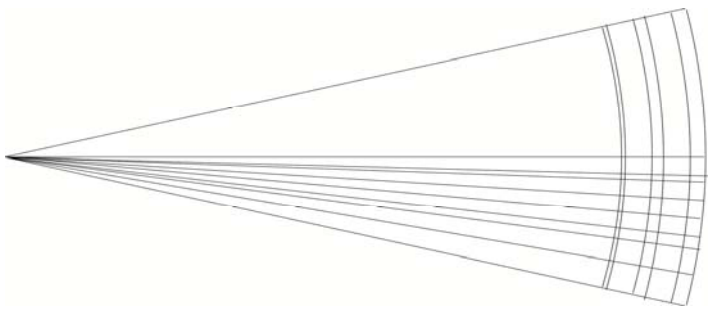

Figure 22: Pseudo-XYZ-grid with a very large innermost radial mesh

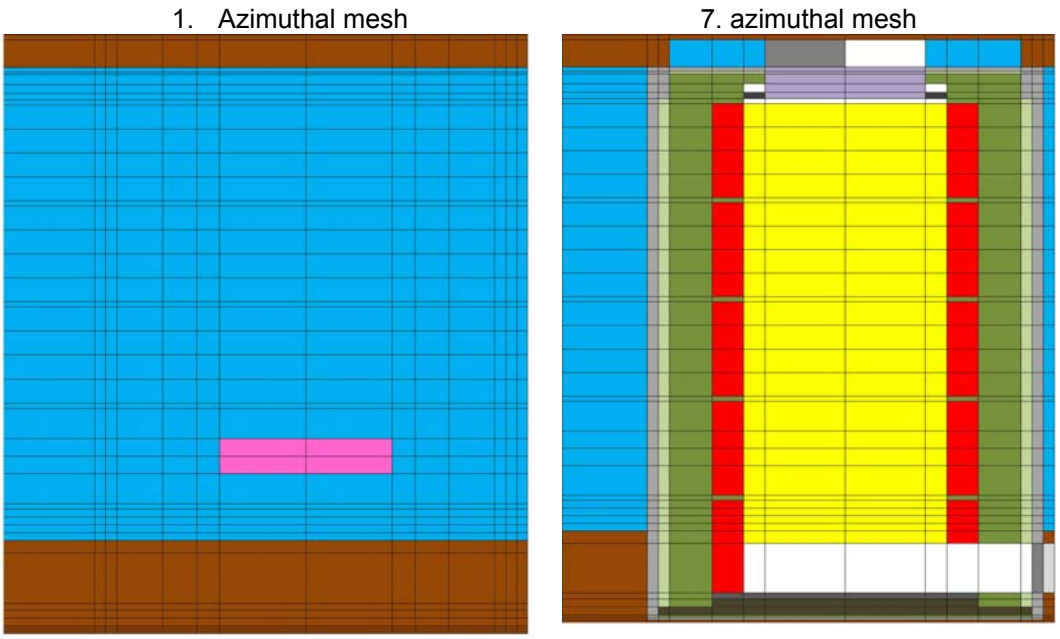

Figure 23: 3D mesh grid in pseudo-xyz geometry

The results of the calculation based on this 3D mesh grid are shown in Fig.24. A very good agreement between the experimental data and the simulation are taken place.

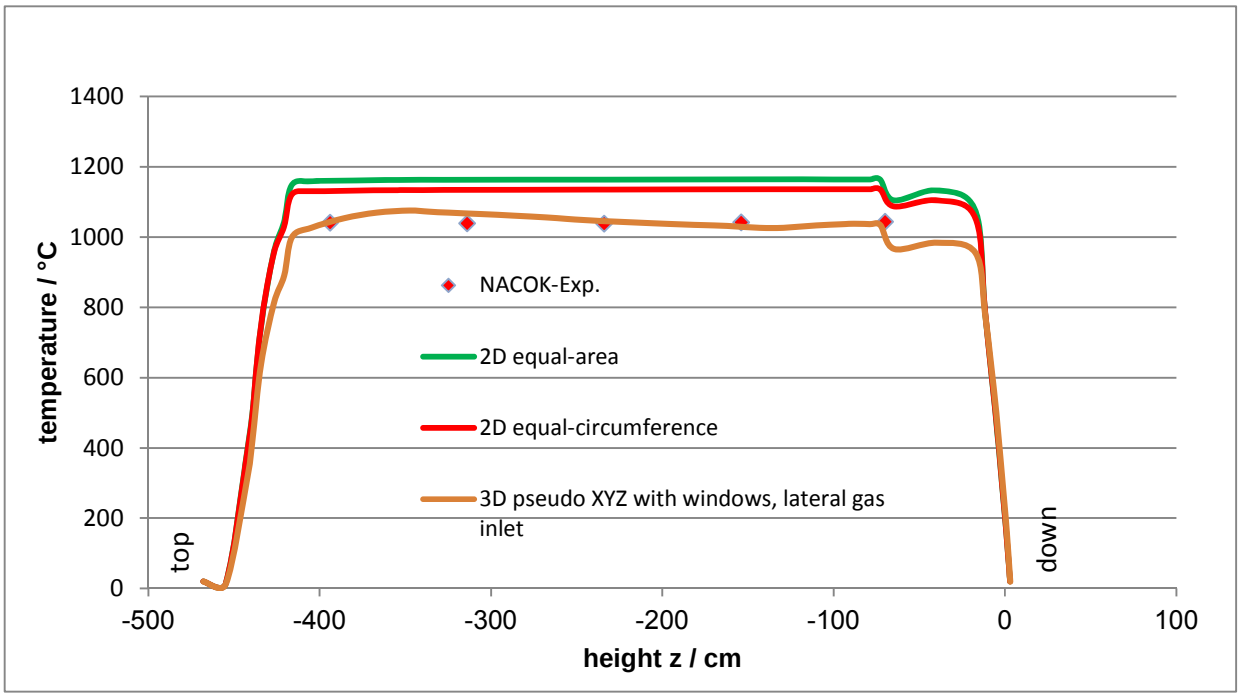

Figure 24: Experimental data and simulation results with different MGT-3D models

Based on these simulation results the decision was made to applicate the 3D model with pseudo xyz-geometry for the pre- and post-calculations in view of the oxidation experiments.

5.2 Pre-calculations for oxidation experiments

To prepare the pre-calculations of the oxidation, the 2D model (r-z-geometry) and the 3D model were used with pseudo-xyz geometry. During the heating phase the test stand is forced to flow through with 100% nitrogen realized with different mass flows. The target temperature for the start point of the oxidation phase is 1100 °C. If the target temperature is reached, 100% nitrogen is converted to a gas mixture (79% nitrogen, 21% CO_2) and the graphite oxidation starts. The phase of the chemical reaction is to be continued for 30 hours. These are the boundary conditions for the MGT-3D pre-calculations.

The first calculations were performed with the 2D model. At the simplified 2D model will be first tested whether MGT drives the internal program modules for the treatment of chemical reactions correctly. In addition, it is an advantage that the calculation time for a two-dimensional mesh is shorter than that of the 3D model. This saves a lot of time in an extensive test phase. Fig. 25 shows the mesh grid used in MGT. The most important material regions are

- 10 graphite blocks (NBG 18) with a height of 20 cm (dark grey)
- One ceramic block below the graphite blocks (light grey)
- Ceramic furnace (light brown)
- Heating zone (red)
- Insulation (green)
- Water cooling (blue)
- Cavities (white)

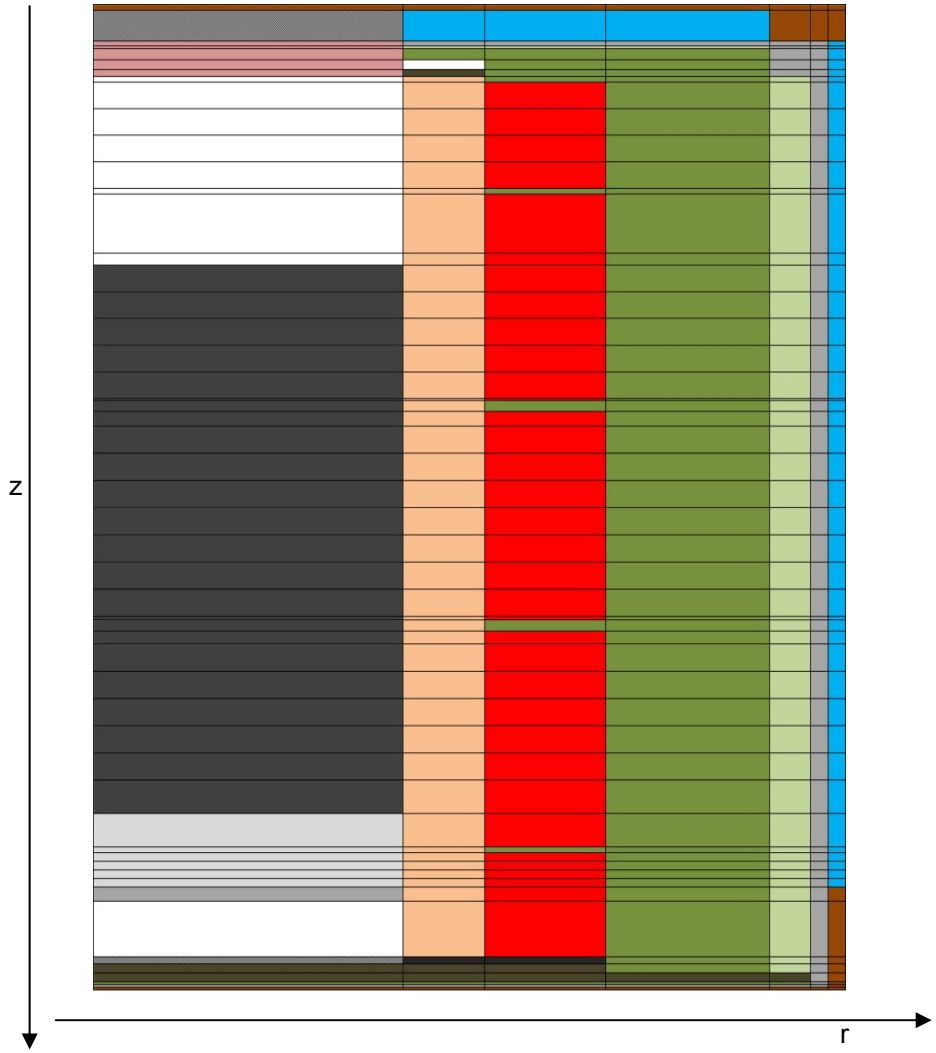

Figure 25: 2D MGT model (r-z-geometry)

The first calculations are used to determine which mass flow for the experiment fits best. For this reason different mass flows are simulated (2, 4, 5, 6, 7, 8, 10 or 15 m^3/h) over a simulation time of 30 hours.

The result of this study is presented in Fig. 26. In this figure the temperature deviations of the first and 5th big block are shown together with the calculated over all graphite burn up. Since the Boudouard reaction is an endothermic chemical reaction in the blocks a decrease in temperature will be observed. It will be appreciated that the decreases in the lowermost block is stronger than in the uppermost blocks. In addition, it can be deduced from the data that the lower block with a mass flow rate of approximately 4m^3/h, the largest decrease in temperature provides, whereas for the block at the top a mass flow rate of 8 m^3/h, the highest temperature difference indicates. Taking the two aspects into account, it can be assumed that an average mass flow rate of approximately 7m^3/h is the appropriate choice.

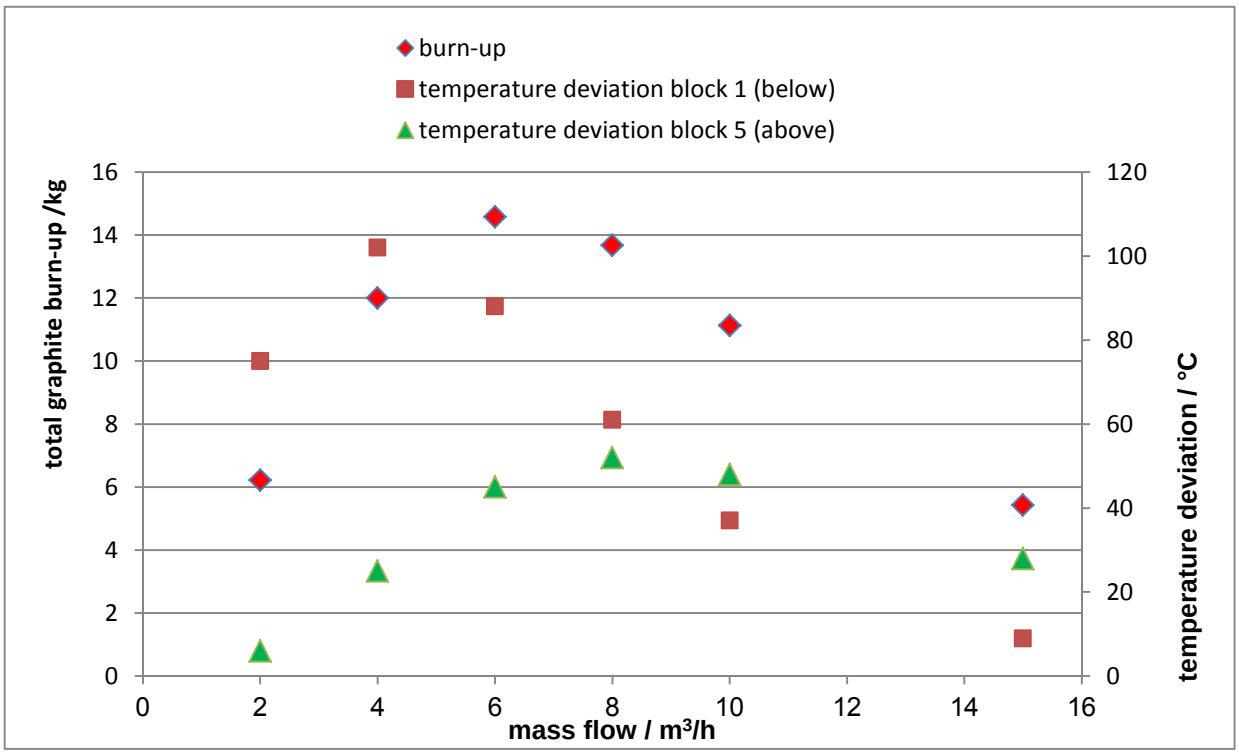

Figure 26: Different mass flows and temperature deviations

For this decision, all further MGT-3D calculations are made with a mass flow of 7 m^3/h. In the next figure (Fig. 27) the graphite burn-up for all five big graphite blocks (10 small blocks 1.1 – 5.2) is given. A simulation time of about 30 hours leads to an overall graphite burn-up value of about 14 kg.

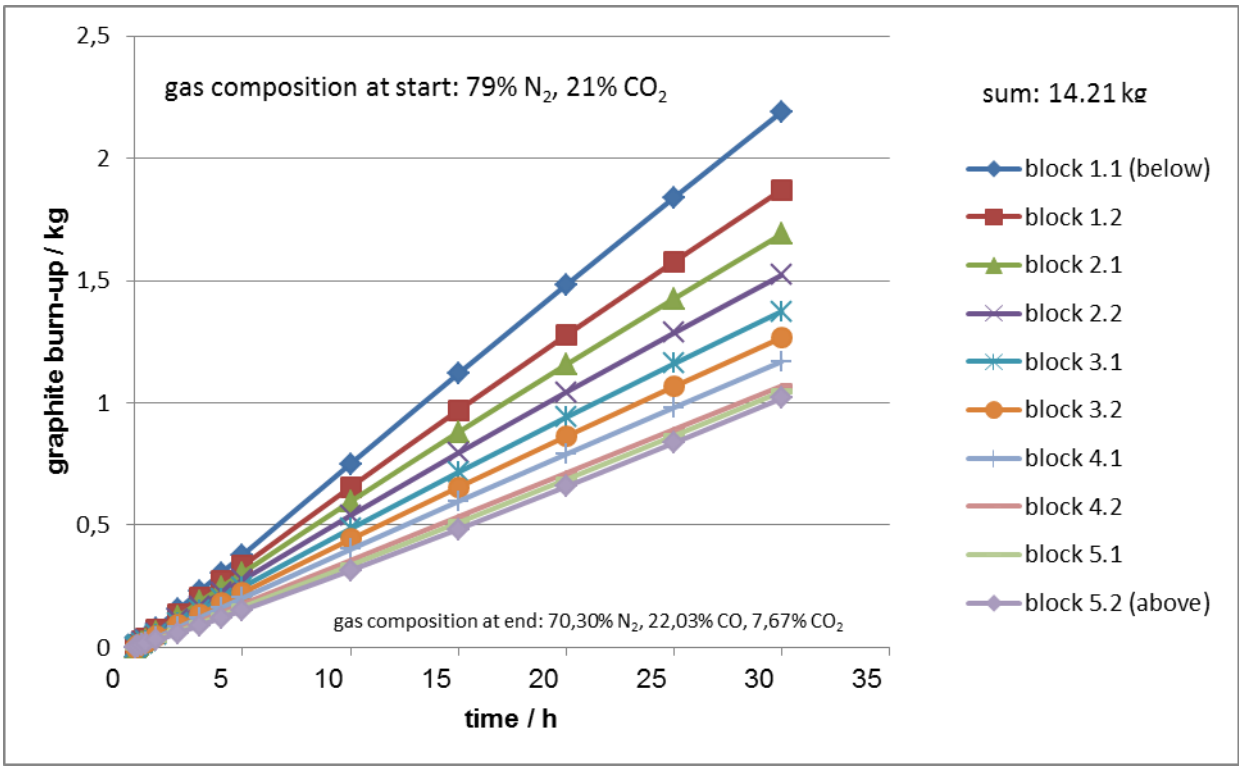

Figure 27: Graphite burn-up for all graphite blocks during the simulation (30 hours)

The gas composition at the end of the transient calculated by MGT is 70,30% N_2, 22,03% CO and 7,67% CO_2. These values show that there is no complete reaction of the CO_2. Fig. 28 represents the decrease in temperatures during the simulation due to the endothermic reaction. It is easily seen, that the loss of temperatures depends on the graphite height. The deeper the block is located, the higher is the temperature decrease in the graphite blocks.

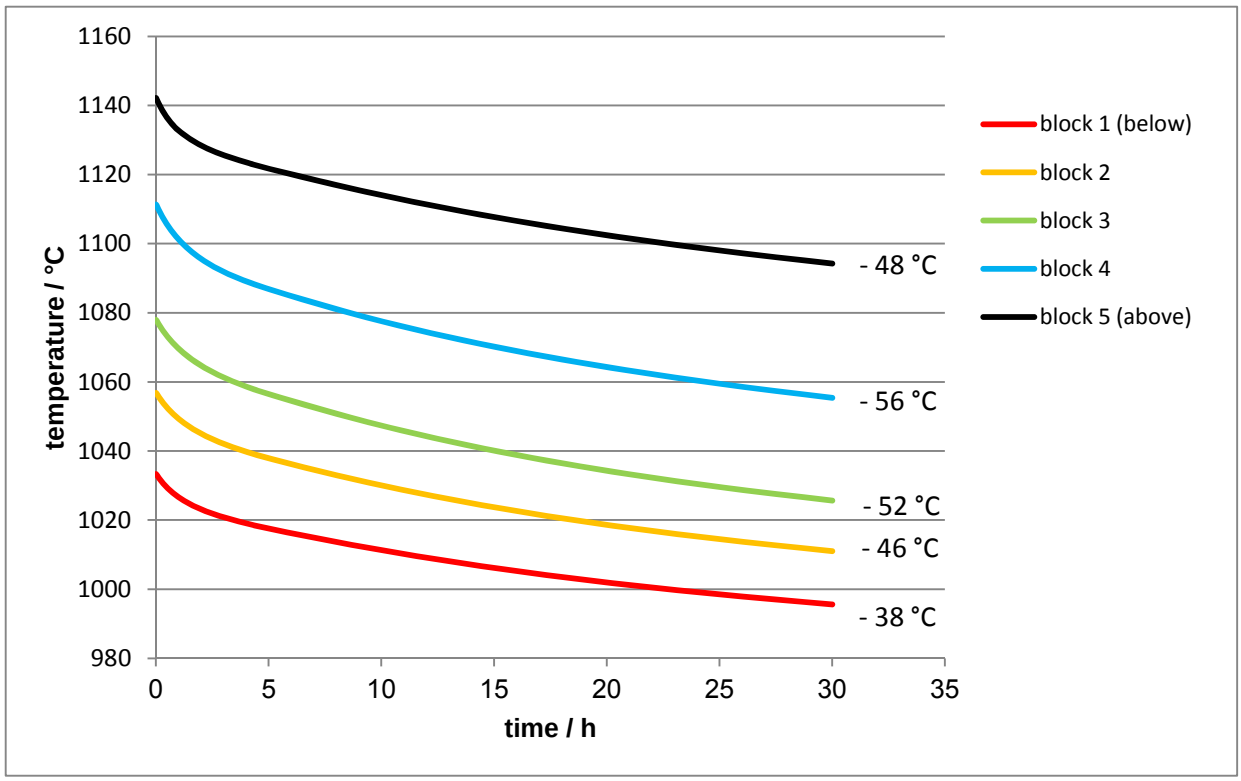

Figure 28: Decreasing temperatures according to the endothermic Boudouard reaction

Now the same calculations are made with the detailed 3D model (pseudo xyz-geometry) as presented in the section before. Two small adaptions are made in this mesh grid. The number of axial meshes has been increased in the region of the lower graphite blocks, since there is the sensitive area in terms of chemical reaction. Moreover, the two windows for optical measurements from the model have been removed, since they are not used in the experiment. The boundary conditions are the same as in the calculations with the 2D model (simulation time of 30 hours, mass flow about 7m^3/h). Figure 29 shows the Fig. 27 corresponding results for the 3D model with respect to the graphite burn-up. Comparing the figures for the entire graphite burn-up, it is found that only slightly differences are arrived (2D model: 14 kg, 3D model: 12 kg). Considering the temperature profiles for the 3D model, this results in a significantly staggered development with increasing height in the graphite blocks (at the bottom 70-80°C, at the top about 30°C deviations). In summary it can be stated - based on the results of the pre-invoicing - that a starting temperature of about 1100°C and a mass flow of approximately 7m^3/h are sufficient to observe the desired reaction. In addition it is expected to see a significant decrease in temperature during the experiment.

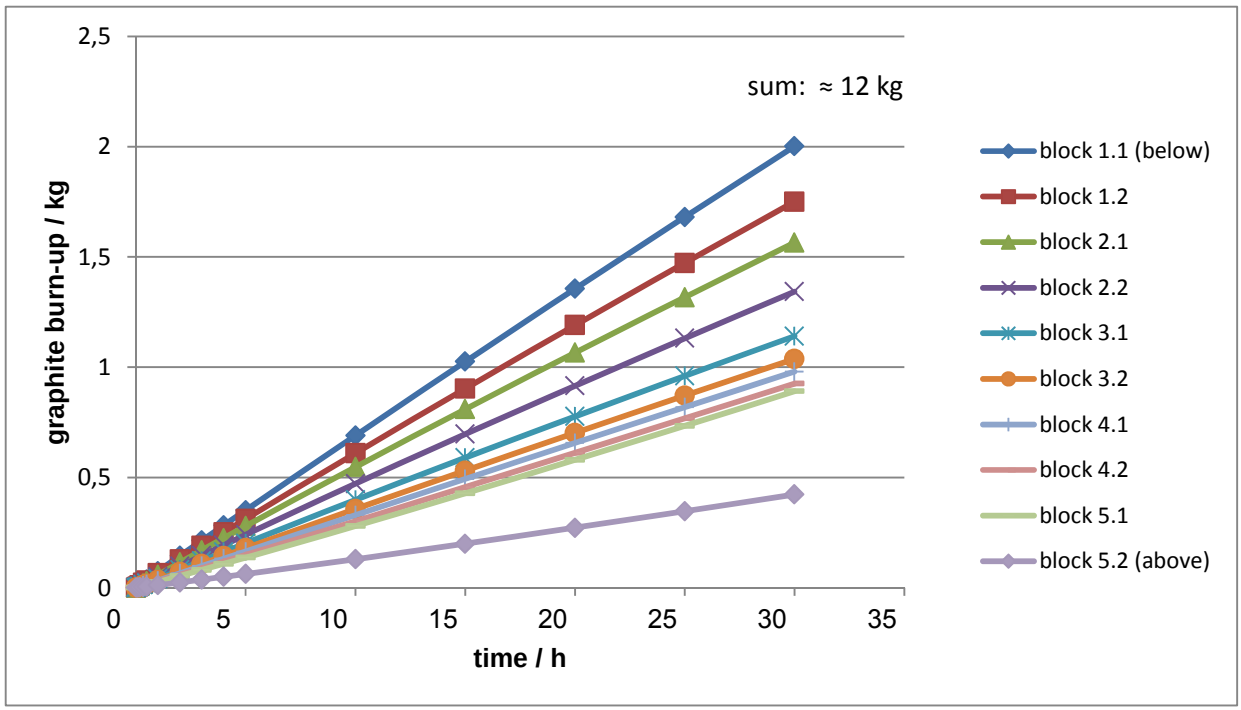

Figure 29: Graphite burn-up calculated with MGT-3D (3D model)

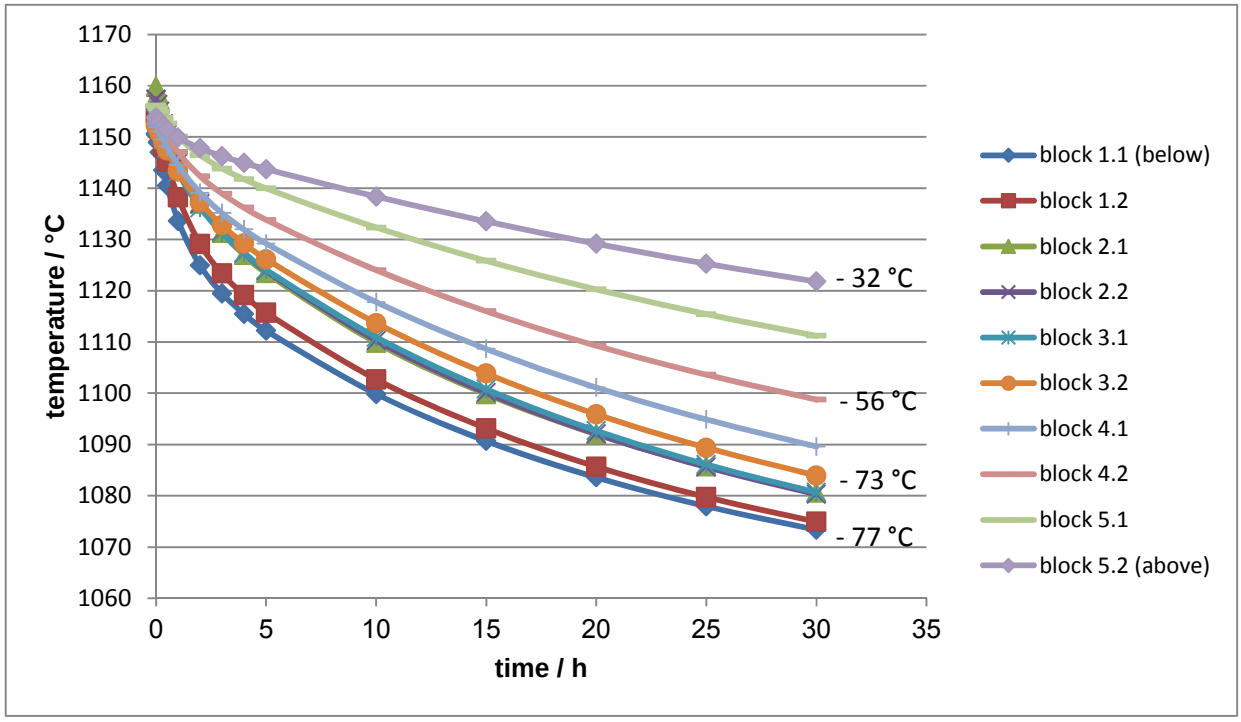

Figure 30: Temperature behavior of the graphite blocks (3D simulation)

6 Experimental data and calculation results

6.1 Experimental data

The experimental procedure of the two oxidation experiments is in principle the same. The heating up of the entire facility is temperature controlled for the furnace-segments, with a heating rate of 30 K/h (the temperature of the graphite geometry is not of interest during the heat up, but it is measured during the whole experiment). After reaching the aimed temperature and some time to steady the entire system, the furnace is switched from temperature control to power controlled operation. It is in the operators hand to adjust the temperature in the graphite geometry preferably similar and within the aimed temperature region only by variation of the electrical power for each segment. After some time (1,5 – 5h) to reach nearly steady-state conditions in the entire facility, the gas supply is switched from nitrogen to the same amount of oxidation gas (7m³N/h, 21Vol.-% CO_2 in N_2). During the oxidation the gas concentration as well as the temperature profile in the experiment, especially in the graphite geometry is observed. After reaching a defined burnup or temperature drop, the oxidation is stopped, the gas supply is switched back to nitrogen. A second and possibly third oxidation phase is done in comparable procedure (with different aimed temperature region and therefore different heating power). When the oxidation-part of the experiment is finished, the operation mode of the furnace is changed to temperature control and the facility is cooled down with a cooling rate of 30K/h.

6.1.1 Block geometry

Experimental setup and instrumentation of the block experiment are described in chapter 4.2.

Figure 31 gives the temperature profile of the first ceramic segment (furnace temperature) during the whole experiment. The vertical bars mark oxidation phase 1 and oxidation phase 2. The heating up (increasing temperature) and cooling down of the facility (strongly decreasing line) are in principle temperature controlled. Especially in the cooling down phase there is no straight line but some disturbances due to the natural cooling curve and some modification of the gas flow in the end of the cooling phase.

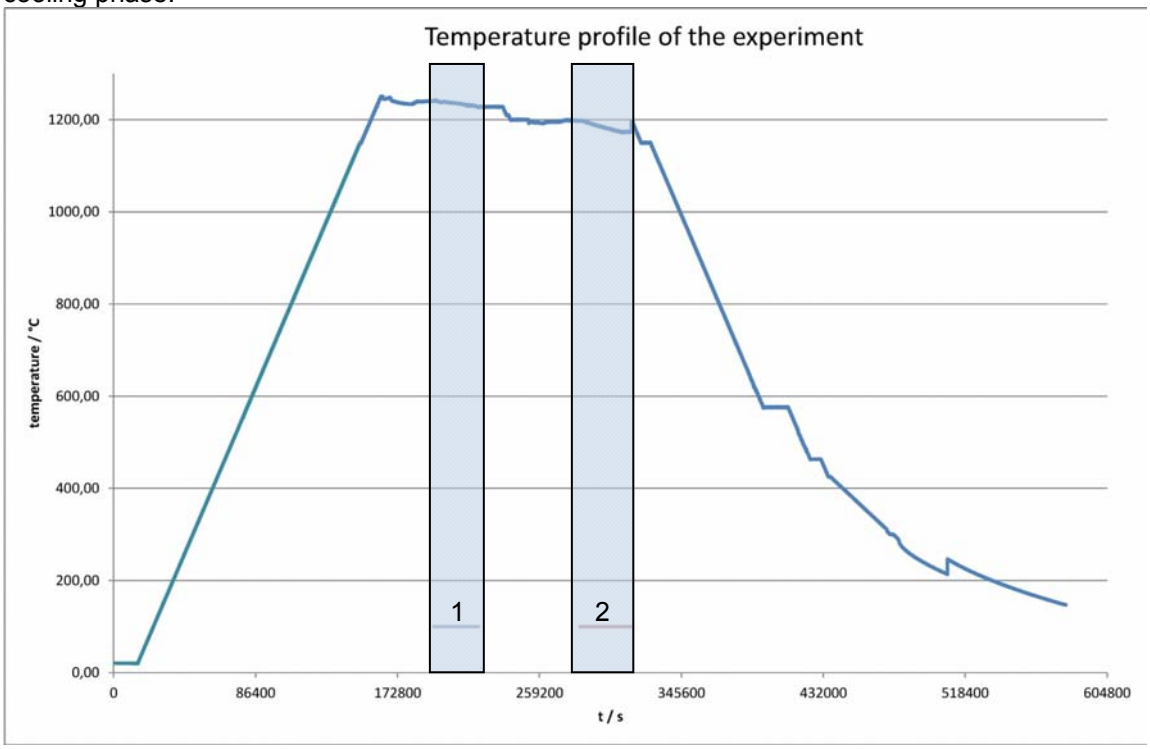

Figure 31: Temperature profile during first experiment

During the “hot” phase of the experiment first there is the adjustment of the power before oxidation phase 1, followed by the first oxidation (duration: 7,5h). Then the temperature for the second oxidation phase is aimed, followed by the power adjustment and the oxidation phase 2 (duration: 8,5h). The short temperature rise after phase 2 is due to a gas change from nitrogen to helium as a pre-experiment. After short time the gas is switched back to nitrogen and the cool down of the facility begins.

Oxidation phase 1:

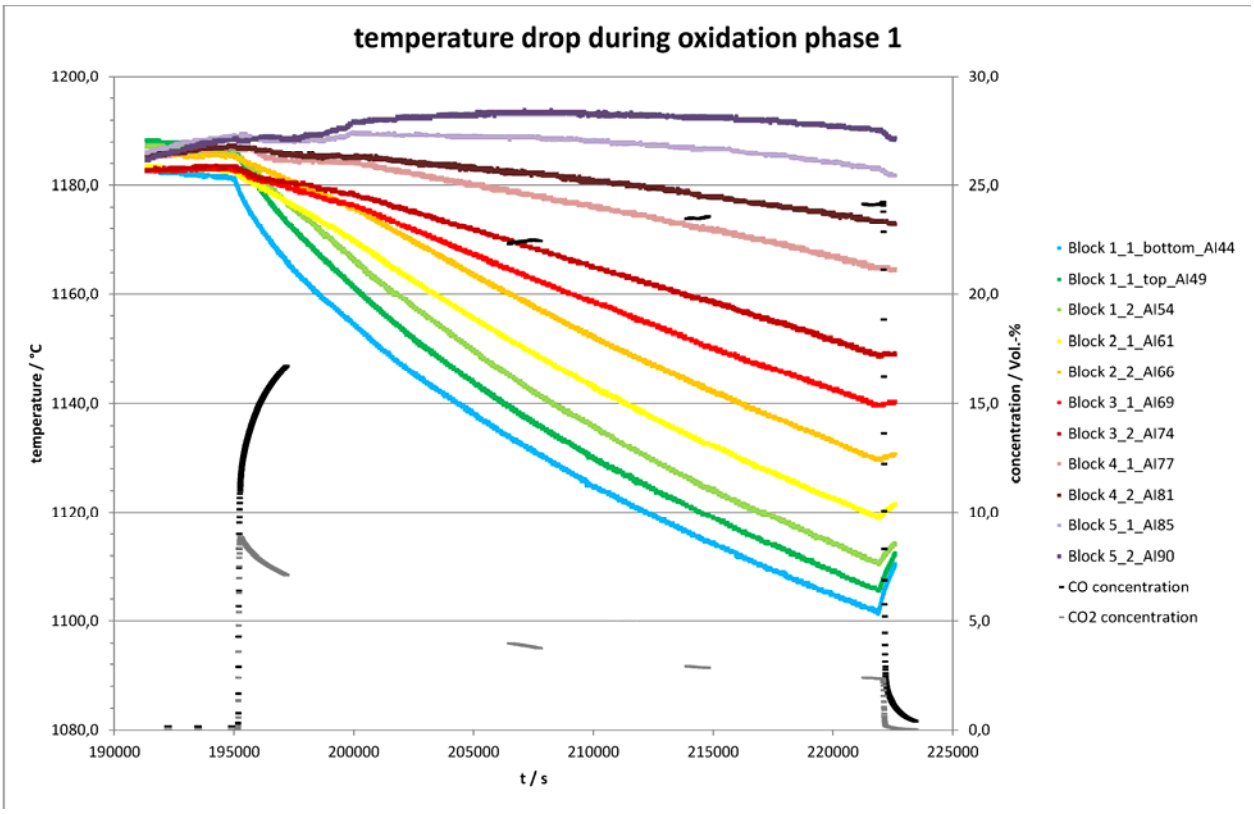

Figure 32: Temperature drop due to first oxidation phase

Beside the temperatures in different heights within the graphite blocks (coloured lines) also the gas concentration of CO (black line) and CO_2 (grey line) at the outlet of the facility are shown in Fig. 32.

The right vertical axis is for the gas concentrations. In the beginning of the first oxidation phase the gas flow is switched from nitrogen to the oxidation gas (21 Vol.-% CO_2 in N_2) and the oxidation starts immediately. The measured CO concentration (black line) as well as the CO_2 concentration (grey line) rise very fast at first. Then the CO_2 concentration drops, the CO concentration continuing rises, which indicates the Boudouard reaction. Due to the fact, that the gas concentration measurement is switched between several measurement points in Fig.32 the black as well as the grey line are interrupted, but a continuous behaviour of both concentrations can be assumed. During oxidation phase 1 the reaction rate for the Boudouard reaction rises with time (further increase of the CO concentration and decrease of the CO_2 concentration).

The temperatures in the graphite geometry (coloured lines) are measured in the middle of each block (Block 1.1 is in the bottom, block 5.2 is at the top of the graphite geometry). As one can see in Fig. 32, the starting temperature at the beginning of the oxidation reaction is 1180 – 1190°C. Once the oxidation gas enters the graphite structure, the temperature drop indicates the beginning of the endothermic reaction. In the lower blocks the temperature decrease is faster than in the upper blocks due to the sinking concentration of remaining CO_2 in the oxidation gas. For a better comparison of the temperature drop in the different graphite blocks in Fig. 33 is the temperature drop relative to the starting temperature given, where the starting temperature is the averaged value over one hour before the begin of the oxidation.

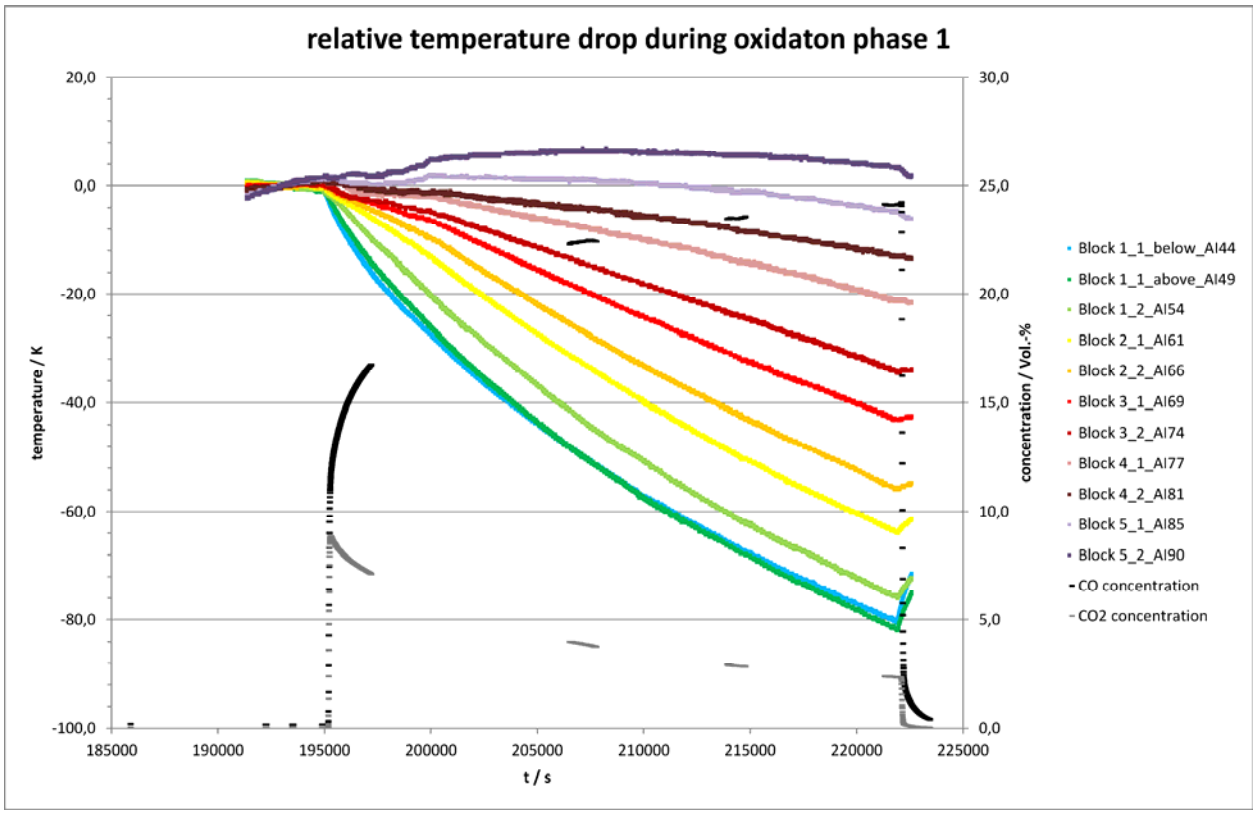

Figure 33: Relative temperature drop

The temperature drop due to the oxidation reaction is strongest in block 1.1 (similar values in the bottom (blue) and the top (dark green) of block 1.1), followed like expected in order of height by block 1.2(light green), 2.1(yellow), 2.2(orange) and so on till block 5.2(dark violet) with the smallest temperature drop. Especially in block 5.1 and 5.2 there is no real temperature drop, in fact, the temperature is still rising. On closer examination even before start of the oxidation the temperature in these two blocks is still rising. This has to be taken into account for the weighting of the temperature profile of the upmost graphite blocks.

The graphite blocks 1.1, 1.2 and 2.1 are located in the second heating segment, block 2.2 to 4.1 in the third heating segment and 4.2, 5.1 and 5.2 in the fourth heating segment of the furnace. Fig. 34 shows the temperature of the different heating zones of the furnace during the oxidation phase. The temperature of the heating segments 1 (dark green), 2 (light green) and 3 (yellow) is nearly stable during the adjustment phase before the oxidation (185 – 195 x 10^3s). In heating segment 4 (orange) and 5 (red) are still rising temperatures, that also have some influence on the temperature of the graphite blocks in the inner ceramic channel (4.2, 5.1, 5.2). At about 200 x 10^3s there is a small jump in the temperature of heating segment 1, 2 and 4 whereas in segment 3 and 5 there is no change. The comparison with the measured voltage of these segments gives also a slight jump in voltage for segment 1, 2 and 4, no change for segment 5 and even a slight decrease in voltage for segment 3 (the set point of the given power for every segment was not changed). Somehow this seems to have some influence on the measured temperatures, especially in block 4.2, 5.1 and 5.2).
The given heating power of segment 5 was at 206 x 10^3s slightly reduced, indicated by the drop in temperature at this time in heating segment 5 (red). Directly after the end of the oxidation phase 1 there was a new temperature aimed for oxidation phase 2.

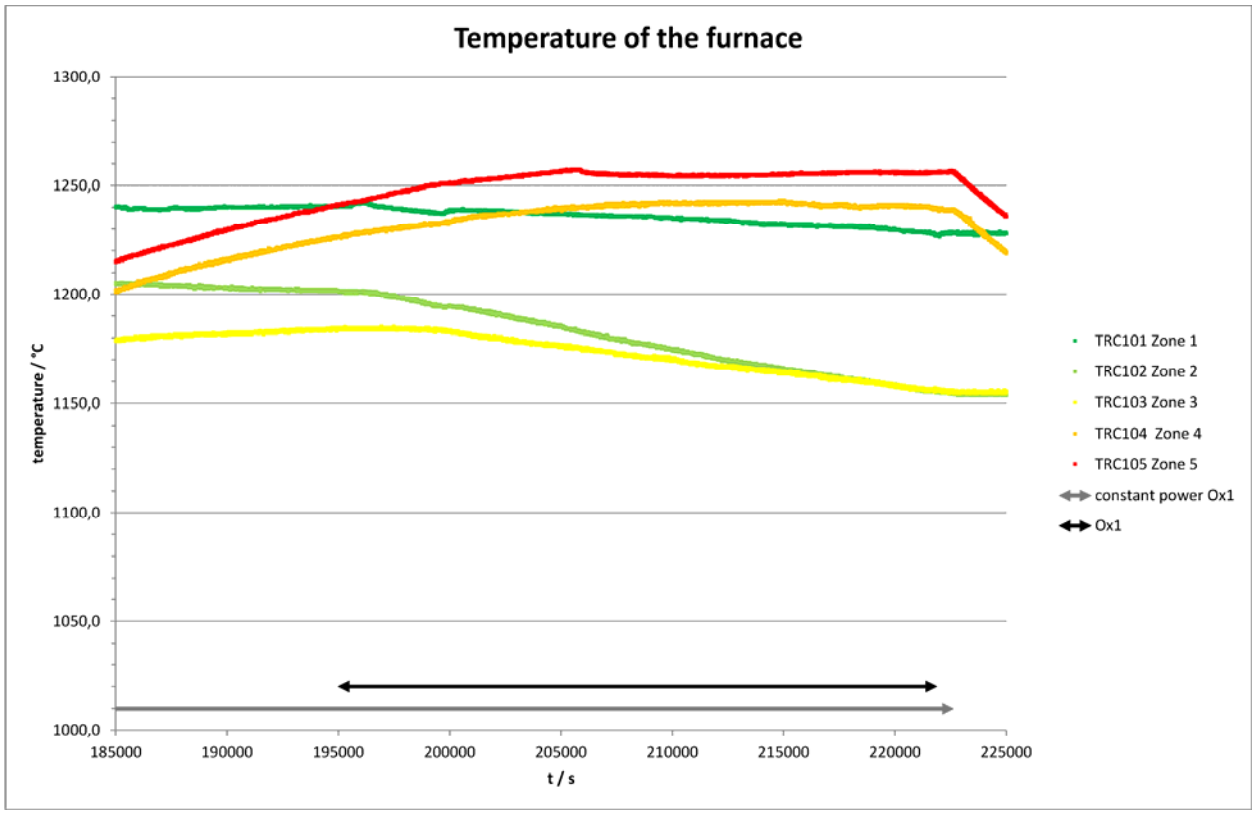

Figure 34: Temperature of the furnace (Ox1)

Oxidation phase 2:

As seen in the first oxidation phase, changes or non-steady state in the heating zones have some not negligible influence on the temperatures of the graphite geometry in the inner channel. Therefore in oxidation phase 2 was special focus on the steady state condition of the furnace before starting the oxidation. The starting temperature in the second oxidation phase is 1120 - 1130°C.

Fig. 35 shows the gas concentration and the temperatures (coloured lines) of the graphite blocks for oxidation phase 2. In the beginning of the first oxidation phase the gas flow is switched from nitrogen to the oxidation gas (21 Vol.-% CO_2 in N_2) and the oxidation starts immediately and even with higher reaction rates (with respect to oxidation phase 1). The concentration of CO_2 (grey line) is increasing with time, the CO concentration (black line) as well as the temperatures of the graphite blocks is decreasing with time. This behaviour can be explained with the temperature dependence of the oxidation reaction.

The temperatures in the graphite geometry (coloured lines) decreases and the lower the blocks are located in the facility, the faster is the temperature drop.

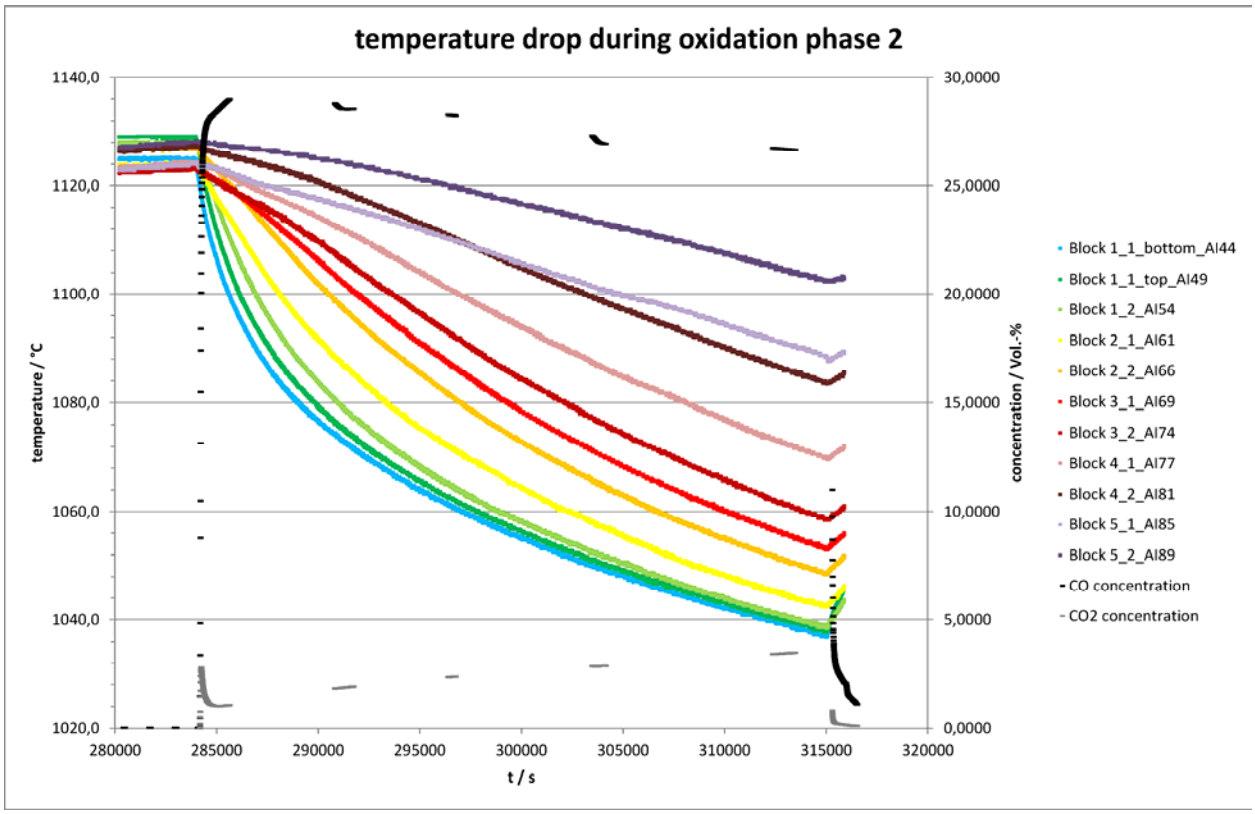

Figure 35: Temperature drop due to second oxidation phase

For a better comparison of the temperature drop in the different graphite blocks, Fig. 36 gives the temperature drop relative to the starting temperature, where the starting temperature is the averaged value over one hour before the begin of the oxidation. In the adjustment phase before begin of oxidation phase 2 the temperatures in the graphite blocks are more stable with respect to oxidation phase 1.

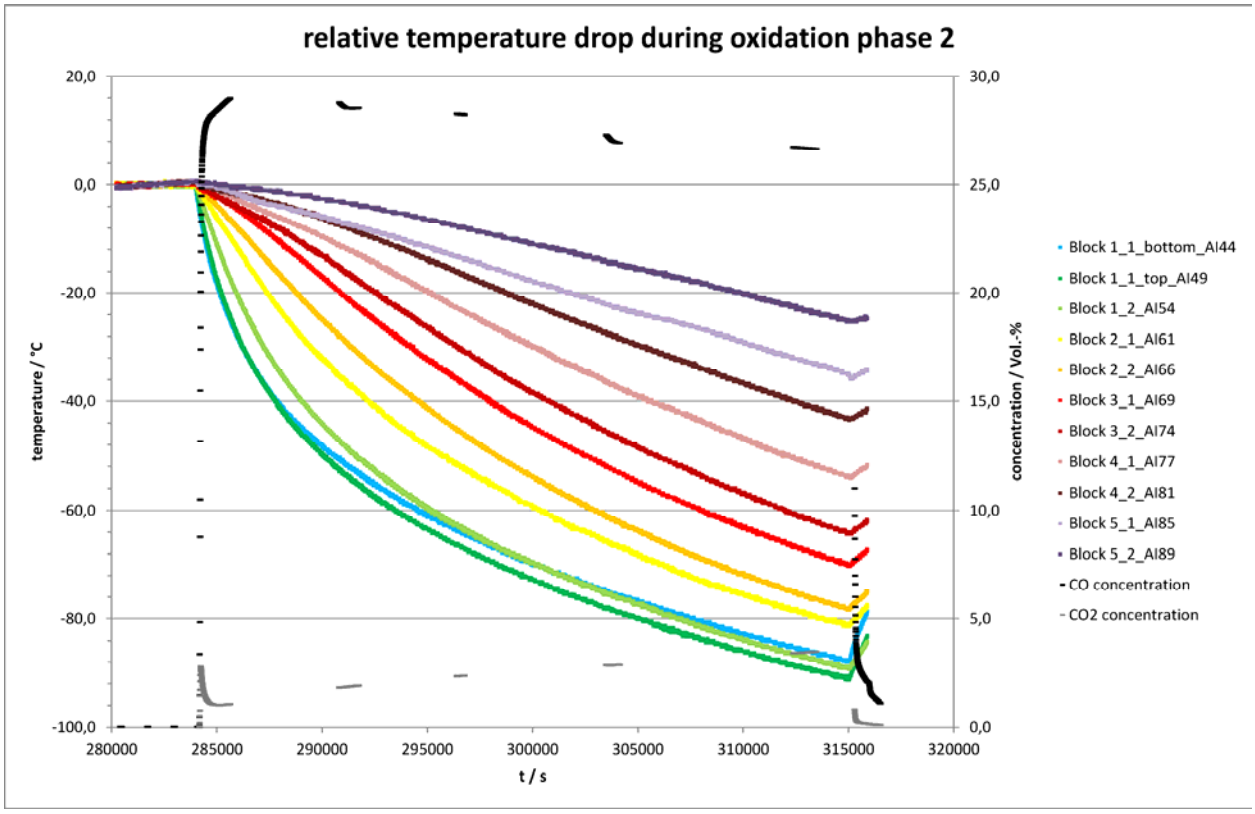

Figure 36: Relative temperature drop

The temperature drop due to the oxidation reaction is strongest in block 1.1 (blue and dark green line), where the temperature drop in the bottom gets slower than in the top. The other blocks follow like expected in order of height (block 1.2 to 5.2 with the smallest temperature drop). Also the temperature profile of the upmost blocks (5.1, 5.2) is in oxidation phase 2 dropping.

Fig. 37 shows the furnace temperatures in oxidation phase 2. Especially in the adjustment phase is the nearly steady state behaviour of the furnace visible. During the reaction phase the influence of the oxidation in the inner part of the ceramic channel on the temperatures in the heating zone is obvious.

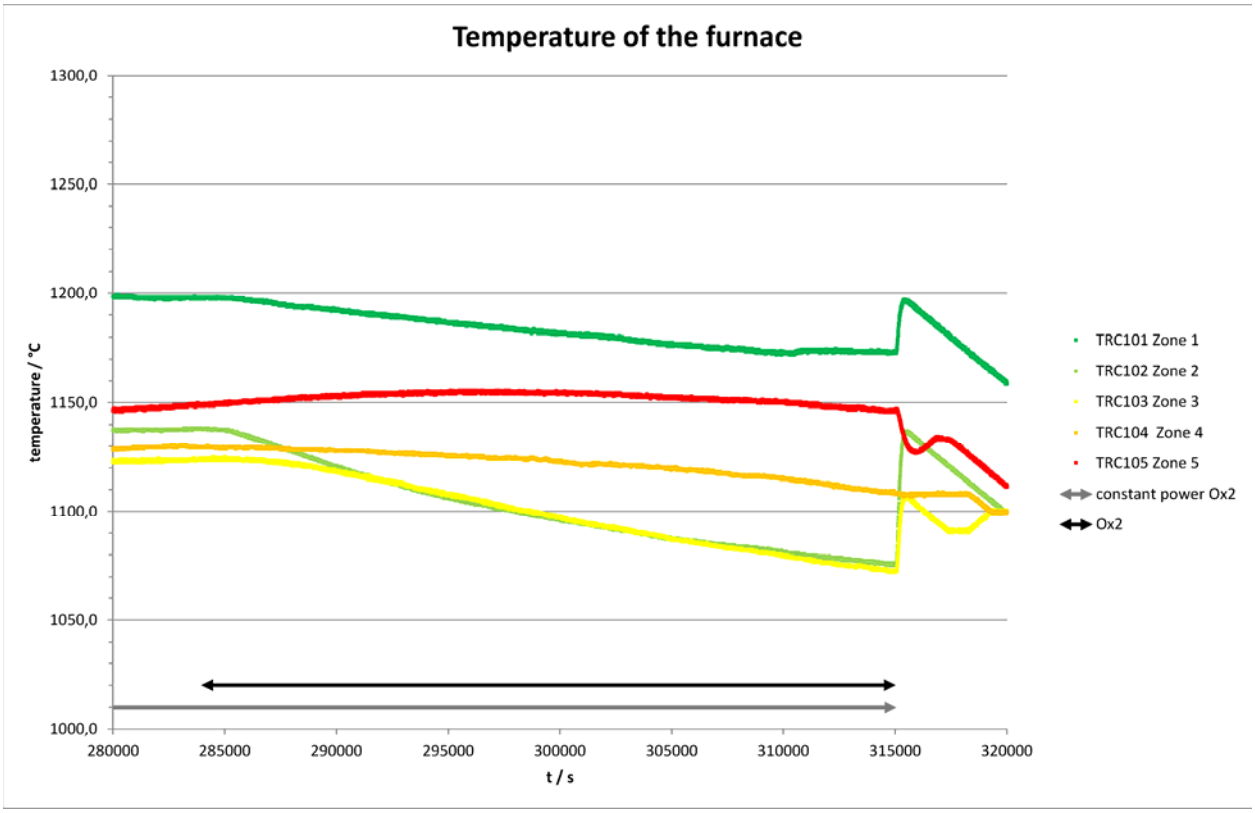

Figure 37: Temperature of the furnace (Ox2)

Examinations after the experiment:

After cooling down and dismounting of the facility, the graphite blocks are examined and weighted separately for the calculation of the burnup in each block.

The visual examination of the blocks as well as the mass loss corresponds with the temperature behaviour during the experiment. The lower the block, the higher is the temperature drop and burn-up. In the upmost blocks there was almost no visible change in shape during oxidation (see Fig. 38 and 39), but in the lower blocks, especially block 1.1 and 1.2, there are significant corrosion effects observed (Fig. 40). The stability of the strongly corroded blocks is still good enough for proper handling of the specimens. In the lower part of block 1.1 (see Fig. 41) there is a quite stable, sponge-like structure, where the initially boreholes are still in good order, but have a far bigger surface now.

Due to the good handling properties of the graphite blocks, there will be additional investigations on selected graphite samples for getting an impression of the size of the surface after oxidation.

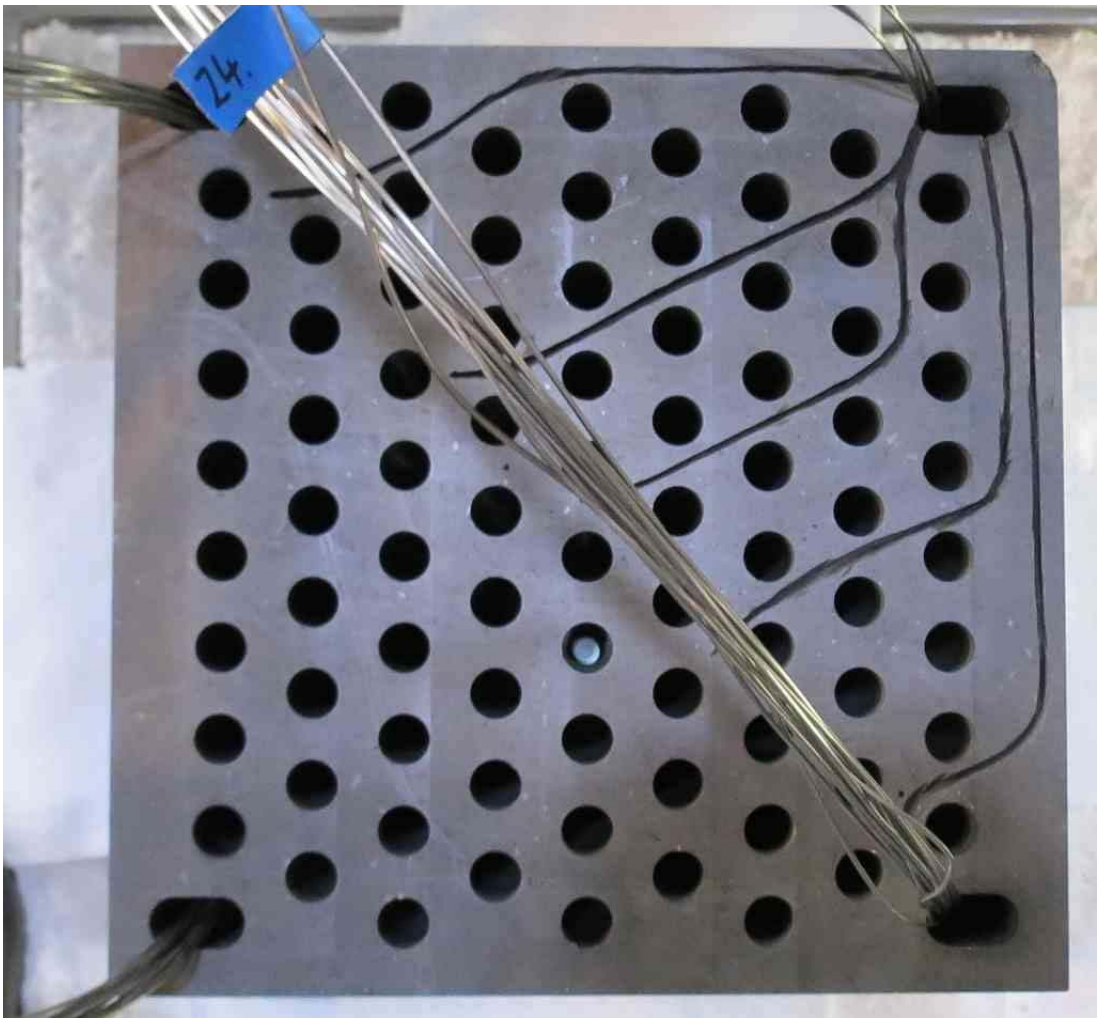

Figure 38: Block before the experiment

Figure 39: Block 5.1 after oxidation

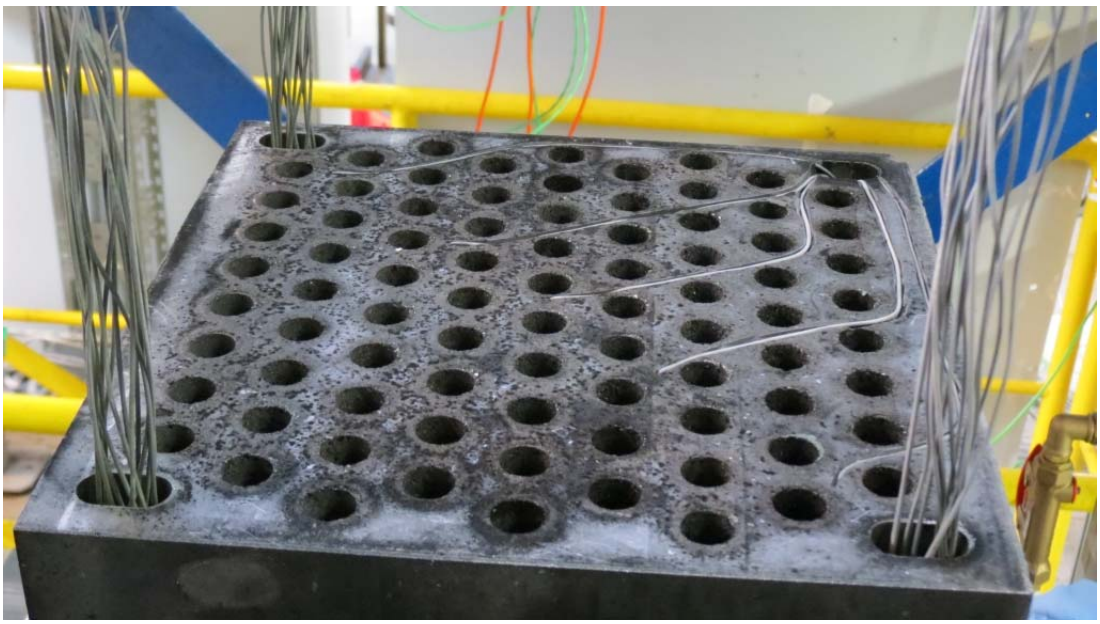

Figure 40: Block 1.1 after oxidation

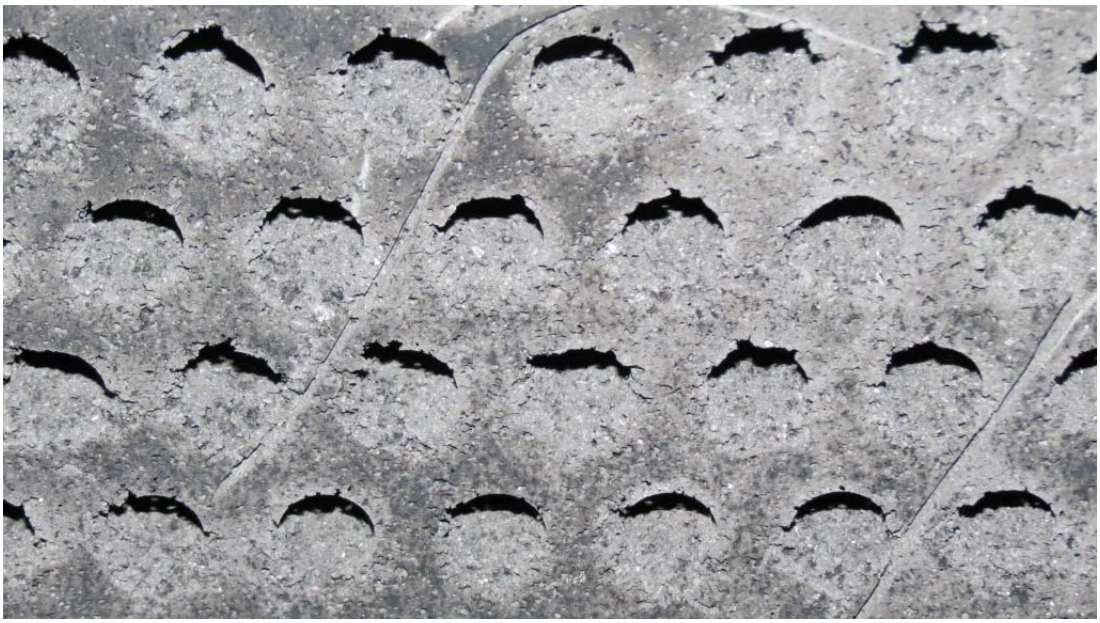

Figure 41: Block 1.1 bottom view after oxidation

The mass loss of the graphite blocks (weighting before and after the experiment) is shown in Fig. 42. Most burn-up is in the lower part of the graphite blocks (1.1, 1.2, 2.1). In the upper part the mass loss gets less, but is still measurable. In total 10,25 kg of initially 250 kg graphite was burned, that's a burn-up of 4.1%.

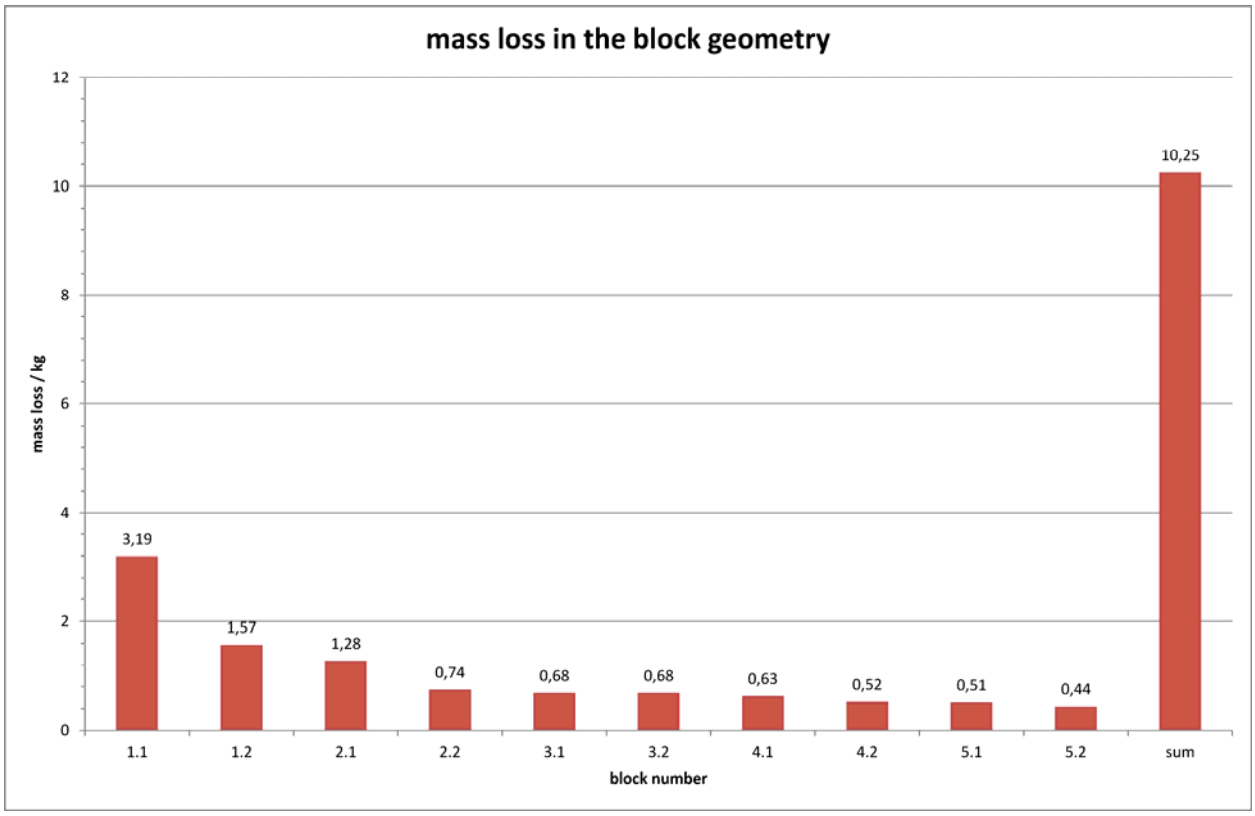

Figure 42: Mass loss of the graphite blocks

6.1.2 Pebble-bed geometry

The experiment with the pebble-bed geometry and the one with the block geometry should be comparable to each other. For this reason the experimental design as well as the experimental performance is chosen carefully. As the surface has a strong influence on the oxidation reaction, this parameter is hold similar to the first experiment. Amount and concentration of the oxidation gas are the same like in the first experiment (7m³N/h, 21 Vol.-% CO_2 in N_2) and also the aimed temperatures are the same.

The experimental setup and the instrumentation of the pebble-bed experiment are described in chapter 4.3.

Fig. 43 gives the temperature profile of the first ceramic segment (furnace temperature) during the whole experiment. The oxidation phases are marked by the vertical bars. The heating up (increasing temperature) and cooling down of the facility (strongly decreasing line) are temperature controlled. Especially in the cooling down phase there is no straight line but some disturbances due to the natural cooling curve and some modification of the gas flow in the end of the cooling phase.

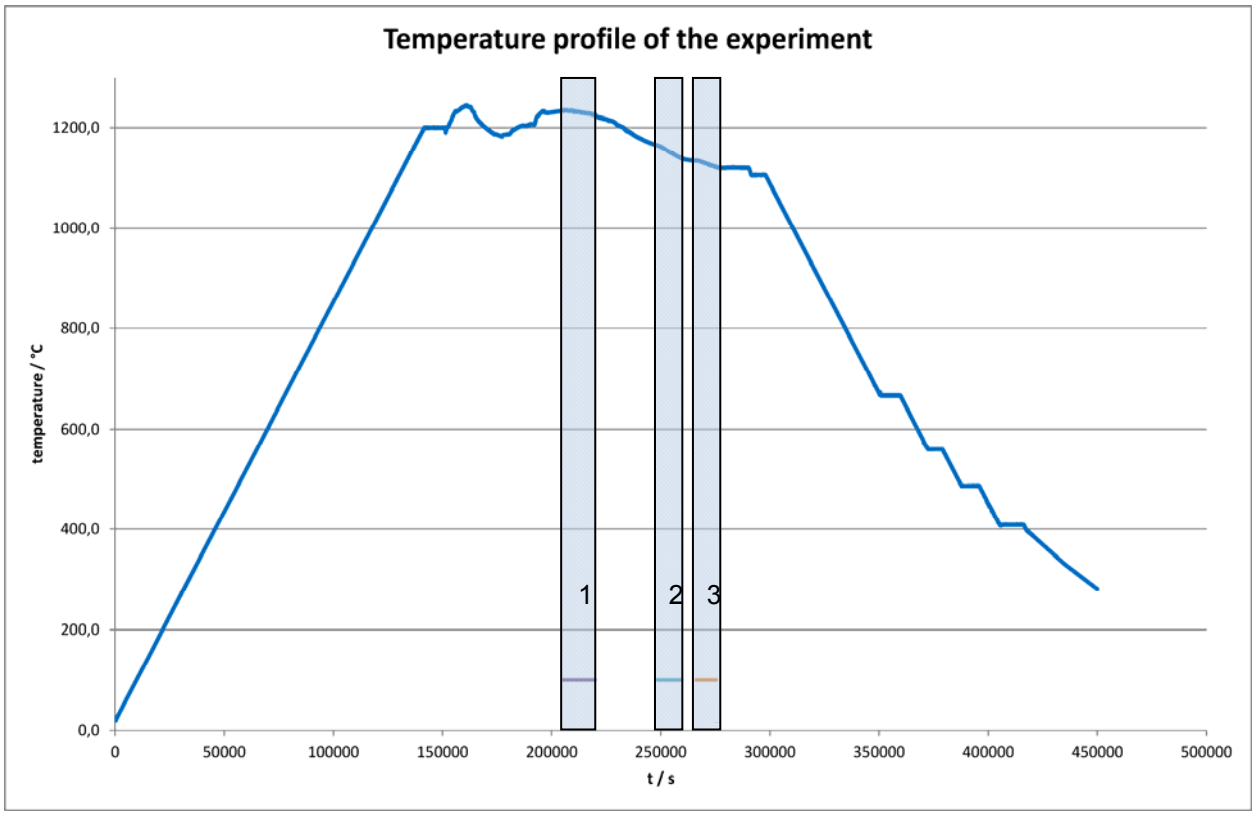

Figure 43: Temperature profile during second experiment

During the “hot” phase of the experiment first there is the adjustment of the power before oxidation phase 1, followed by the first oxidation (duration: 4h). Then the temperature for the second oxidation phase is aimed, followed by the power adjustment and the oxidation phase 2 (duration: 3h). To get a comparable relative graphite burn-of with respect to the experiment with block geometry, an additional oxidation phase 3 (duration: 2,5h) is done. There was no power adjustment between the second and third oxidation phase, so this is a real transient behaviour.

Oxidation phase 1:

Beside the temperatures in different pebble layers (coloured lines) also the gas concentration of CO (black line) and CO_2 (grey line) at the outlet of the facility are shown in Fig. 44 .

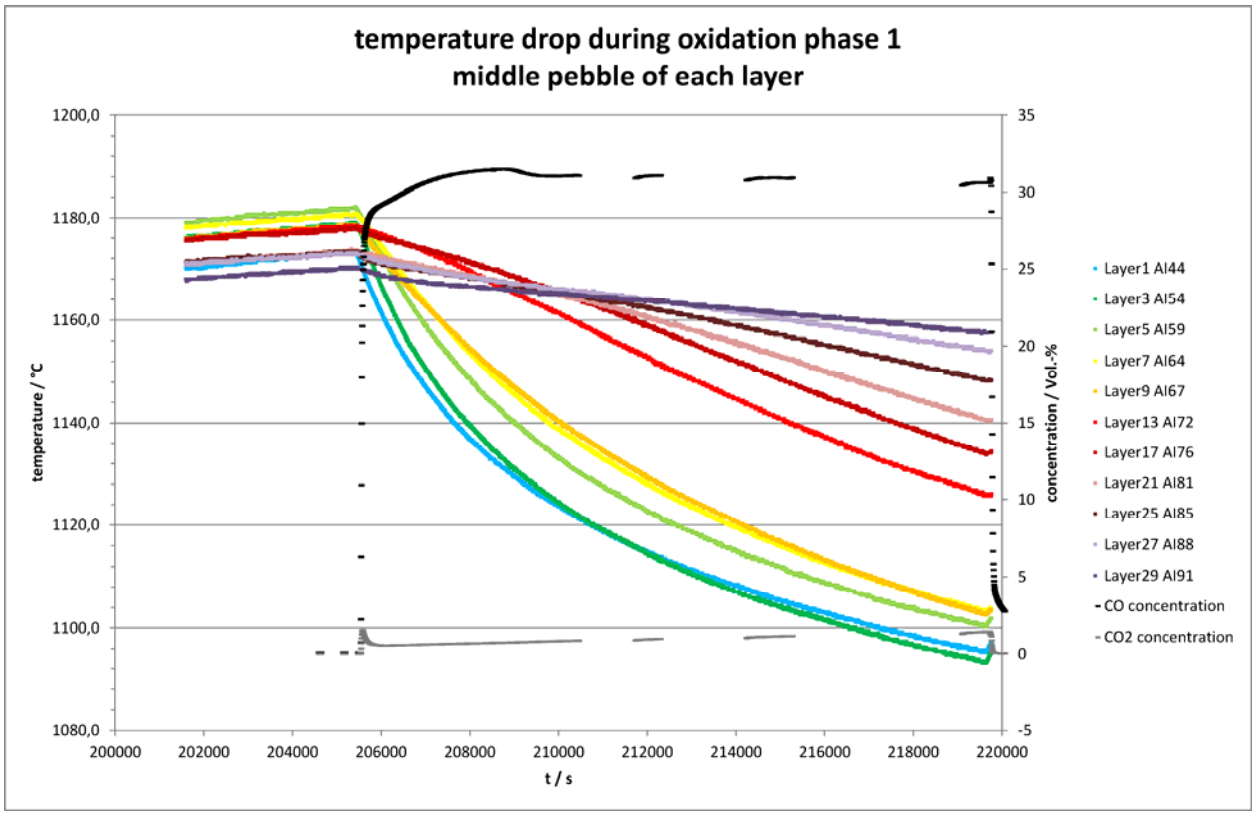

Figure 44: Temperature drop due to first oxidation phase

The right vertical axis is for the gas concentrations. In the beginning of the first oxidation phase the gas flow is switched from nitrogen to the oxidation gas (21 Vol.-% CO_2 in N_2) and the oxidation starts immediately. The measured CO concentration (black line) rises very fast at first. The CO_2 concentration (grey line) has a little jump in the beginning and then drops again, which both indicates the Boudouard reaction. Due to the fact, that the gas concentration measurement is switched between several measurement points in Fig. 44 the black as well as the grey line are interrupted, but a continuous behaviour of both concentrations can be assumed. During oxidation phase 1 the reaction rate for the Boudouard reaction first drops with time (decrease of the CO concentration and increase of the CO_2 concentration).

The temperatures in the graphite geometry (coloured lines) are measured in the middle of each layer (layer 1 is in the bottom, layer 29 is at the top of the graphite geometry). As one can see in Fig. 44, the starting temperature at the beginning of the oxidation reaction is 1170 – 1180°C. Once the oxidation gas enters the graphite structure, the temperature drop indicates the beginning of the endothermic reaction. In the lower pebble layers the temperature decrease is faster than in the upper blocks due to the sinking concentration of remaining CO_2 in the oxidation gas. For a better comparison of the temperature drop in the different graphite layers in Fig. 45 is the maximal temperature drop for every layer relative to the starting temperature given, where the starting temperature is the averaged value over one hour before the begin of the oxidation.

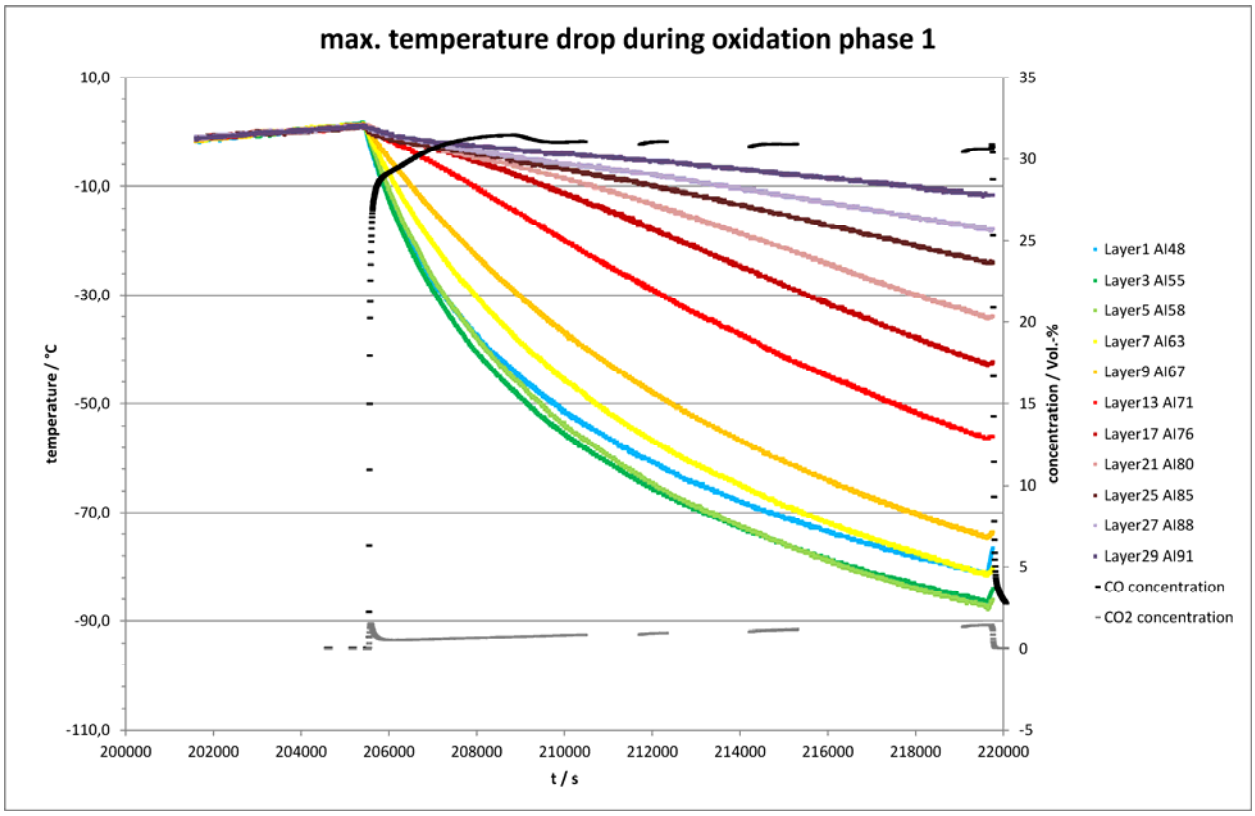

Figure 45: Relative temperature drop

The temperature drop due to the oxidation reaction is strongest in layer 3 (dark green), followed like expected in order of height by layer 5 (light green), 7 (yellow), 9 (orange) and so on till layer 29 (dark violet) with the smallest temperature drop. Layer 1 (blue) has in the beginning of the oxidation a similar drop like Layer 3 and 5, but then the drop gets slighter.

Oxidation phase 2:

The starting temperature in the second oxidation phase is 1135 - 1145°C.

Fig. 46 shows the gas concentration and the temperatures (coloured lines) of the pebble bed for oxidation phase 2. In the beginning of the second oxidation phase the gas flow is switched from nitrogen to the oxidation gas (21 Vol.-% CO_2 in N_2) and the oxidation starts immediately and even with higher reaction rates (with respect to oxidation phase 1). The concentration of CO jumps directly from 0 Vol.-% to the value of about 30 Vol.-%. Due to the non-continuous measurement of the gas concentrations, the jump in concentration itself is not measured in the exact time of the start of the oxidation. The CO_2 concentration (grey line) is almost very slightly increasing with time, the CO concentration (black line) as well as the temperatures of the graphite blocks is decreasing with time. This behaviour can be explained with the temperature dependence of the oxidation reaction.

The temperatures in the graphite geometry (coloured lines) decreases and the lower the pebble layer is located in the facility, the faster is the temperature drop. Layer 1 is an exception like seen in the first oxidation phase.

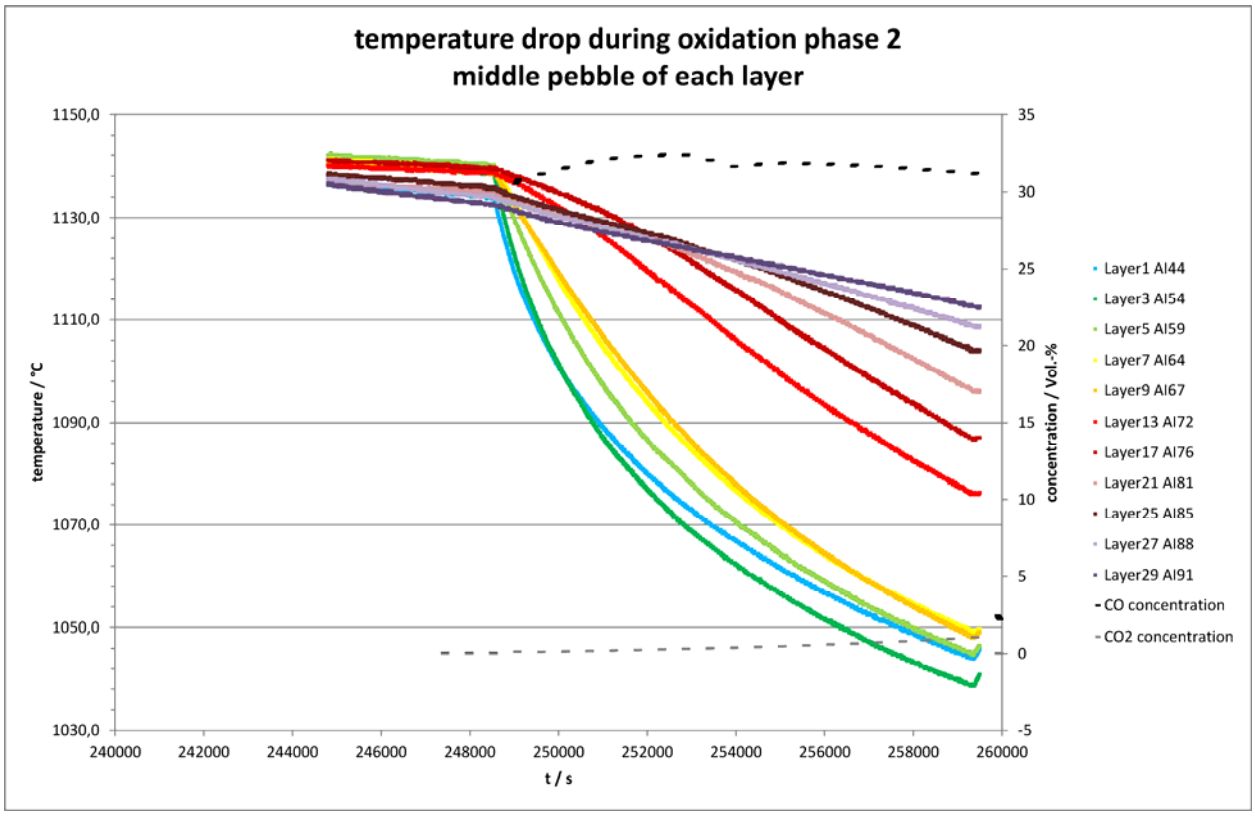

Figure 46: Temperature drop due to second oxidation phase

For a better comparison of the temperature drop in the different pebble layers, fig. 47 gives the temperature drop relative to the starting temperature, where the starting temperature is the averaged value over one hour before the begin of the oxidation.

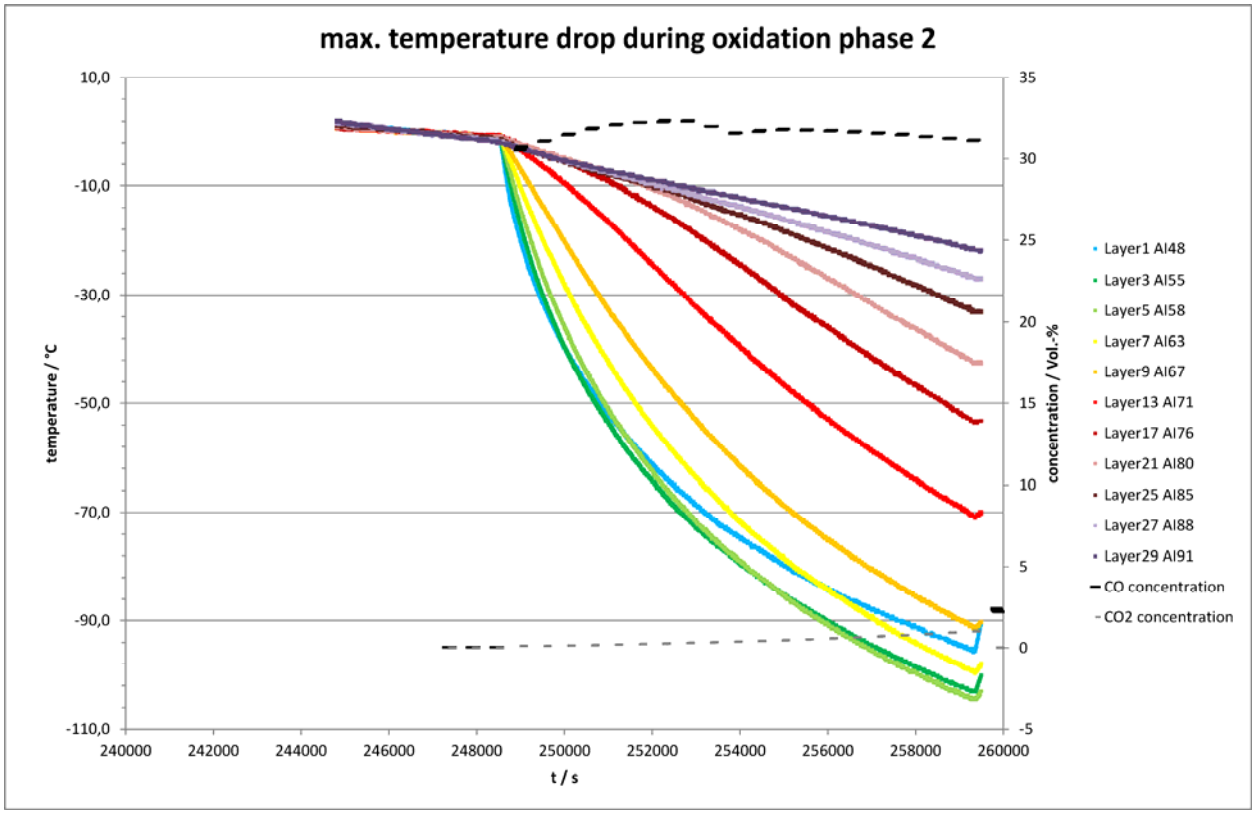

Figure 47: Relative temperature drop

The temperature drop due to the oxidation reaction is strongest in the lower part of the pebble bed (layer 1-5), where in layer one the temperature drop gets less with time (in comparison to the other temperatures). The temperature in the other layers follow like expected in order of height (layer 7 to 29 with the smallest temperature drop).

Oxidation phase 3:

Different to the mode of operation between oxidation phase 1 and 2 (in the block type as well as in the pebble-bed experiment) after oxidation phase 2 the power is not adjusted to another temperature, but hold constant and just waited for several time. With this important data are generated for the transient behaviour of the experimental facility.

The starting temperature for the third oxidation phase could therefore not be adjusted properly and is between 1070 – 1110°C.

Fig. 48 shows the gas concentration and the temperatures (coloured lines) of the pebble bed for oxidation phase 3. In the beginning of the third oxidation phase the gas flow is switched from nitrogen to the oxidation gas (21 Vol.-% CO_2 in N_2) and the oxidation starts immediately. The CO_2 concentration (grey line) is increasing with time, the CO concentration (black line) as well as the temperatures of the graphite blocks is decreasing with time. This behaviour can be explained with the temperature dependence of the oxidation reaction. The drop of the CO concentration in the middle of each oxidation reaction cannot be brought into accordance with a raise in the CO_2 concentration and has to be discussed later.

The temperatures in the graphite geometry (coloured lines) decreases and the lower the pebble layer is located in the facility, the faster is the temperature drop. Layer 1 is an exception like seen in the first two oxidation phases.

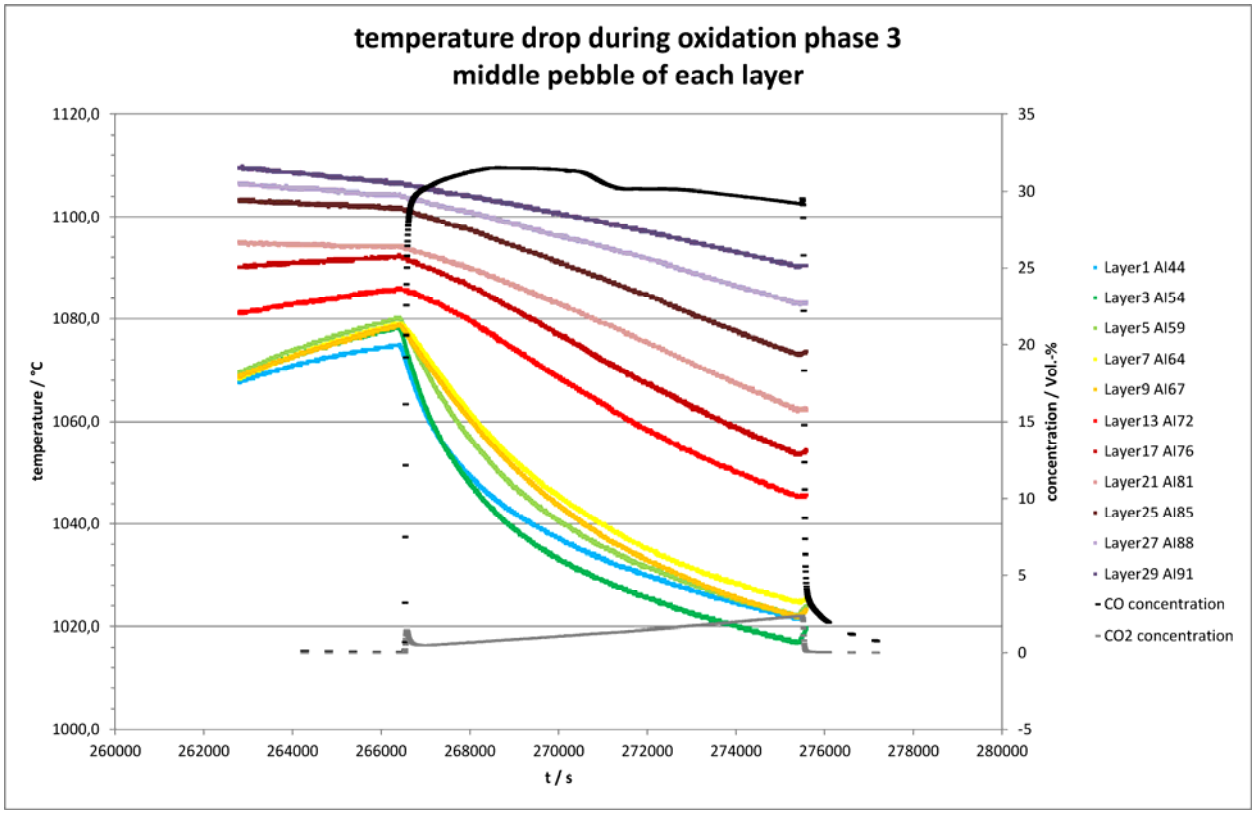

Figure 48: Temperature drop due to second oxidation phase

For a better comparison of the temperature drop in the different pebble layers, fig. 49 gives the temperature drop relative to the starting temperature, where the starting temperature is the averaged value over one hour before the begin of the oxidation.

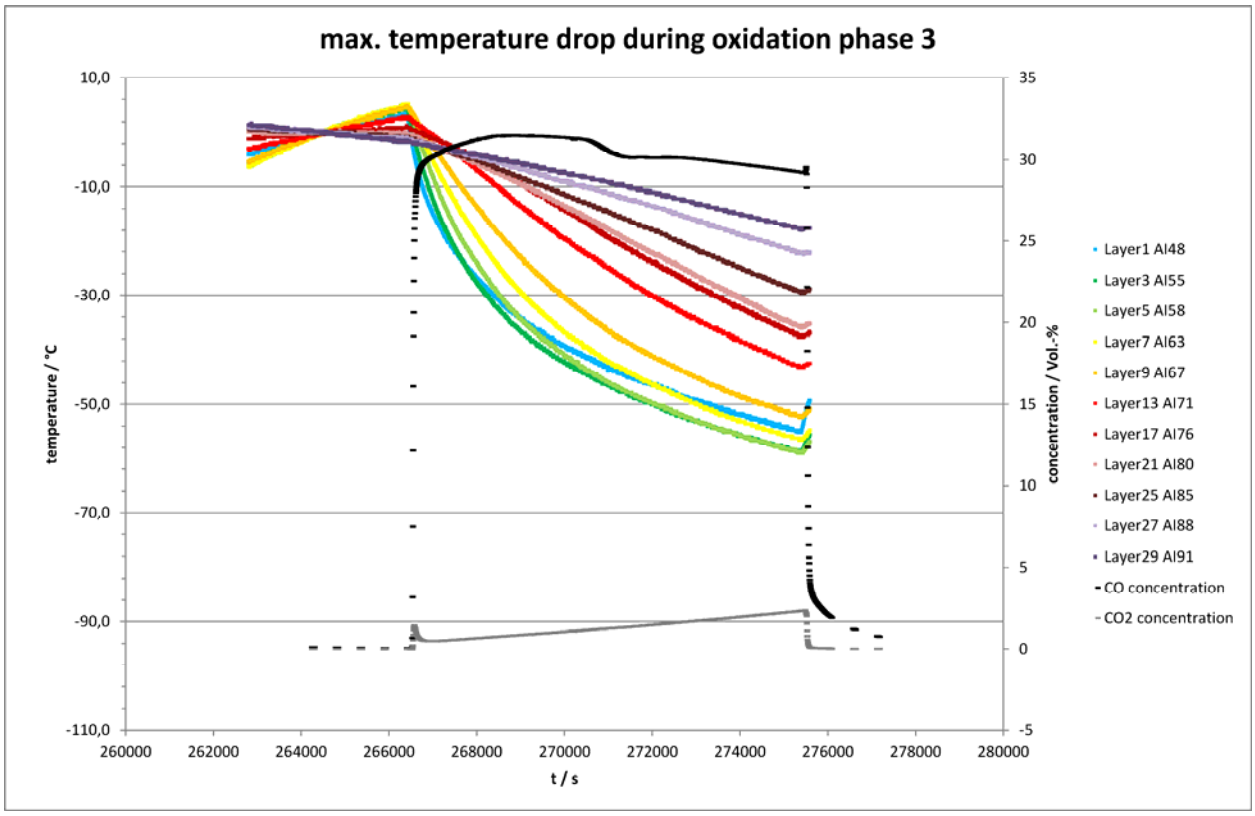

Figure 49: Relative temperature drop

The temperature drop due to the oxidation reaction is strongest in the lower part of the pebble bed (layer 1-5), where in layer one the temperature drop gets less with time (in comparison to the other temperatures). The temperature in the other layers follow like expected in order of height (layer 7 to 29 with the smallest temperature drop).

Examinations after the experiment:

After cooling down and dismounting of the facility, each layer of graphite pebbles is examined and weighted separately for the calculation of the burnup in each layer.

The visual examination of the pebble-bed layers as well as the mass loss corresponds with the temperature behaviour during the experiment. The lower the pebble layer, the higher is the temperature drop and burn-up. In Fig 50 and 51 one see as example layer 9 before and after the oxidation. In the upmost layers there was almost no visible change in shape during oxidation (Fig. 52), but in the lower layers of the pebble-bed (especially layer 1-7) there are significant corrosion effects observed (Fig. 53). At the points of contact between the pebbles, there is obvious less corrosion in comparison to the parts that can be flown around by the oxidation gas (Fig. 51, 55). Especially in the lower pebble layers (Fig. 53, layer 1) one can see that strongly corroded pebbles lay next to pebbles that still have the original shape. The stability of the corroded pebbles is not comparable with the stability of the corroded graphite blocks (Fig. 55, 56). Even the top layers loose some graphite dust during dismounting (Fig.54).

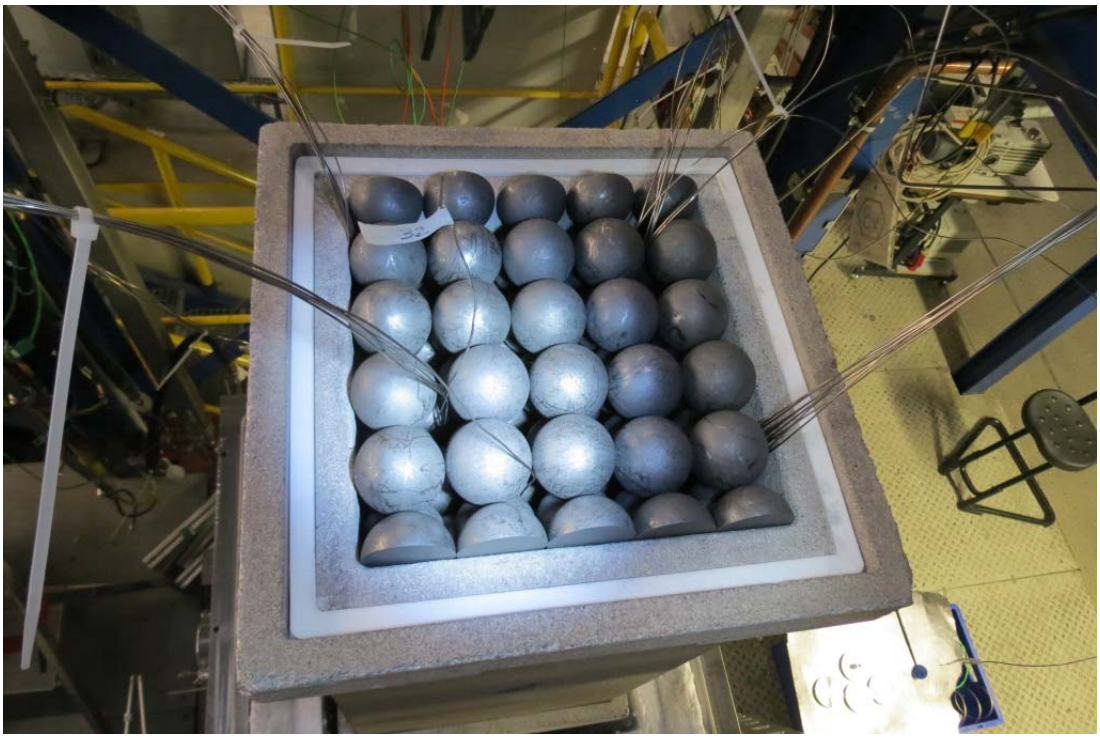

Figure 50: Layer 9 before the experiment

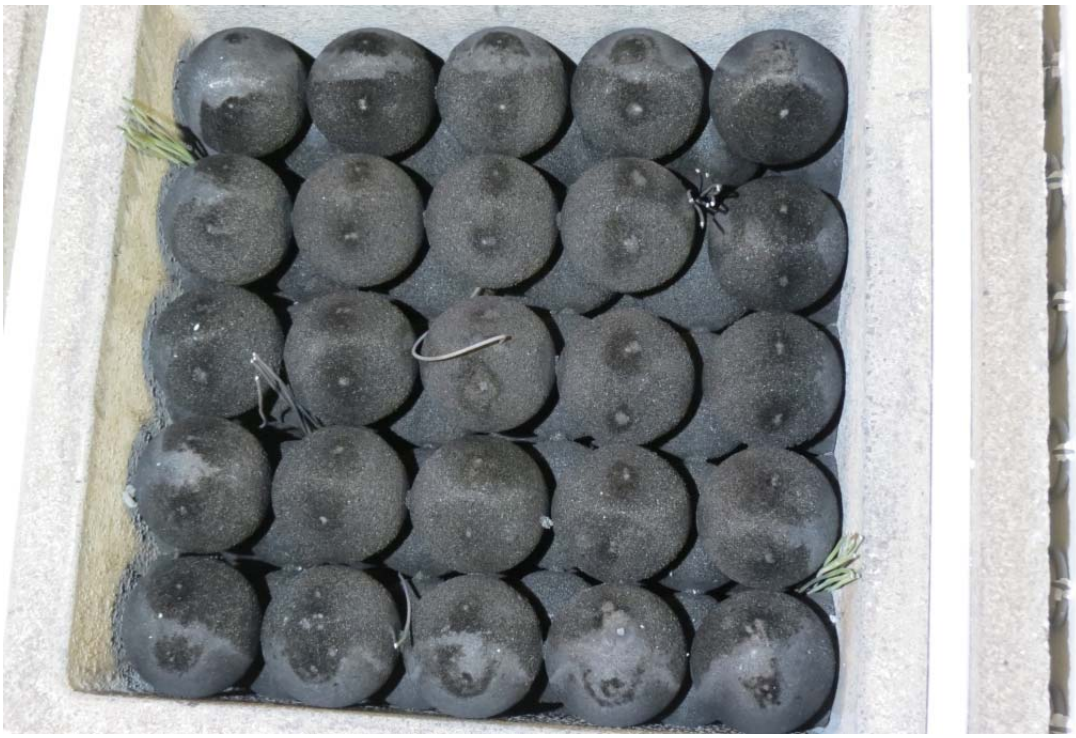

Figure 51: Layer 9 after oxidation

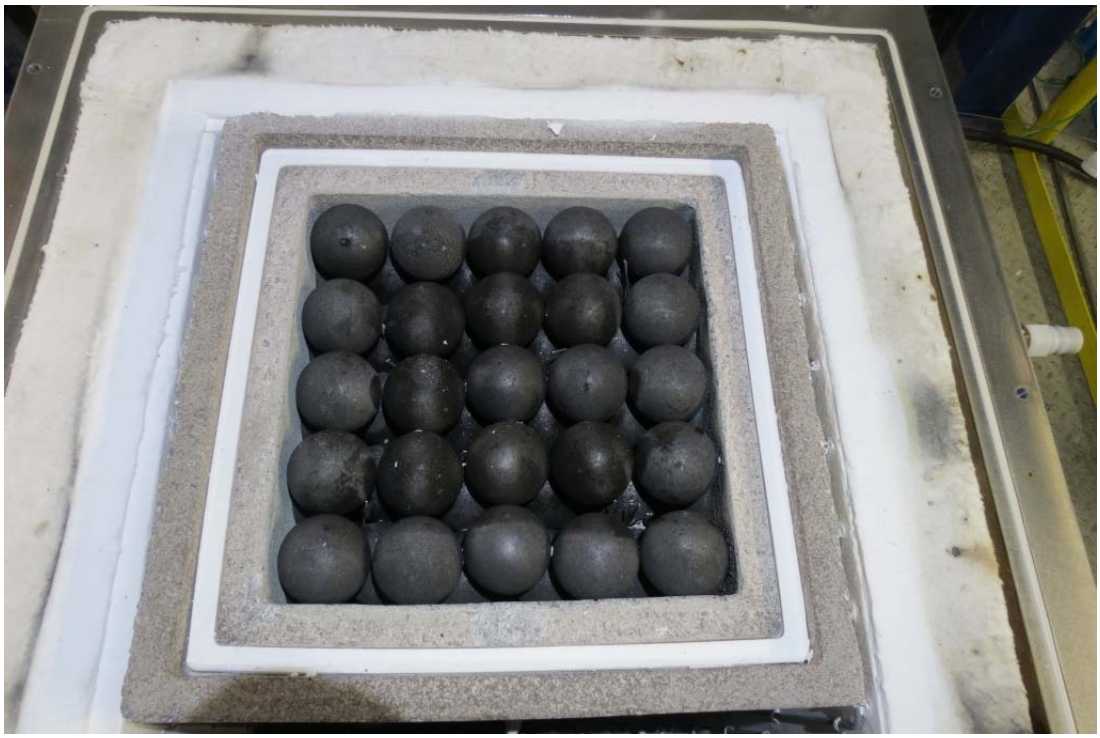

Figure 52: Layer 25 after oxidation

Figure 53: Layer 1 after oxidation

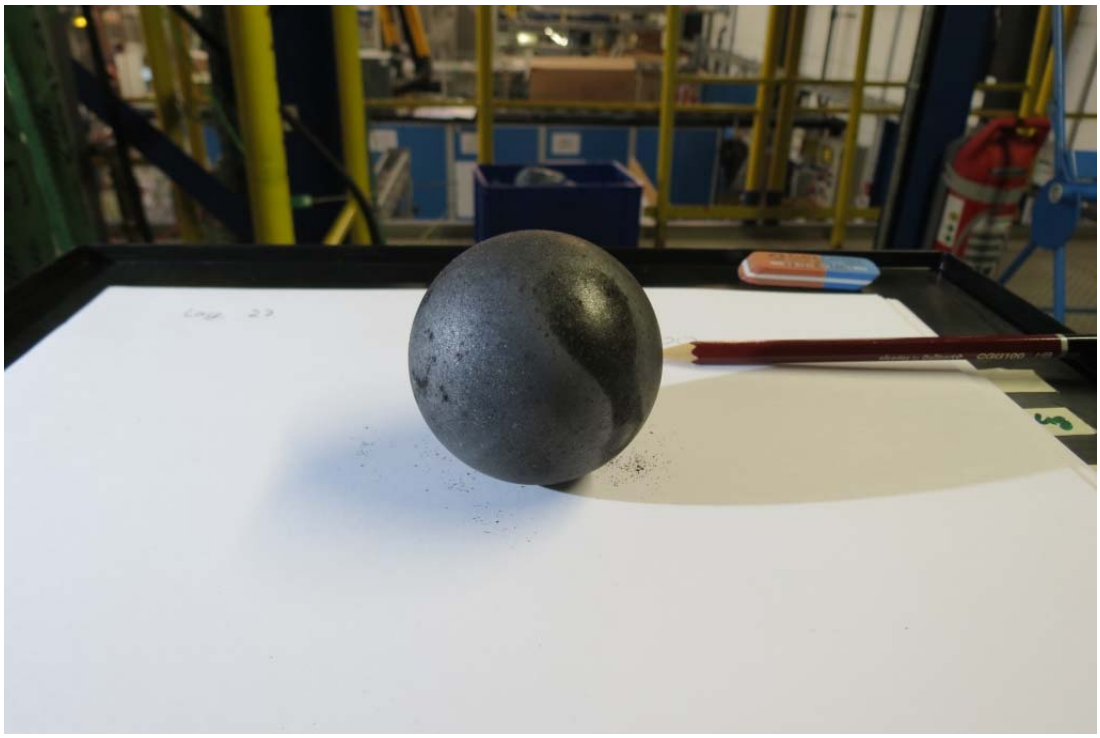

Figure 54: Pebble of upper layer after oxidation

Figure 55: Pebble of middle layer after oxidation

Figure 56: Pebble of lower layer after oxidation

The mass loss of the pebble-bed (weighting before and after the experiment) is shown in Fig. 57. Most burn-up is in the lower part of the pebble-bed (layer 1-9). In the upper part the mass loss gets less. In total 7,47 kg of initially 147,2 kg graphite was burned, that's a burn-up of 5,2%.

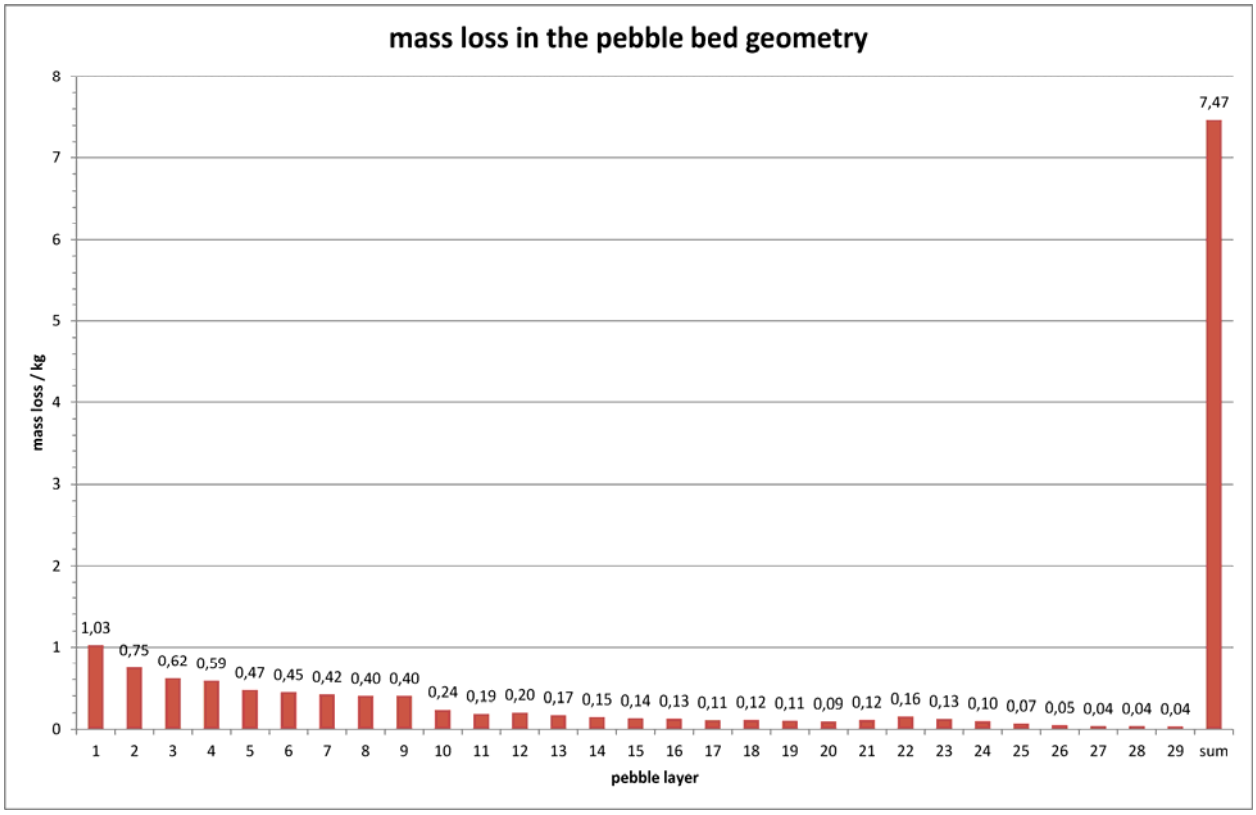

Figure 57: Mass loss of the pebble bed

6.2 Post-Calculation results

Based on the model that was designed to accompany the oxidation and preliminary experiments, the recalculations will now be made to the performed experiments. The first experiment deals with 10 small graphite blocks and one ceramic block below the graphite to get the correct temperatures at the bottom of the first graphite block. As seen in the section before the simulation time was reduced to a total of about 16 hours split into two oxidation phases (phase I and phase II).

6.2.1 Post-calculation results for the block experiment

The first oxidation phase starts at ca. 1190°C. Fig. 58 shows the temperature curves for all 10 graphite blocks during the first oxidation. The temperature decrease due to the Boudouard reaction is clearly visible for all 10 blocks. In this case, the result of the post-calculation confirmed that the decrease in temperature in the lower blocks is greater than the upper.

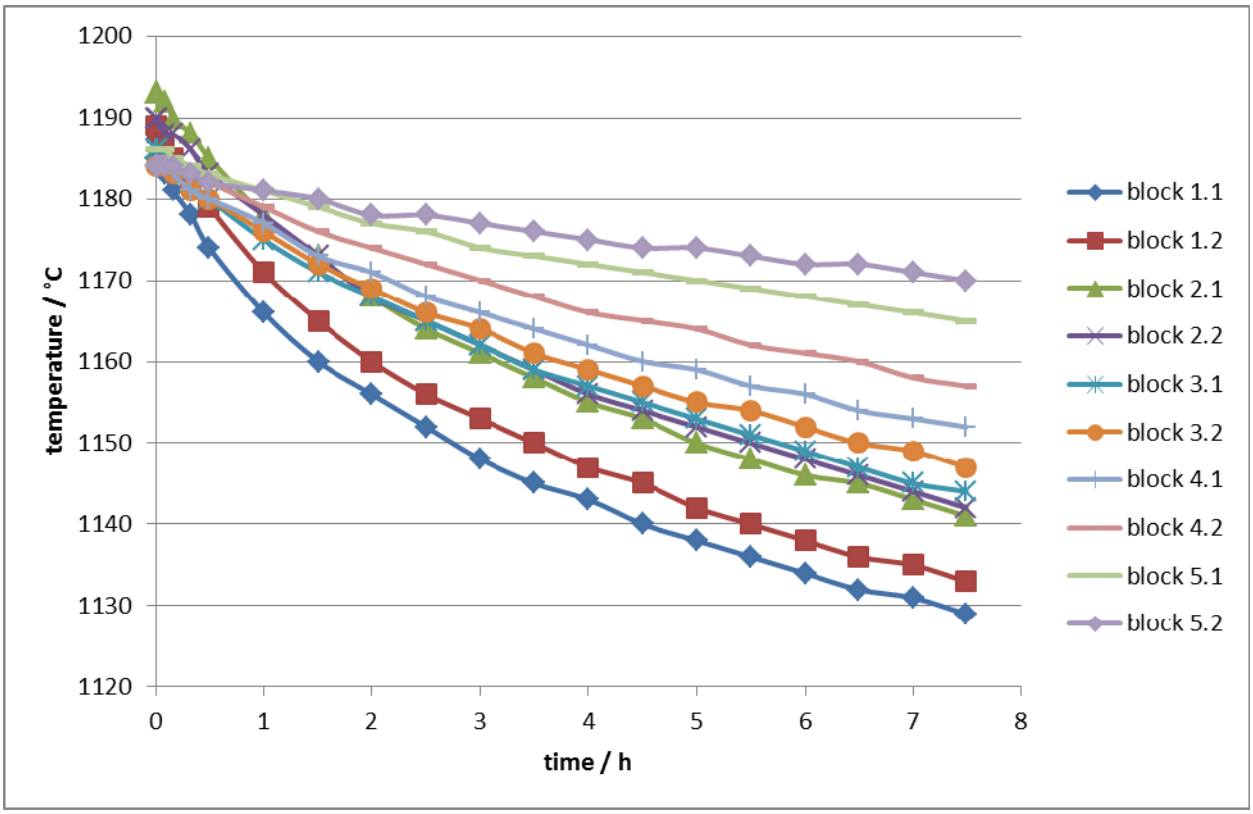

Figure 58: Temperature curves of 10 graphite blocks during first oxidation phase

The temperature of the lower blocks decreases by 56°C, whereas it decreases by only about 14°C in the upper block. After the first oxidation stage and the re-conversion to 100% nitrogen, the heating power of the pilot plant was adjusted so that an approximately constant temperature level of 1130 ° C in the graphite blocks is reached. Then the second oxidation phase starts with a gas mixture as defined before (79% N_2, 21% CO_2). The second phase takes a bit longer than the first phase, but started on a lower temperature level. The temperature curves for this phase are shown in Fig. 59. The trend in the lower blocks in terms of the temperature decrease is stronger than in the upper blocks But it can also be seen here. However, the spread is smaller, since the temperature loss is located in the lower blocks at about 40 °C and in the upper portions at approximately 15 °C.

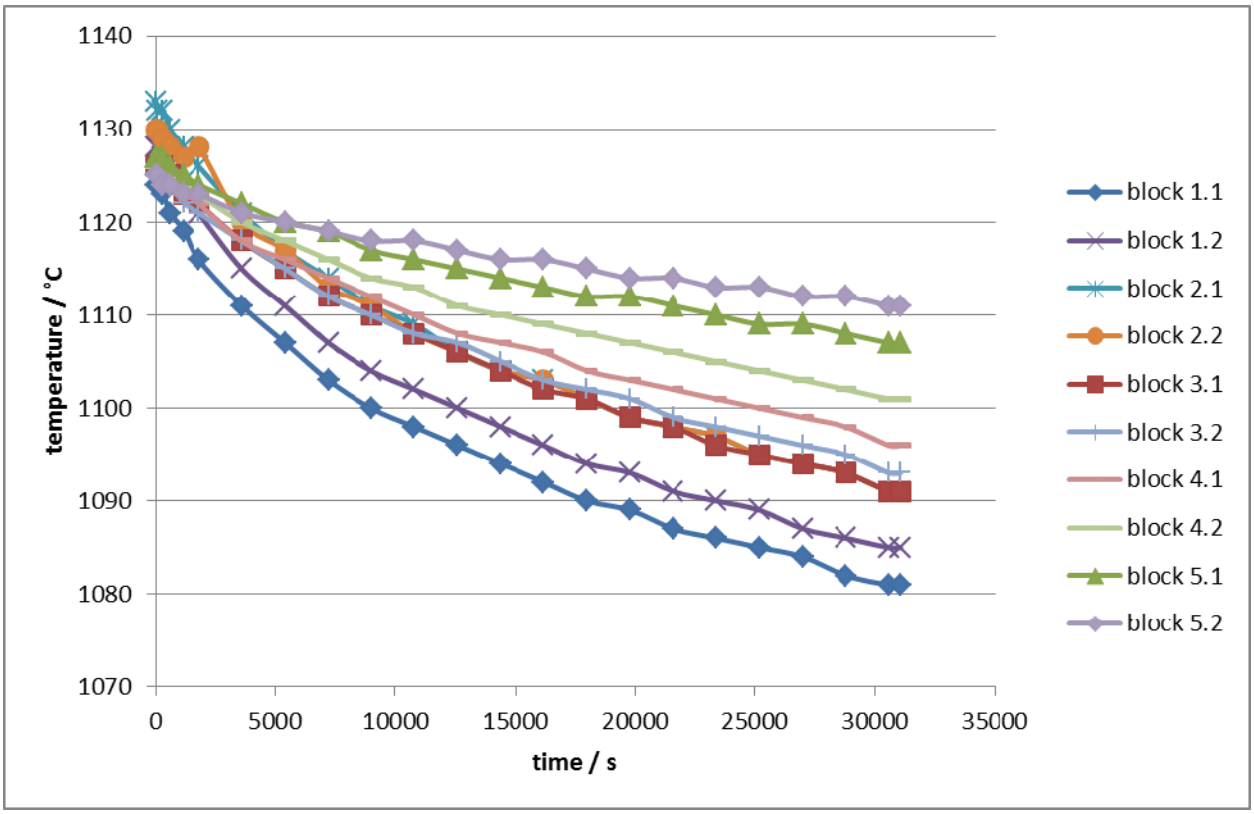

Figure 59: Temperature curves of 10 graphite blocks during second oxidation phase

Table 6 lists the total graphite burn-up of the ten blocks via two oxidation phases and indicates the total sum, which can then be compared later with the data of the experiment.

	block 1.1	block 1.2	block 2.1	block 2.2	block 3.1	block 3.2	block 4.1	block 4.2	block 5.1	block 5.2	sum /kg
phase 1	0,648	0,565	0,502	0,431	0,359	0,317	0,287	0,257	0,231	0,106	3,703
phase 2	0,506	0,462	0,425	0,375	0,327	0,3	0,282	0,262	0,249	0,117	3,305
sum / kg	1,154	1,027	0,927	0,806	0,686	0,617	0,569	0,519	0,48	0,223	**7,008**

Table 6: Graphite burn-up after both oxidation phases

Comparing the results of the two phases, it can be seen that the burn-up of the second phase was lower, although the duration of this phase was greater than that of the first oxidation. A possible explanation for this may lie in the lower starting temperature for the second Boudouard reaction. As a result of the experimental conditions (no weighing of the graphite blocks could take place between the oxidation phases) this assumption cannot be validated experimentally. Thus, only the entire graphite corrosion after completion of the two phases is compared with the simulation results (see section 6.3.1).

6.2.2 Post-calculation results for the pebble bed experiment

The next three figures show the temperature curves of the pebble layers during the Boudouard reaction in the pebble bed. The total oxidation time was only 9.5 hours in this experiment, while trying with the graphite blocks, there were more than 16 hours. This also explains the lower total burnup. The three oxidation phases in the pebble bed start at different temperature levels. The first phase began at about 1175°C, the second at approximately 1130°C and the third at approximately 1085 °C. Fig. 60 (first phase) shows the decrease in temperature due to the endothermic reaction in the lower layers of spheres is significantly higher than in the upper layers. This behavior was already in the block test visible due to the fact that in the upper graphite areas, the CO_2 concentration is not as high as in the lower layers due to the reaction already taken place. For the first oxidation phase, the decrease in temperature is between 50°C

(layers 1-5) and 10°C (layers 27-29). In the second oxidation phase (see Fig. 61) the spread is lower (35°C - 10°C) and lasting the third phase reduces the temperature in the lowest layers only about 25°C. In the upper layers of the value is comparable to those of the first two phases.

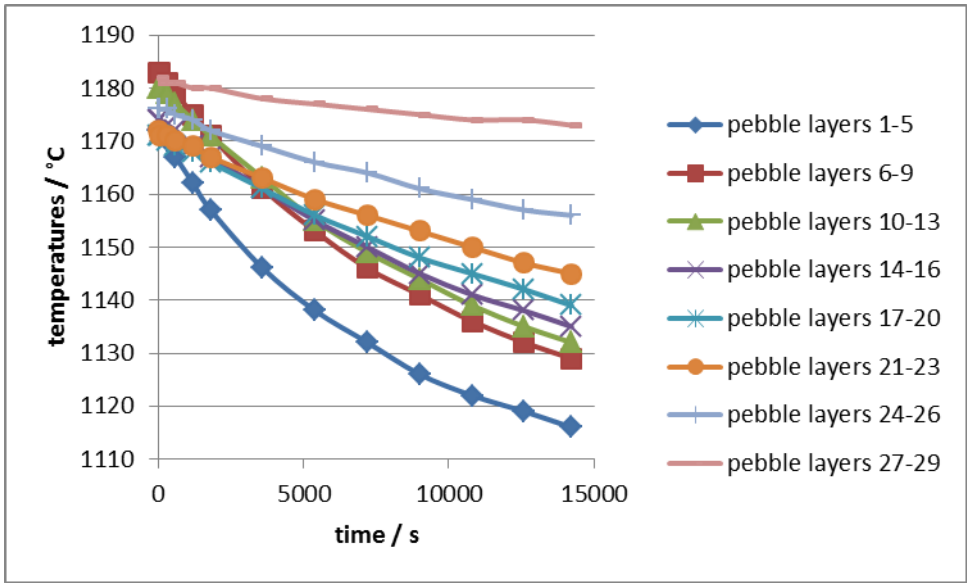

Figure 60: Graphite burn-up during first oxidation phase

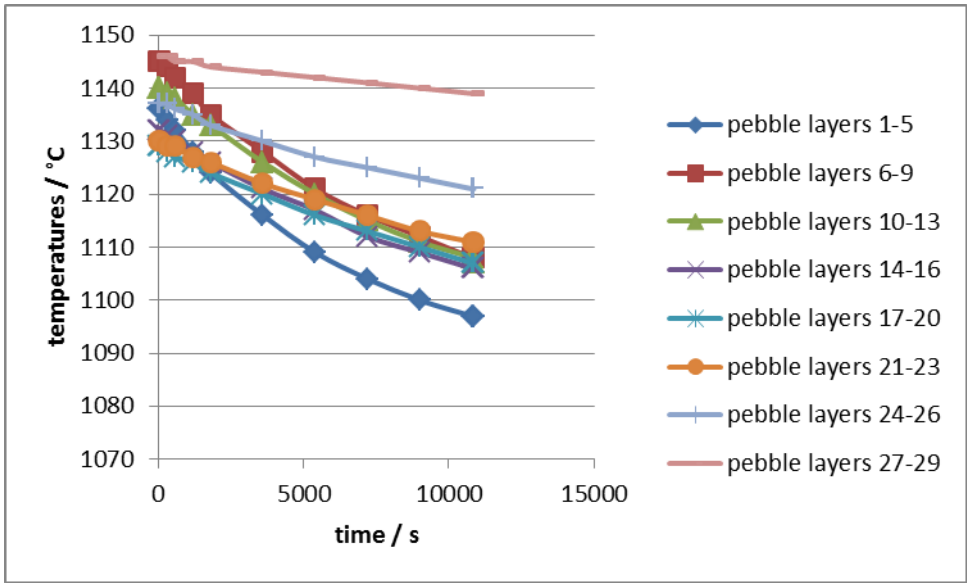

Figure 61: Graphite burn-up during second oxidation phase

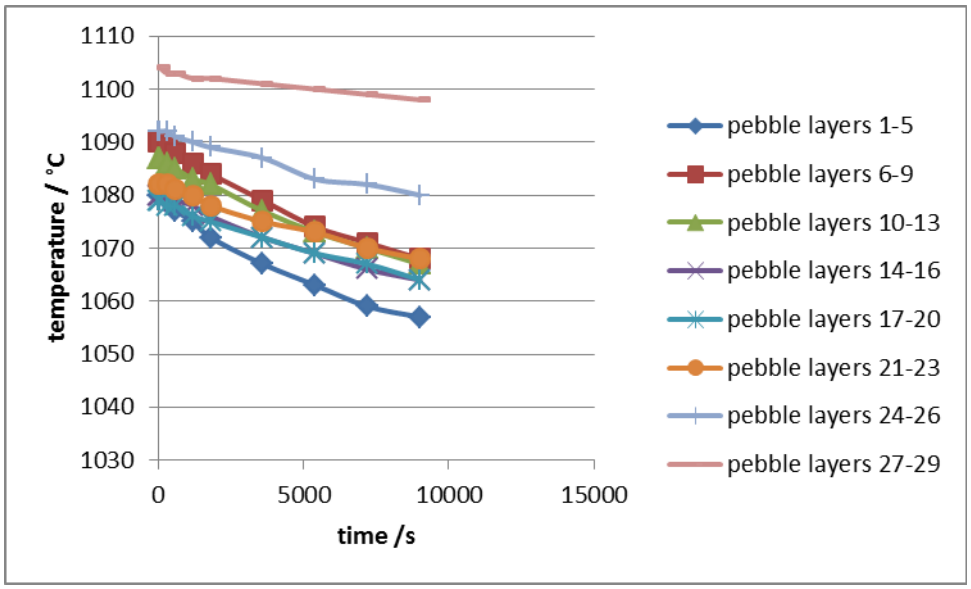

Figure 62: Graphite burn-up during third oxidation phase

Table 7 shows the values of the burn-up in all phases of oxidation und the sum. Only the sum is comparable with the experimental data (see section 6.3.2). The amount of graphite, which was burned during the test is significantly lower than in the block attempt.

	time	pebble layers 1 - 5	pebble layers 6 - 9	pebble layers 10 - 13	pebble layers 14 -16	pebble layers 17 - 20	pebble layers 21 - 23	pebble layers 24 - 26	pebble layers 27 - 29	sum /kg
phase 1	3h 57 min	0,623	0,417	0,333	0,260	0,215	0,183	0,167	0,087	2,285
phase 2	3h 1 min	0,374	0,258	0,208	0,165	0,141	0,126	0,124	0,069	1,465
phase 3	2h 30 min	0,195	0,144	0,121	0,101	0,09	0,085	0,091	0,054	0,881
sum / kg	9h 28 min	1,192	0,819	0,662	0,526	0,446	0,394	0,382	0,21	**4,631**

Table 7: Graphite burn-up after three oxidation phases

6.3 Comparison

In this section the experimental data from the two oxidation tests are compared to the simulation results. The similarities and differences are pointed out and explained if possible. In table 8 the main characteristics of the two Boudouard experiments are collectively represented. Because the graphite surface is decisive for the Boudouard reaction, the surface of the graphite blocks 10 provided the number of layers of spheres in the second experiment.

	Block	**Pebble-bed**
Graphite surface	1,892 m^2	1,900 m^2
Material	NBG-18	MLRF-1
Total mass	250 kg	143 kg
Mass loss	10,2 kg (4,2%)	7,4 kg (5,1%)
Tempera-ture	Ox1: 1185°C Ox2: 1125°C	Ox1: 1175°C Ox2: 1135°C Ox3: 1095°C
Oxidation time	Ox1: 7h 29 min Ox2: 8h 38 min	Ox1: 3h 57 min Ox2: 3h 1 min Ox3: 2h 30 min

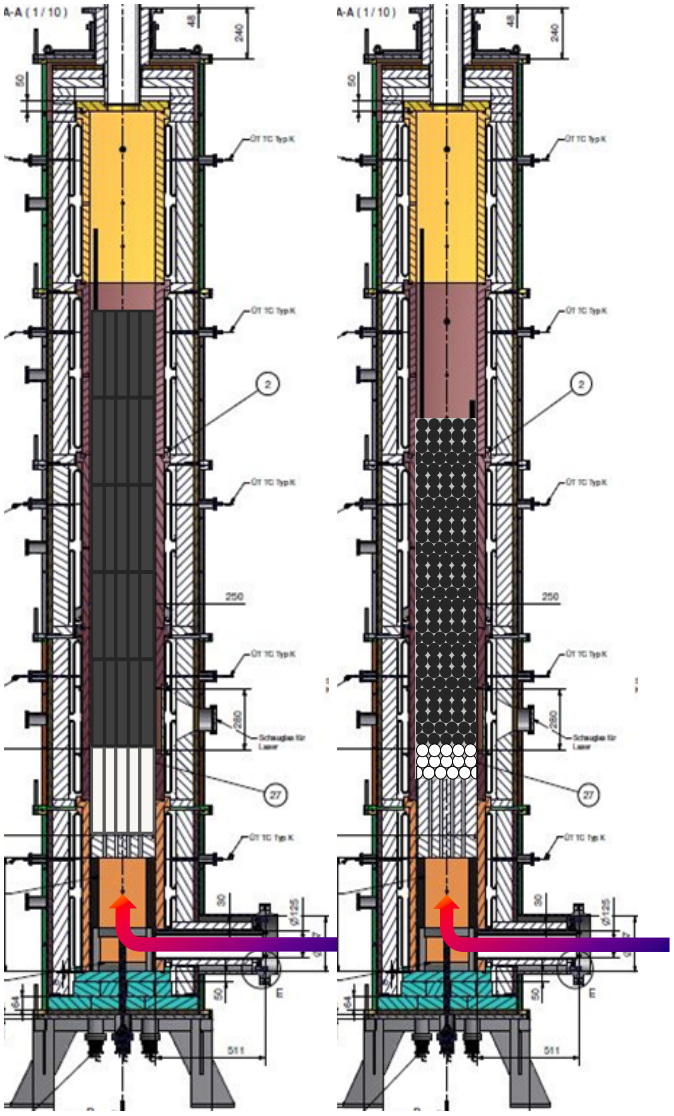

Table 8: Comparison between experimental boundary conditions of block and pebble-bed geometry

6.3.1 Block geometry

A comparison between the calculated graphite burn-up and the graphite loss that arose after the experiment by weighing the blocks is first shown in Table 9.

	block 1.1	block 1.2	block 2.1	Block 2.2	block 3.1	block 3.2	block 4.1	block 4.2	block 5.1	block 5.2	sum /kg
MGT-3D	1,154	1,027	0,927	0,806	0,686	0,617	0,569	0,519	0,48	0,223	**7,008**
experiment	3,19	1,57	1,28	0,745	0,685	0,685	0,625	0,52	0,51	0,435	**10,245**
abs. deviation	2,036	0,543	0,353	0,061	0,001	0,068	0,056	0,001	0,03	0,212	**3,237**
(%)	-64%	-35%	-28%	+8%	<+1%	-10%	-9%	<-1%	-6%	-49%	**-32%**

Table 9: Comparison of graphite burn-up for the block experiment

The graphite corrosion in the blocks calculated by MGT deviates about 32% from the experimentally measured burn-up. However, considering the results for the individual blocks, it is found that the results in the central region (blocks 2.2 to 5.1) fit very well. In the lower blocks the oxidation and the pores in the graphite starts to dilate quickly. So that there is an increase in block surface and thus an expansion of the oxidation surface. This surface modification is not taken into account in the calculation program and therefore provides an explanation for the relatively large variations in this region.

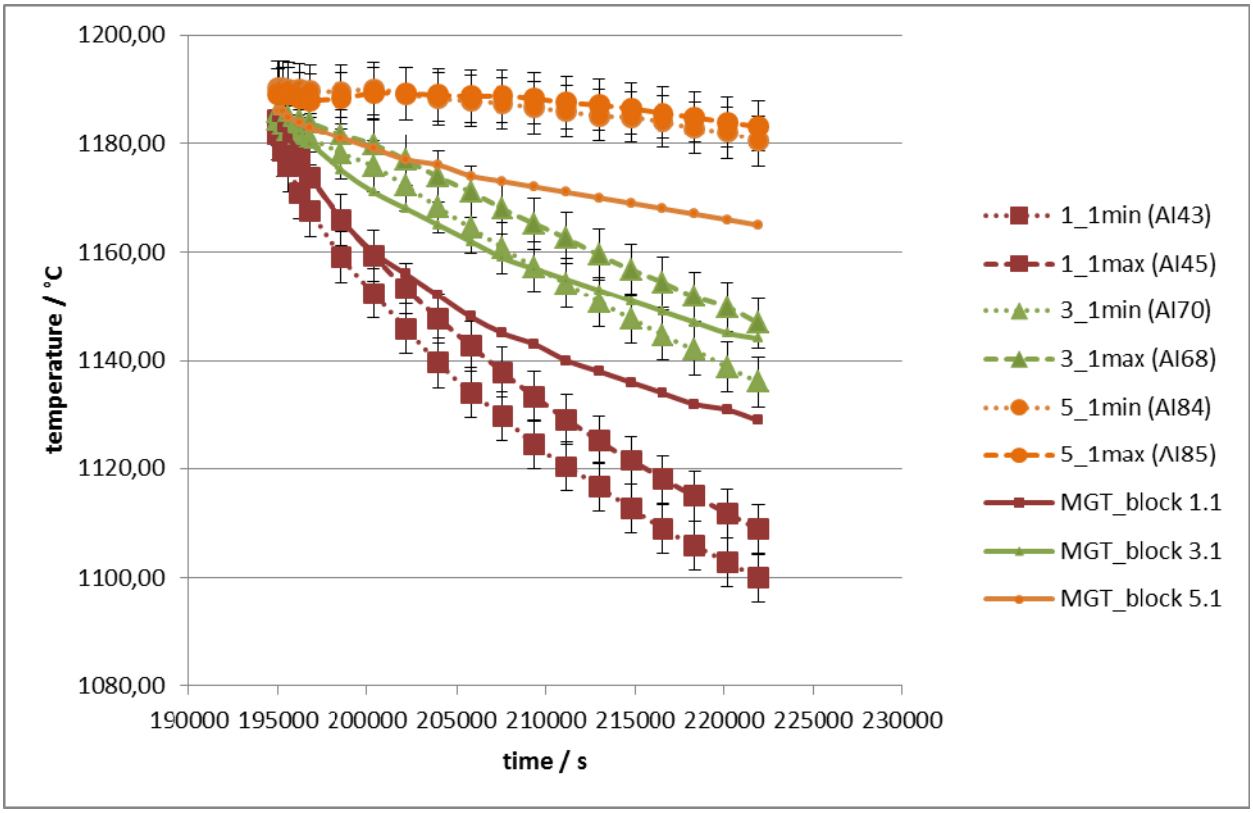

Figure 63: Temperature drop due to Boudouard reaction (first oxidation phase)

Fig. 63 confirms this fact. It is clearly seen that the calculated temperature profile of MGT is good at the beginning of the first oxidation phase within the first blocks. The values are in the range of measured temperatures. With increasing pore diffusion, however, increases the temperature decrease in the experiment. This also explains that the temperature profiles of the second oxidation phase show significantly greater discrepancy between simulation and experiment (see Fig. 64).

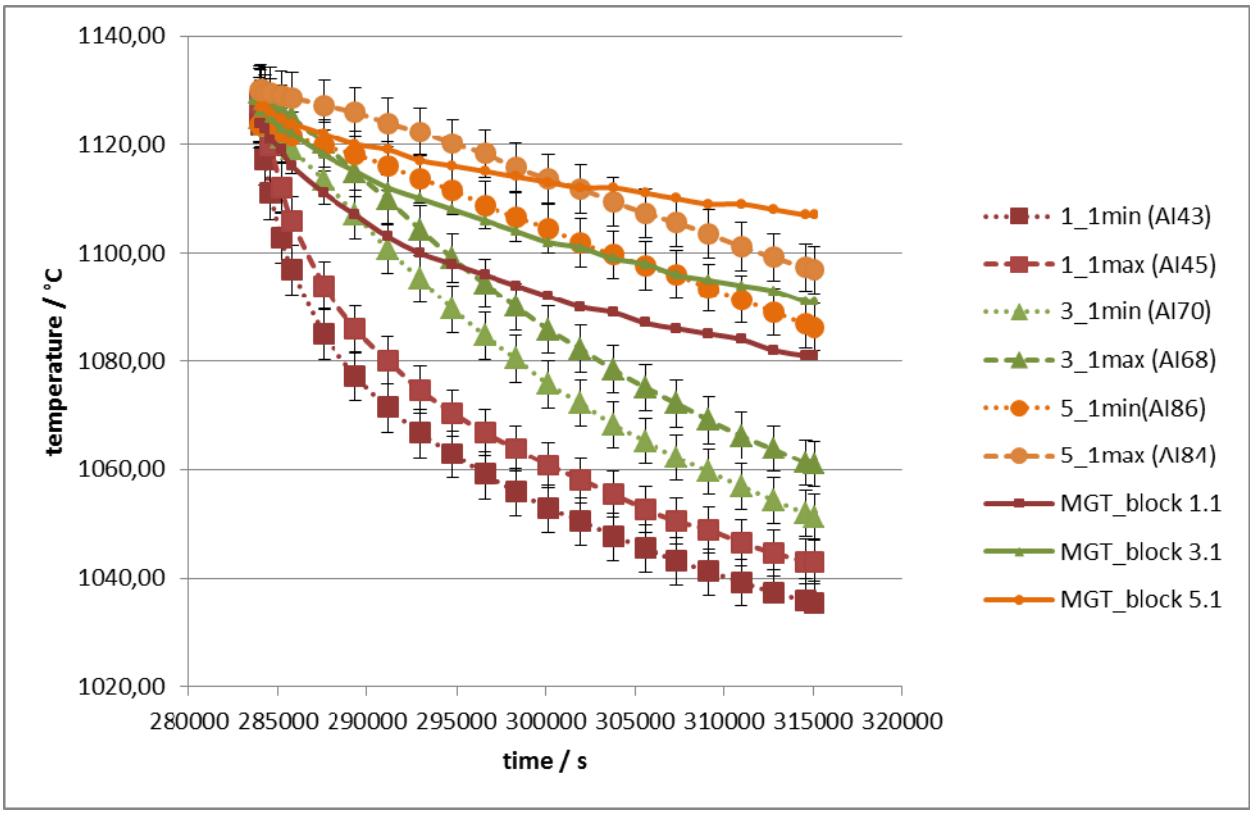

Figure 64: Temperature drop due to Boudouard reaction (2nd oxidation phase)

6.3.2 Pebble bed geometry

In the pebble-bed experiment the difference between calculation and experiment with respect to the graphite corrosion is around 38%, which is in the same order as in the block experiment (see Table 10). There is a good agreement seen in the central pebble layers. The deviations at the bottom and top of the pebble bed are much larger and also can be explained by the change in the surface due to the pore diffusion (see section before).

	pebble layers 1 - 5	pebble layers 6 - 9	pebble layers 10 - 13	pebble layers 14 -16	pebble layers 17 - 20	pebble layers 21 - 23	pebble layers 24 - 26	pebble layers 27 - 29		sum /kg
MGT-3D	1,192	0,819	0,662	0,526	0,446	0,394	0,382	0,21		**4,631**
Experiment	3,445	1,665	0,79	0,415	0,425	0,395	0,22	0,115	0,080 kg less dust	**7,39**
Abs. deviation	2,253	0,846	0,128	0,111	0,021	0,001	0,162	0,095		**2,759**
(%)	-65%	-51%	-16%	+27%	+5%	<+1%	+74%	+83%		**-38%**

Table 10: Graphite burn-up in the experiment and calculated with MGT

Fig. 65 shows the temperature behavior during the first oxidation phase. The solid lines represent the results of MGT calculations in different heights of the pebble bed (bottom – middle – top). The dotted lines mark the experimental results of the corresponding regions. The experimental data are also provided with error bars result from the use of thermocouples. This shows the same trend as in the figures above. There is a reasonably well agreement in the central region (layers 17 – 20), but significant deviations at the bottom (layers 1 – 5) and the top (layers 27 – 29). Looking at the begin of the oxidation time (the first 15 minutes) the simulated values are lying between the minimum and maximum values of the experiment. Then the pore diffusion starts and the temperature decreasing caused by the Boudouard effect takes place but is not realized in the simulation.

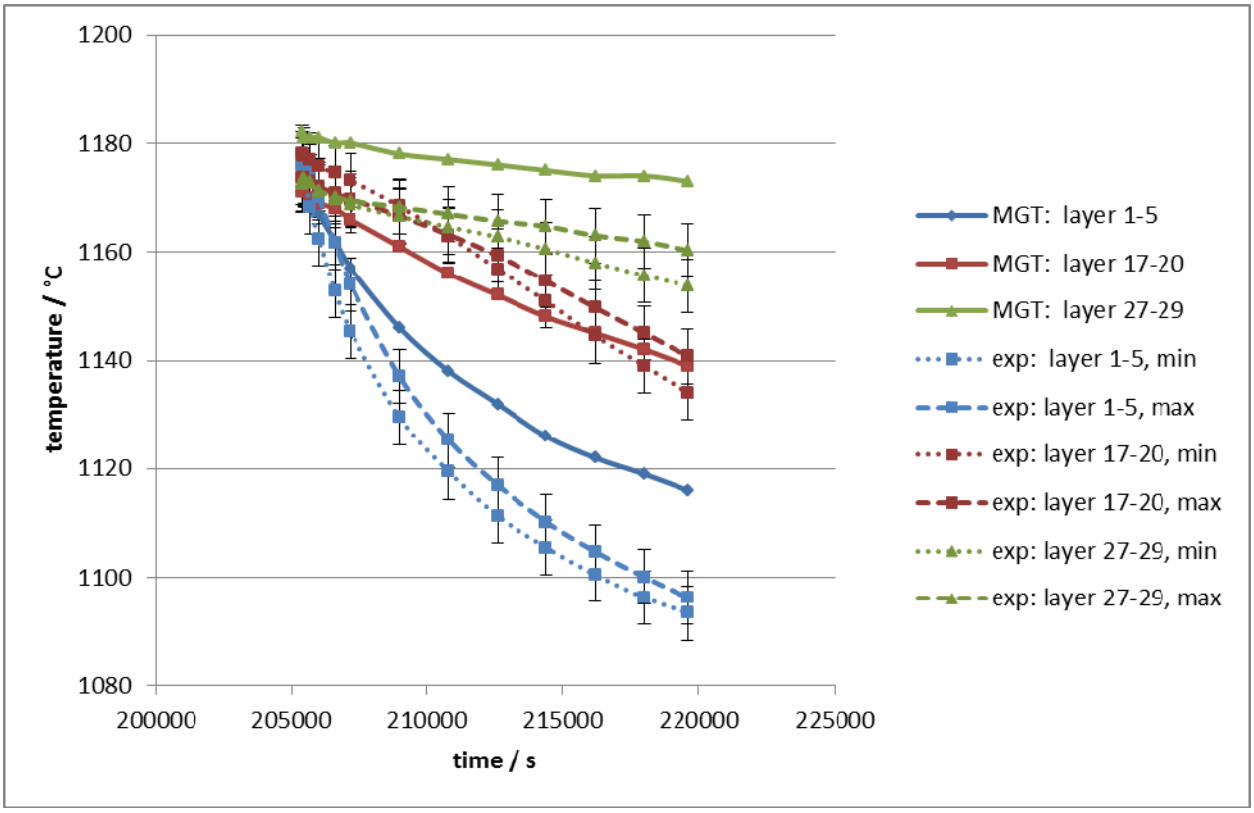

Figure 65: Temperature drop due to Boudouard reaction (first oxidation phase)
Comparison between MGT and experimental data

During the experiment, a total of three oxidation phases were performed in the pebble-bed. Between the second and third oxidation phase, the heating power in the experiment was not changed. Only the gas composition changed accordingly (100% nitrogen and 79% nitrogen mixture, 21% CO2 in the oxidation). Therefore, this experimental phase (Phase 2 oxidation - no oxidation - oxidation phase 3) has been estimated in terms of the temperature evolution with a transient in MGT. The result of this transient is shown in Fig. 66. The trend of the curves (temperature decrease during the oxidation temperature rise in the meantime) is similar. But as seen before the temperature variations in the experiment are much more pronounced than the calculated.

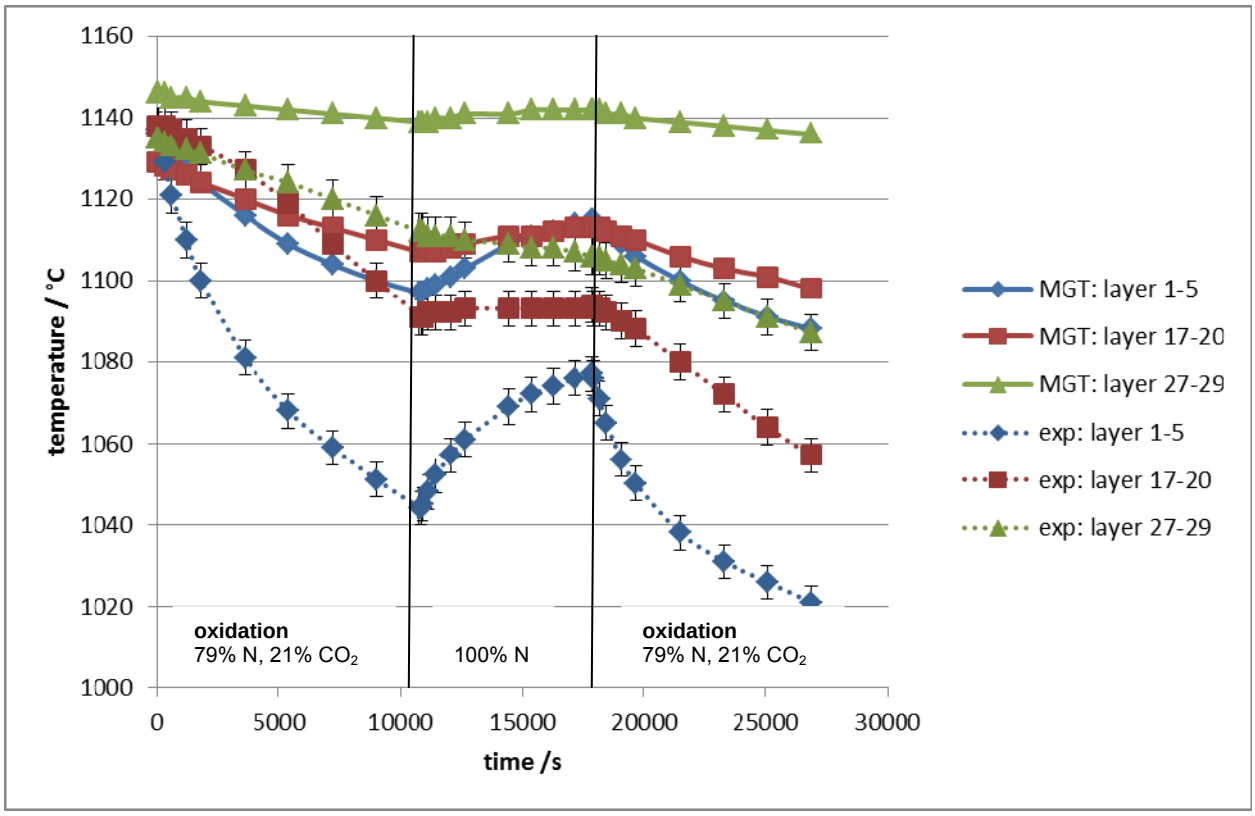

Figure 66: Transient behavior of oxidation phases 2 and 3

Figure 67 shows an overall comparison between the results of the block and the pebble-bed test. The relative mass loss as a function of the overflown graphite surface is specified. Both geometries show a similar burn up related to the overflown surface. The surfaces that are available for the oxidation were identical at the beginning of each experiment, but the reaction times differ significantly (16h 7min for the block experiment, 9h 28min for the pebble bed experiment). The similar values of the graphite burn-up for the two geometries despite the different oxidation time allow the conclusion that the flow distribution of the reaction gas in the graphite structure plays an important role. The flow within a pebble-bed differs significantly from that within the graphite blocks.

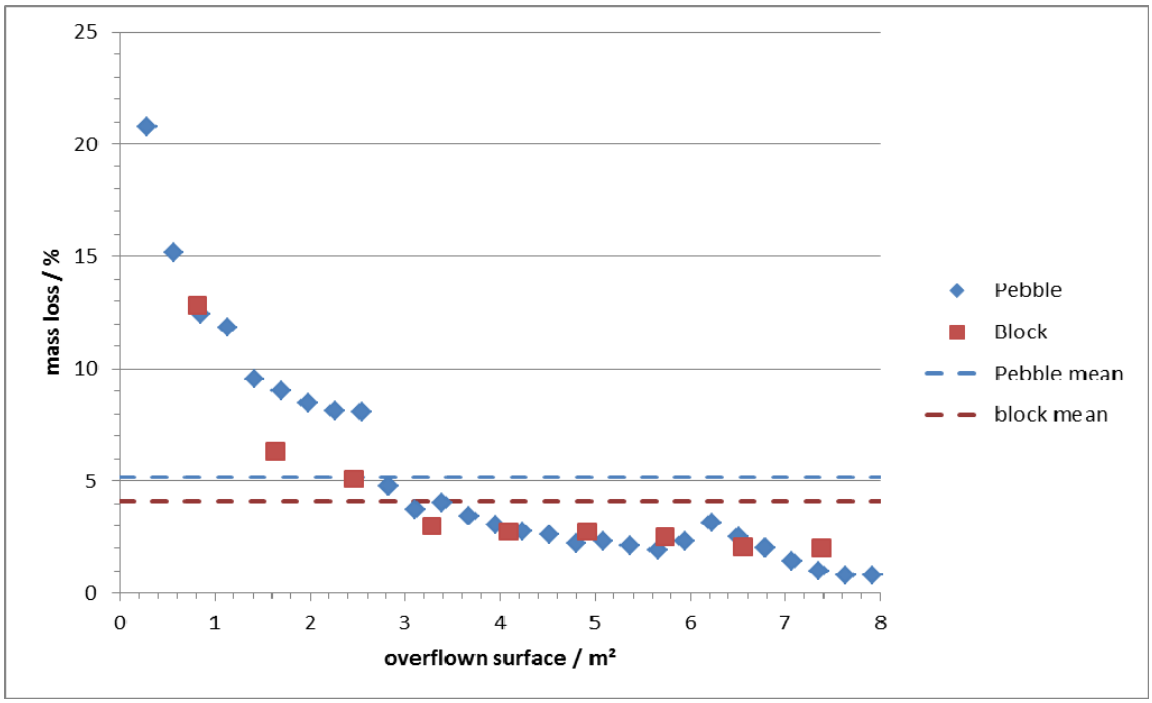

Figure 67: Mass loss for pebbles and blocks.

7 Evaluation of graphite samples

In addition to the comparison of experimental and simulated data, a further focus of the evaluation is to examine the test pieces. For this REM (Reflection Electron Microscope) and BET measurements are performed. The BET method is based on adsorption of gas on a surface. The amount of gas adsorbed at a given pressure allows to determine the surface area of a sample. The BET- measurements were carried out with the Apparatus AUTOSORB-1 from Quantachrome. The AUTOSORB-1 operates be measuring the quantity of gas adsorbed onto or desorbed from a solid surface at some equilibrium vapour pressure by static volumetric method. The data are obtained by admitting or removing a known quantity of adsorbate gas into or out of a sample cell containing the solid adsorbent maintained at a constant temperature below the critical temperature of the adsorbate. As adsorption or desorption occurs the pressure in the sample cell changes until equilibrium is established. The quantity of gas adsorbed or desorbed at the equilibrium pressure is the difference between the amount of gas admitted or removed and the amount required to fill the space around the adsorbent (void space).
Figure 68 shows the measurement cell developed for measurements at solid pieces instead of powder. With these measurements the difference of graphite structure in the process of oxidising should be made visible.

Figure 68: measurement cell

Fig. 69 shows a schematic representation of the areas in a block of graphite, which are provided for such measurement. Unfortunately, these additional studies could not be completed within the ARCHER project.

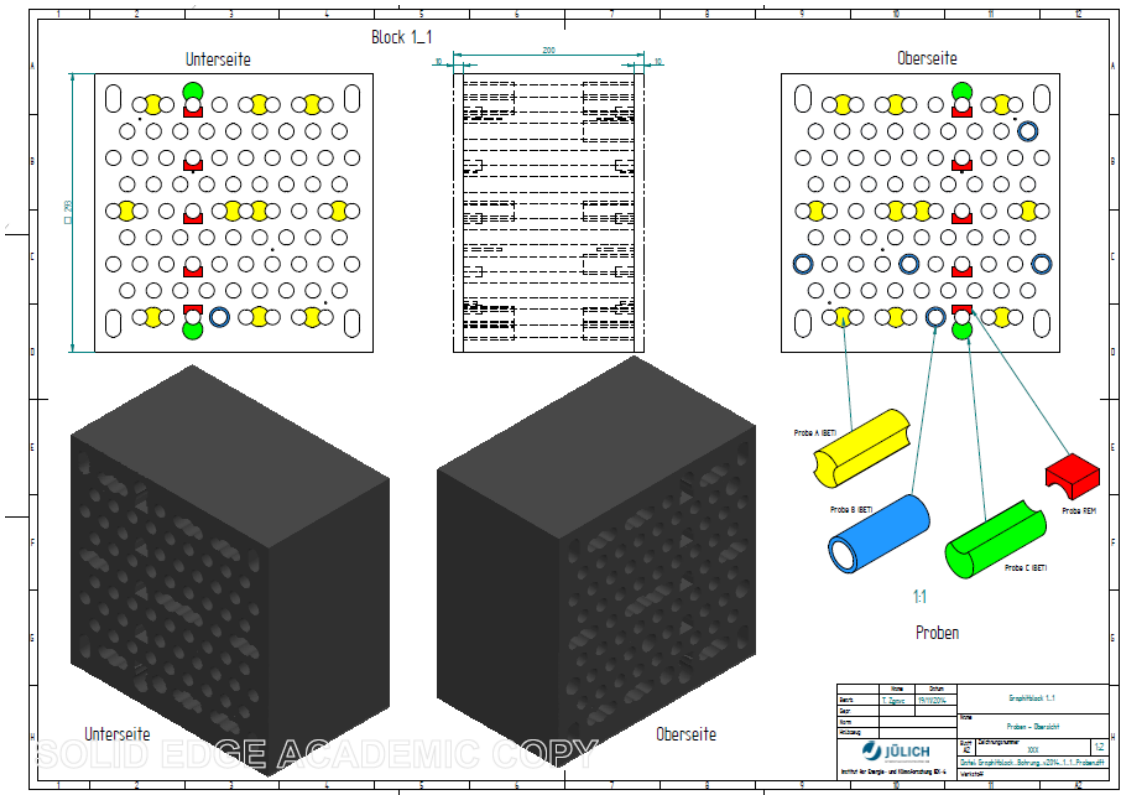

Figure 69: Schematic representation of the areas in a block of graphite, which are provided for measurement

8 Summary

The two oxidation experiments which were performed within the framework of the project ARCHER, are one of the few graphite corrosion experiments dealing with the pure Boudouard reaction. So far, very few data were available. The results (see chapter 6) show that we reached the aimed oxidation range (regime II, in-pore diffusion region, see chapter 2). Clearly visible is the endothermic reaction, both in the experiments and in the accompanying MGT calculations. After the oxidation the blocks show a clear sponge-like structure, which also underlines, that the desired experimental conditions were met. For the spherical test it must be noted that strong differences in erosion can be observed within a pebble layer. This shows that the burn-up is strongly dependent on the local gas flow. But the mass balance (relative burn-up) for each pebble layer fits well together with the results of the block test (see chapter 6.3).

The pre- and post-calculations with MGT-3D have shown that MGT can simulate the effects associated with the Boudouard reaction. The comparison with the experiments show, that the simulation results are better in the early stages of oxidation and identify only very small deviations in the mean altitude of both, blocks and pebble-bed. The relatively large deviations at other times and in the peripheral areas of the graphite geometry must be investigated in further parameter studies. It has to be stressed that MGT has been applied only to graphite corrosion problems inside of pebble beds. The calculations for block geometries meant a new application within the ARCHER project. The pre-calculations (heating experiments and simulation of graphite oxidation) have influenced the design of the experiments and were confirmed by the good results of the experiments.

The surface-analysis of the test pieces (see chapter 7) will give additional information on the Boudouard reaction and the interpretation of the experimental data. Therefore, even if the surface-analysis was not within the proposed program, the generated date will be added after the final completion of the project.